

**EFFECTS OF MANGANESE (IV) OXIDE ON THE PHYSICAL,  
MECHANICAL AND MICROSTRUCTURAL PROPERTIES OF ALUMINA**

**CHENG CHUEN RONG**

**A project report submitted in partial fulfilment of the  
requirements for the award of the degree of  
Bachelor of Engineering (Hons) Mechanical Engineering**

**Faculty of Engineering and Science  
Universiti Tunku Abdul Rahman**

**May 2011**

## DECLARATION

I hereby declare that this project report is based on my original work except for citations and quotations which have been duly acknowledged. I also declare that it has not been previously and concurrently submitted for any other degree or award at UTAR or other institutions.

Signature : \_\_\_\_\_

Name : Cheng Chuen Rong

ID No. : 07UEB06168

Date : 2010-08-24

**APPROVAL FOR SUBMISSION**

I certify that this project report entitled **“EFFECTS OF MANGANESE OXIDE, MnO<sub>2</sub> ON THE PHYSICAL, MECHANICAL AND MICROSTRUCTURAL PROPERTIES OF ALUMINA”** was prepared by **CHENG CHUEN RONG** has met the required standard for submission in partial fulfilment of the requirements for the award of Bachelor of Engineering (Hons.) Mechanical Engineering at Universiti Tunku Abdul Rahman.

Approved by,

Signature : \_\_\_\_\_

Supervisor : \_\_\_\_\_

Date : \_\_\_\_\_

The copyright of this report belongs to the author under the terms of the copyright Act 1987 as qualified by Intellectual Property Policy of University Tunku Abdul Rahman. Due acknowledgement shall always be made of the use of any material contained in, or derived from, this report.

© 2011, Cheng Chuen Rong. All right reserved.

## ACKNOWLEDGEMENTS

I would like to thank everyone who had contributed to the successful completion of this project, especially my group members Choo Wei Seng, Lim Wee Keat, Tan Ye Lock, Wai Jie Sheng and Yong Chan Han. Moreover, I would prefer to express my gratitude to my research supervisor, Mr. Ting Chen Hunt for his helpful advice, guidance and his enormous patience throughout the development of the research. Besides, he also spent much of his time in explaining and providing ideas for us to further understand the scope of the research.

Besides that, I also wish to express my appreciation to Zoey Kang, who is a chemical lab assistant because she has spent plenty of her time on explaining additional information regarding the X-Ray Diffraction (XRD) analysis and helping me to perform the Scanning Electron Microscope (SEM) analysis.

In addition, I would also like to express my gratitude to my loving parents and friends who had helped and gave me encouragement during the research.

## **EFFECTS OF MANGANESE (IV) OXIDE ON THE PHYSICAL, MECHANICAL AND MICROSTRUCTURAL PROPERTIES OF ALUMINA**

### **ABSTRACT**

The primary objective of this final year project is mainly focusing on the enhancement of the mechanical property which is the hardness of the alumina ceramics through a series of fabrication processes which include uniaxial pressing, cold isostatic pressing and pressureless single step sintering. Besides, the influences of manganese (IV) oxide,  $\text{MnO}_2$  addition on the physical, mechanical and microstructural properties of alumina ceramics were also studied. Some standard experimental equipments and techniques such as powder preparation, green body preparation, sintering, grinding, polishing, bulk density measurement, Young's Modulus determination, Vickers hardness determination, SEM microstructure examination and X-ray diffraction (XRD) were applied throughout the entire alumina research work. The results showed that Vickers hardness of samples doped with  $\text{MnO}_2$  would be greater if compared to undoped samples. The positive effect of  $\text{MnO}_2$  addition on the hardness of the alumina ceramics could be further enhanced with the increasing amount of  $\text{MnO}_2$  addition and sintering temperature. Similarly, the modulus of elasticity of the alumina ceramics could also be improved by the addition of  $\text{MnO}_2$  and increasing the sintering temperature. Furthermore, small quantities of  $\text{MnO}_2$  addition could lead to the enhancement of the densification process. The grain growth would also be promoted with the increasing amount of  $\text{MnO}_2$  addition and sintering temperature. In the interim,  $\text{MnO}_2$  addition would also cause the formation of intragranular and intergranular pores while only intergranular pores could be observed on the undoped alumina ceramics. Moreover, no secondary phase formation was detected, thus this shows that the  $\text{MnO}_2$  is in solid solution of alumina.

## TABLE OF CONTENTS

<b>DECLARATION</b>	<b>ii</b>
<b>APPROVAL FOR SUBMISSION</b>	<b>iii</b>
<b>ACKNOWLEDGEMENTS</b>	<b>v</b>
<b>ABSTRACT</b>	<b>vi</b>
<b>TABLE OF CONTENTS</b>	<b>vii</b>
<b>LIST OF TABLES</b>	<b>x</b>
<b>LIST OF FIGURES</b>	<b>xii</b>
<b>LIST OF SYMBOLS / ABBREVIATIONS</b>	<b>xvi</b>
<b>LIST OF APPENDICES</b>	<b>xvii</b>

### CHAPTER

<b>1</b>	<b>INTRODUCTION</b>	<b>1</b>
	1.1 Background	1
	1.2 Aims and Objectives	2
	1.3 Structure of the Thesis	2
<b>2</b>	<b>CERAMICS</b>	<b>3</b>
	2.1 Definition of Ceramic	3
	2.2 History and Evolution of Ceramics	4
	2.3 Properties of Ceramics	5
	2.3.1 Mechanical Properties	5
	2.3.2 Physical Properties	6
	2.3.3 Functional Properties	7
	2.4 Atomic Bonding and Crystal Structure of Ceramics	8

2.5	Microstructure of Ceramic	10
2.6	Types and Applications of Ceramics	12
<b>3</b>	<b>ALUMINA</b>	<b>13</b>
3.1	Introduction	13
3.2	Grades of alumina powder	14
3.3	Phases of alumina	15
3.4	Crystal structures of transition aluminas	16
3.5	Properties of alumina	17
3.5.1	Mechanical properties	17
3.5.2	Physical properties	18
3.5.3	Chemical properties	18
3.6	Applications of alumina	19
3.7	Consolidation Approach	20
3.7.1	Uniaxial pressing	20
3.7.2	Hot pressing	21
3.7.3	Isostatic pressing	22
3.8	Sintering Approach	24
3.8.1	Pressureless sintering	24
3.8.2	Spark plasma sintering	26
3.8.3	Microwave sintering	27
3.9	Various types of additives	28
3.9.1	Niobium oxide	28
3.9.2	Titanium oxide	29
3.9.3	Zirconium oxide	31
3.9.4	Magnesium oxide	32
3.9.5	Manganese (II) oxide, MnO	33
3.9.6	Manganese (IV) oxide, MnO <sub>2</sub>	35
<b>4</b>	<b>METHODOLOGY</b>	<b>39</b>
4.1	Introduction	39
4.2	Powder Preparation	39
4.3	Green Body Preparation	41



4.4	Sintering	41
4.5	Grinding and Polishing	42
4.6	Bulk Density Measurement	42
4.7	Young's Modulus Determination	43
4.8	Vickers Hardness Determination	44
4.9	Microstructure Examination	45
4.10	X-Ray Diffraction (XRD)	45
<b>5</b>	<b>RESULTS AND DISCUSSIONS</b>	<b>47</b>
5.1	Bulk Density and Average Shrinkage	47
5.2	Young Modulus	52
5.3	Vickers Hardness	55
5.4	X-Ray Diffraction (XRD) Analysis	58
5.5	Grain Size	63
<b>6</b>	<b>CONCLUSION AND RECOMMENDATIONS</b>	<b>73</b>
6.1	Conclusion	73
6.2	Recommendations	74
	<b>REFERENCES</b>	<b>76</b>
	<b>APPENDICES</b>	<b>80</b>

## LIST OF TABLES

TABLE	TITLE	PAGE
2.1	Knoop Hardness Number of Ceramic Materials (Richerson, 2005).	5
2.2	Melting Temperatures of Ceramics (Groover, 2010).	7
2.3	Degree of Ionic Character for Ceramic Materials (Callister, 2007).	8
2.4	Types of Crystal Structures (Callister, 2007).	9
2.5	Types and Applications of Ceramics (Callister, 2007).	12
3.1	Crystallographic Information of Transition Alumina (Lee and Rainforth, 1994).	16
3.2	Mechanical Properties of Alpha-Alumina at Room Temperature (Black and Hastings, 1998).	17
3.3	Physical Properties of $\alpha$ -Alumina at Room Temperature (Lide, 2004).	18
3.4	Relative Density and Grain Size of Alumina with 3.0 wt% MnO <sub>2</sub> .	36
4.1	Characteristics of the Starting Pure Alumina, Al <sub>2</sub> O <sub>3</sub> Powder.	40
4.2	Characteristics of the Doping manganese oxide, MnO <sub>2</sub> Powder.	40
4.3	Sample Identification Codes Employed in Present Study.	41

5.1	Summary of Compounds found in Samples before and after Sintering (A and M represents $\text{Al}_2\text{O}_3$ and $\text{MnO}_2$ respectively).	62
-----	--	----

## LIST OF FIGURES

FIGURE	TITLE	PAGE
2.1	Ceramic Materials.	3
2.2	(a) Historical Pottery. (b) Historical Animal Statue.	4
2.3	Densities of Various Materials (Callister, 2007).	6
2.4	Stable and Unstable Anion-Cation Configurations (Callister, 2007).	8
2.5	Orientation of Crystal Lattice of Ceramic's Microstructure (Barsoum, 1997).	10
2.6	Schematic Microstructure of Ceramics (Barsoum, 1997).	11
2.7	Photomicrograph of Silicon nitride, $\text{Si}_3\text{N}_4$ (Barsoum, 1997).	11
3.1	(a) Fine and (b) Coarse Alumina Powder	13
3.2	(a) Brown and (b) White Fused Alumina.	14
3.3	(a) Boehmite, (b) Gibbsite and (c) Diaspore.	15
3.4	Hexagonal Crystal Structure of $\alpha$ -Alumina (Bär, 2004).	16
3.5	Vickers Hardness of Materials (Lide, 2004).	17
3.6	Various Applications of Alumina: (a) Bricks, (b) Radomes, (c) Hip Prostheses, (d) Spark Plug.	19
3.7	Uniaxial Pressing Process (Materials, 2010).	20
3.8	Hot Pressing (Materials, 2010).	21
3.9	Hot Isostatic Pressing (Franklin and Wang, 1976).	22

3.10	Cold Isostatic Pressing (Mitsue Koizumi et al., 1991).	23
3.11	Temperature Profile of Conventional Sintering (Oghbaei et al., 2010).	24
3.12	Temperature Profile of Two-Step Sintering (Wang et al., 2009).	25
3.13	Schematic Diagram of Spark Plasma Sintering (Guo and Tuan, 2004).	26
3.14	Schematic Diagram of Microwave Sintering (Bengisu, 2001).	27
3.15	Relative Density as a Function of Sintering Temperature for Various Compositions of Alumina Ceramic (Hsu et al., 2007).	28
3.16	Grain Size as a Function of Sintering Temperature for Various Compositions of Alumina Ceramics (Hsu et al., 2007).	29
3.17	Grain Size as a Function of Sintering Time for Various Compositions of Alumina Ceramic (Hsu et al., 2007)	29
3.18	Effect of Sintering Temperature on Sintered Density of TiO <sub>2</sub> doped Alumina Ceramics (Sathiyakumar et al., 2002).	30
3.19	Microstructures of Full Dense Alumina prepared by (A) Constant Heating Rate Sintering (1600 °C/0 h) and (B) Two-Step Sintering (T <sub>1</sub> = 1450 °C, T <sub>2</sub> = 1350 °C/12 h) (Wang et al., 2009).	31
3.20	Micrographs of Alumina Sintered at 1550 °C, (a) Pure or 0 wt. %, (b) 0.1 wt. %, (c) 1.5 wt. % Manganese Oxide (Sathiyakumar, 2002).	34
3.21	Micrographs of Undoped Alumina Samples after Sintering at (a) 1550 °C, (b) 1650 °C (Toy et al., 1995).	36
3.22	Micrographs of Alumina with 0.5% Manganese addition after Sintering at (a) 1550 °C, (b) 1650 °C (Toy et al., 1995)	37
3.23	The Phase Diagram of MnO-Al <sub>2</sub> O <sub>3</sub> System (Erkalfa et al., 1995).	37

4.1	Schematic Indentation Fracture Pattern of an Idealized Vickers Palmqvist Crack System.	44
5.1	Graph of Bulk and Relative Density against Sintering Temperature for Various Concentration of MnO <sub>2</sub> Addition	47
5.2	Graph of Bulk and Relative Density against Concentration of MnO <sub>2</sub> Addition for Various Sintering Temperature	48
5.3	Comparison of Relative Density between Experimental Result and Researcher's Result (Erkalfa et al., 1995).	49
5.4	Comparison of Bulk and Relative Density of Alumina Samples which were doped with MnO <sub>2</sub> and MgO independently and sintered at 1450 ° C	50
5.5	Graph of Average Shrinkage against Sintering Temperature for Various Concentrations of MnO <sub>2</sub> Addition	51
5.6	Graph of Average Shrinkage against Concentrations of MnO <sub>2</sub> Addition for Various Sintering Temperatures	51
5.7	Graph of Modulus of Elasticity against Sintering Temperature for Various Concentration of MnO <sub>2</sub> Addition	52
5.8	Graph of Modulus of Elasticity against Concentration of MnO <sub>2</sub> Addition for Various Sintering Temperature	53
5.9	Comparison of Modulus of Elasticity of Alumina Samples doped with MnO <sub>2</sub> and MgO independently and sintered at 1450 ° C	54
5.10	Graph of Vickers Hardness against Sintering Temperature for Various Concentration of MnO <sub>2</sub> Addition	55
5.11	Graph of Vickers Hardness against Concentration of MnO <sub>2</sub> Addition for Various Sintering Temperatures	56
5.12	Comparison of Vickers Hardness of Alumina Samples doped with MnO <sub>2</sub> , MgO and TiO <sub>2</sub> independently and sintered at 1450 ° C	57

5.13	XRD Analysis of Samples Doped with (a) 0 wt. %, (b) 0.5 wt. %, (c) 1.5 wt. %, (d) 3.0 wt. %, (e) 5.0 wt. % of MnO <sub>2</sub> before Sintering	59
5.14	XRD Analysis of Samples Doped with (a) 0 wt. %, (b) 0.5 wt. %, (c) 1.5 wt. %, (d) 3.0 wt. %, (e) 5.0 wt. % of MnO <sub>2</sub> after Sintering at 1250 °C	60
5.15	XRD Analysis of Samples Doped with (a) 0 wt. %, (b) 0.5 wt. %, (c) 1.5 wt. %, (d) 3.0 wt. %, (e) 5.0 wt. % of MnO <sub>2</sub> after Sintering at 1350 °C	61
5.16	XRD Analysis of Samples Doped with (a) 0 wt. %, (b) 0.5 wt. %, (c) 1.5 wt. %, (d) 3.0 wt. %, (e) 5.0 wt. % of MnO <sub>2</sub> after Sintering at 1450 °C	62
5.17	SEM Analysis of Pure Alumina Samples Sintered at (a) 1250 °C, (b) 1350 °C and (c) 1450 °C	64
5.18	SEM Analysis of Samples Doped with 0.5 wt. % MnO <sub>2</sub> Sintered at (a) 1250 °C, (b) 1350 °C and (c) 1450 °C	65
5.19	SEM Analysis of Samples Doped with 1.5 wt. % MnO <sub>2</sub> Sintered at (a) 1250 °C, (b) 1350 °C and (c) 1450 °C	66
5.20	SEM Analysis of Samples Doped with 3.0 wt. % MnO <sub>2</sub> Sintered at (a) 1250 °C, (b) 1350 °C and (c) 1450 °C	67
5.21	SEM Analysis of Samples Doped with 5.0 wt. % MnO <sub>2</sub> Sintered at (a) 1250 °C, (b) 1350 °C and (c) 1450 °C	68
5.22	Graph of Average Grain Size against Temperature for Various Concentration of MnO <sub>2</sub> Addition	69
5.23	Graph of Average Grain Size against Concentration of MnO <sub>2</sub> Addition for Various Sintering Temperatures.	70
5.24	Comparison of Average Grain Size between Experimental Result and Researcher's Result (Erkalfa et al., 1995).	71
5.25	Comparison of Average Grain Size of Alumina Ceramics with Various Concentrations of Additives.	72

**LIST OF SYMBOLS / ABBREVIATIONS**

$\rho$	Bulk density of the sample
$W_a$	Weight of the sample in air
$W_w$	Weight of the sample in water and
$\rho_w$	Density of the distilled water which vary with temperature
$E$	Young's Modulus (Pa)
$m$	Mass of the rectangular bar (g)
$b$	Width of the bar (mm)
$L$	Length of the bar (mm)
$t$	Thickness of the bar (mm)
$F_f$	Fundamental resonant frequency of bar in flexure, (Hz)
$T_1$	Correction factor for fundamental flexural mode to account for finite thickness of bar, Poisson's ratio etc.
$P$	Applied load
$D$	Average diagonals
$\mu$	Poisson's ratio



**LIST OF APPENDICES**

<b>APPENDIX</b>	<b>TITLE</b>	<b>PAGE</b>
A	Experimental Data	80
B	X-Ray Diffraction Card Data Information	82
C	Gantt Chart and Flow Chart	87

## CHAPTER 1

### INTRODUCTION

#### 1.1 Background

By referring to the past researches, some of the authors had encountered several problems or issues regarding to the studies of alumina. For instance, some of the authors faced the difficulty in achieving desirable physical and microstructural properties of alumina at the same instant. In details, the sintering temperature of pure alumina must be high enough in order to obtain desirable level of relative density. However, high sintering temperature tends to promote the grain growth of alumina, which is usually undesirable in most of the cases since it gives adverse effects to the mechanical properties of alumina. As a consequence, either the physical or microstructural properties of alumina have to be compromised for the better achievement of another.

In fact, this topic is of researchers' interest because there is a great potential for alumina ceramics to be widely used in various structural applications due to its high melting temperature, chemical stability, corrosion resistance and mechanical properties such as hardness and wear resistance at elevated temperatures. Therefore, it is reasonable and rational to expect that alumina ceramics would be extensively used for a variety of engineering applications if the mechanical properties of alumina are further improved.

In the research, there are several limitations due to the limited resources and facilities available. For instance, microwave sintering is believed to have positive

effects on alumina in which higher relative density could be achieved at lower sintering temperatures. However, microwave sintering could not be applied in the research due to the lack of related equipment or device. Besides that, cold or hot isostatic pressing which could yield green compacts with higher and more uniform density, could only be performed by using the facilities in other universities.

## **1.2 Aims and Objectives**

The main objective of this project is to study the influence of manganese oxide,  $\text{MnO}_2$  addition on the physical, mechanical and microstructural properties of alumina. The aim of the present work is to improve the hardness of alumina ceramics at low sintering temperature with  $\text{MnO}_2$  addition through a series of fabrication processes such as uniaxial pressing, cold isostatic pressing and pressureless single step sintering processes.

## **1.3 Structure of the Thesis**

The final year project thesis consists of several important sections such as literature review, methodology, results analysis, discussions, conclusion and recommendations.

## CHAPTER 2

### CERAMICS

#### 2.1 Definition of Ceramic

There are various sources of information which explain about the actual meaning of ceramic. From the aspect of terminology, the word - “ceramic” is actually derived from “keramikos”, which is a Greek word. By definition, “keramikos” can be interpreted as “a burnt substance”. This is owing to the people at ancient times would use clay to make different products by mixing it with a small amount of water, shaping the paste into desired form and finally drying it under the hot sun or in a furnace with high temperature. According to Dr. W. David Kingery, who was the father of modern ceramic engineering, proposed that ceramic could be anything as long as it was not an organic or metallic material. Meanwhile, from the aspect of material science, ceramic is often treated as a compound that is formed from metallic and nonmetallic elements with the application of heat treatment, usually in the form of carbides, oxides and nitrides (Callister, 2007).



**Figure 2.1: Ceramic Materials.**

## 2.2 History and Evolution of Ceramics

The use of ceramics in daily activities of mankind started around 24,000 BC, where animals and human statues were made from clay. Around 9,000 or 10,000 BC, products such as tiles, potteries and bricks started to be used widely among the populations. However, these traditional ceramics were porous in nature. Consequently, in ancient times, pottery was seldom used to store and carry water due to leakage tended to occur. This problem was solved successfully when the transparent and water resistant glass was created. During the Middle Ages, refractories which could withstand high temperature were used mainly in constructing the furnace for the metal industry American Ceramic Society [ACS] (2010).



**Figure 2.2: (a) Historical Pottery. (b) Historical Animal Statue.**

Due to certain limitations and shortcomings of traditional ceramics, researchers had tried various methods in refining their microstructural properties so that ceramic materials with better physical, chemical and mechanical properties could be synthesized for highly developed engineering applications. As the time passes, traditional ceramics have now evolved into modern and advanced ceramics which are widely used in different fields and industries such as aeronautic, medical, communication, electrical and electronic. The classical examples of modern and advanced ceramics are magnetic ceramics, optical ceramics, high strength ceramics, piezoelectric, semiconductor ceramics and electrochemical ceramics (ACS, 2010).

## 2.3 Properties of Ceramics

### 2.3.1 Mechanical Properties

From ancient to modern times, most of the people would perceive that metal is definitely stronger than ceramic in term of mechanical behaviour. This is owing to most of the metallic materials would usually possess better mechanical properties such as strength, elasticity and fracture toughness. As a consequence of these stereotyping effects, the application of ceramic materials in our daily life products is much lesser if compared to metals. For instance, vehicles like cars, ships and aircrafts are usually made of metals such as steel alloys and titanium alloys instead of pure ceramics materials. However, in actual fact, the stiffness and strength of some ceramic materials such as silicon carbide and alumina are comparable to those metals (Richerson, 2005).

The hardness of ceramic materials is considerably high but most of them are brittle and very vulnerable to fracture in nature. This is owing to most of them are having relatively low fracture toughness if compared to metals. As a proof, both crystalline and noncrystalline ceramics which own very little energy absorption, tend to fracture instantly without undergoing any plastic deformation when they are applied with tensile stress at room temperature. As we know, some imperfections such as microvoids, microcracks, notches, scratches and surface cracks might exist on the surface or internal regions of ceramic materials. As a result, these defects are likely to act as stress concentration sites which would magnify the applied tensile stress and lead to brittle fracture easily (Richerson, 2005).

**Table 2.1: Knoop Hardness Number of Ceramic Materials (Richerson, 2005).**

Ceramic Material	Knoop Hardness Number
Alumina, $\text{Al}_2\text{O}_3$	200
Silicon dioxide, $\text{SiO}_2$	800
Silicon carbide, $\text{SiC}$	2500
Boron carbide, $\text{B}_4\text{C}$	2800
Diamond, C	7000

From the past experiments, researchers found that most of the ceramics are noticeably strong when they are subjected to compressive load while they would become weak as the tensile force is applied on them. For example, the compressive strength of porcelain is approximately ten times greater than its tensile strength. In addition, ceramic materials would have relatively low flexural strength due to their high tendency to fracture when the tensile strain is more than or equivalent to 0.1%. Moreover, creep deformation would usually occur when the ceramic materials are subjected to compressive or tensile stresses at elevated temperature. Different from brittle fracture, creep deformation would not occur right after the exertion of stress. However, deformation or strain experienced by ceramic materials would accumulate as stress is applied continuously until failure occurs. Due to their molecular structures, ceramic materials generally own fine tribological properties with wear and erosion resistance (Richerson, 2005).

### 2.3.2 Physical Properties

In actual fact, most of the ceramic materials would have densities which are lower than metals but higher than polymers. As a result, ceramics are usually lighter than metals but heavier than polymers (Callister, 2007).

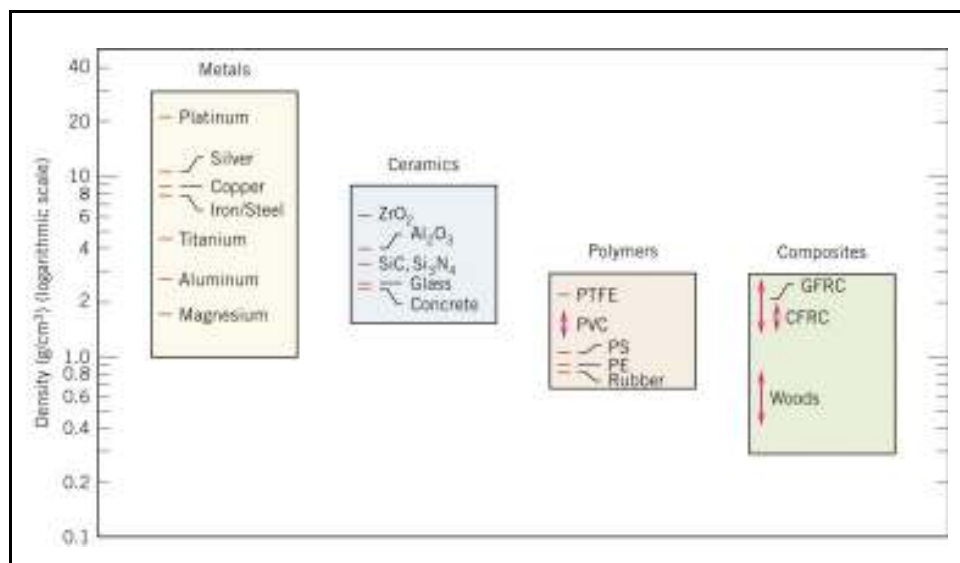


Figure 2.3: Densities of Various Materials (Callister, 2007).

Meanwhile, most of the ceramics are electrically and thermally insulative, which means that their electrical or thermal conductivities are much lower than metals, which are excellent electrical and thermal conductors. Even though the thermal expansion coefficients of ceramic materials are relatively lesser than metals, they are more prone to thermal shock or thermal crack, resulting from rapid thermal changes. This phenomenon usually occurs on ceramic materials as a result of their high thermal expansion coefficients, low thermal conductivities and brittleness or low toughness. However, they are still widely used in the engineering applications which involve high temperature operating conditions. This is owing to their melting temperature are significantly higher than most of the metals, allowing them to have good mechanical resistance even at elevated temperatures (Groover, 2010).

**Table 2.2: Melting Temperatures of Ceramics (Groover, 2010).**

<b>Ceramic Materials</b>	<b>Melting Temperature (°C)</b>
Silicon oxide, SiO <sub>2</sub>	1400
Alumina, Al <sub>2</sub> O <sub>3</sub>	2054
Tungsten carbide, WC	2870
Titanium carbide, TiC	3250
Silicon carbide, SiC	27,007
Cubic boron nitride, BN	30,007

### 2.3.3 Functional Properties

In general, functional properties consist of magnetic, optical and chemical properties of a material. By viewing the chemical properties of ceramic materials, most of them are found to be highly resistant to oxidation, corrosion and chemical attack. As a proof, many scientific researches have shown that ceramics would have higher resistance to harsh environment than metals and polymers. Meanwhile, some ceramics might possess optical characteristics such as transparent, translucent or opaque, depending on their microstructures and types of dopant. As we know, not only metals such as pure irons are magnetic, but some of the oxide ceramics such as ferum oxide (Fe<sub>3</sub>O<sub>4</sub>) also exhibits magnetic behaviour (Ashby et al., 2009).



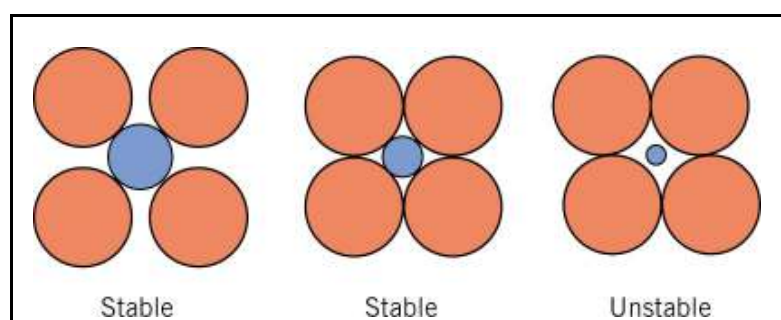
## 2.4 Atomic Bonding and Crystal Structure of Ceramics

Different types of ceramics would have dissimilar atomic bonding. Some of their atomic bonding might be purely ionic, totally covalent or even combination of both, depending on the degree of ionic character of the compounds. Ionic bonding involves transferring of electrons from one atom to another while covalent bonding is the sharing of electrons between atoms in order to achieve electrically neutral. Therefore, the degree of ionic character would be equivalent to zero if the atoms are sharing electron to achieve octet. From the table 2.3, the atomic bonding of magnesium oxide, MgO and silicon carbide, SiC is ionic and covalent accordingly due to their respective degree of ionic character (Callister, 2007).

**Table 2.3: Degree of Ionic Character for Ceramic Materials (Callister, 2007).**

Ceramic Material	Degree of Ionic Character
Magnesium oxide, MgO	73
Sodium Chloride, NaCl	67
Alumina, Al <sub>2</sub> O <sub>3</sub>	63
Silicon dioxide, SiO <sub>2</sub>	51
Zinc sulfide, ZnS	18
Silicon carbide, SiC	12

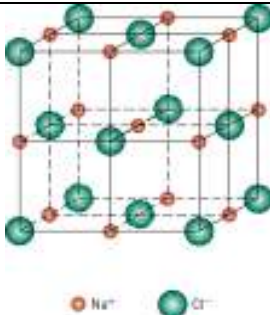
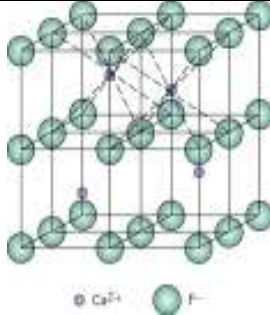
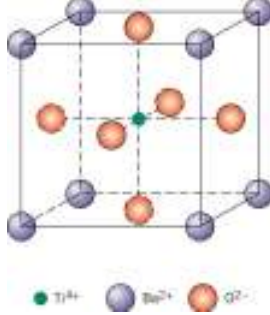
The crystal structures can be assumed to be formed from electrically charged ions instead of atoms for those ceramic materials which own predominantly ionic bonding. Indeed, cations are smaller than anions due to the electrons are usually transferred from metallic to non-metallic elements during the ionization processes. Moreover, the crystal structure of the ceramic would be stable if those anions which enclose a cation are all in contact with the cation (Callister, 2007).



**Figure 2.4: Stable and Unstable Anion-Cation Configurations (Callister, 2007).**

There are various crystal structures such as AX,  $A_mX_p$  and  $A_mB_nX_p$  for a wide range of ceramic materials. By comparison, AX-type crystal structure owns equal number of cations and anions,  $A_mX_p$ -type crystal structure has different number of cations and anions while  $A_mB_nX_p$ -type crystal structure is mainly for those ceramic compounds with more than one type of cation. The types of crystal structures and their respective examples are summarized in Table 2.4 (Callister, 2007).

**Table 2.4: Types of Crystal Structures (Callister, 2007).**

Structure Name	Structure Type	Examples	Figure
Rock Salt (Sodium Chloride)	AX	NaCl, MgO, FeO	
Fluorite	AX <sub>2</sub> ( $A_mX_p$ )	CaF <sub>2</sub> , UO <sub>2</sub> , ThO <sub>2</sub> , ZrO <sub>2</sub> , PuO <sub>2</sub>	
Perovskite	ABX <sub>3</sub> ( $A_mB_nX_p$ )	BaTiO <sub>3</sub> , SrZrO <sub>3</sub> , SrSnO <sub>3</sub>	

## 2.5 Microstructure of Ceramic

By comparing their microstructures, ceramics can be classified into crystalline and non-crystalline. As indicated by their nomenclature, crystalline ceramics would form polycrystalline microstructure while non-crystalline ceramics own non-crystalline or amorphous microstructure. For instance, most of the ceramics such as alumina,  $\text{Al}_2\text{O}_3$ , zirconia,  $\text{ZrO}_2$ , Magnesium oxide,  $\text{MgO}$  and calcium fluoride,  $\text{CaF}_2$  are considered as crystalline ceramics, except glasses and glass ceramics (Callister, 2007).

Microstructure of ceramic materials consists of grain boundaries, pores, secondary phases, orientation of crystal lattice, shape and size of grains. Polycrystalline microstructure is made up of many small interlocking crystals or usually known as grains. The distribution of grains can only be observed with the aid of microscope due to the extremely small grain sizes of ceramics, ranging from 1 to 50  $\mu\text{m}$ . Moreover, each of the grains is separated from one and another by area of disorder or grain boundary. Owing to ceramics are composed of at least two elements, more than one phase would usually exist in the microstructure. Moreover, the structure, composition and properties of each phase generally vary from one and another. Even though the composition of each grain is identical, the orientation of crystal lattice would change from one grain to another (Barsoum, 1997).

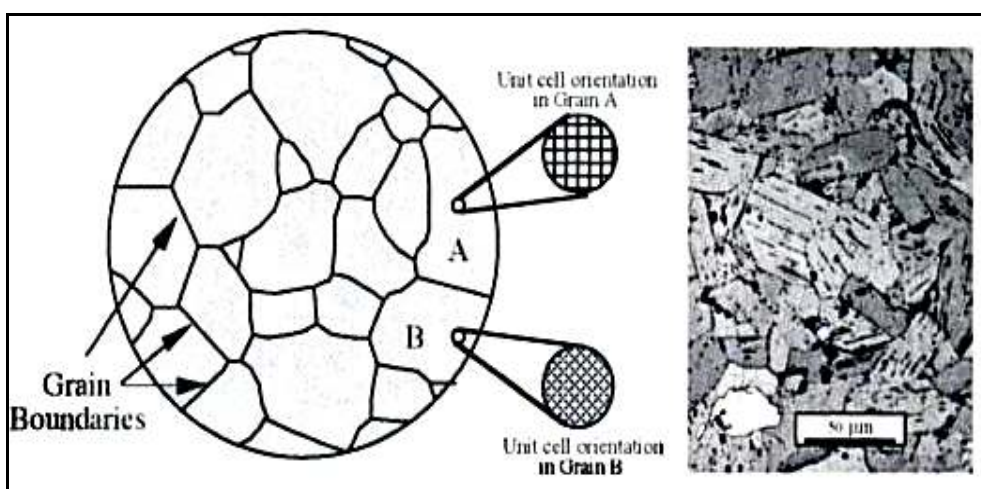


**Figure 2.5: Orientation of Crystal Lattice of Ceramic's Microstructure (Barsoum, 1997).**

Mechanical, functional and physical properties of ceramics are influenced by porosity, boundaries, size, shape, orientation and distribution of grains. For instance, grains with smaller size would improve the mechanical strength and density of ceramic materials. Although a fine grained ceramic offers better mechanical strength at room temperature, it is more prone to creep failure if compared to a coarse grained ceramic. According to literature, most ceramics are not completely dense due to the presence of pores in the microstructure. As a result, the mechanical performance of ceramic materials would be deteriorated (Barsoum, 1997).

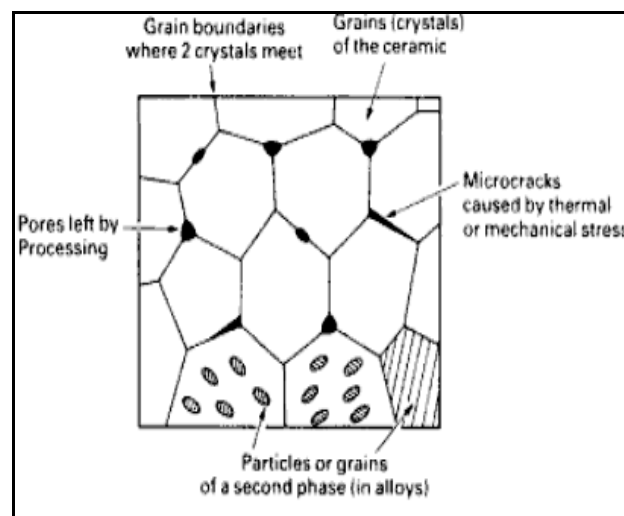


**Figure 2.6: Schematic Microstructure of Ceramics (Barsoum, 1997).**

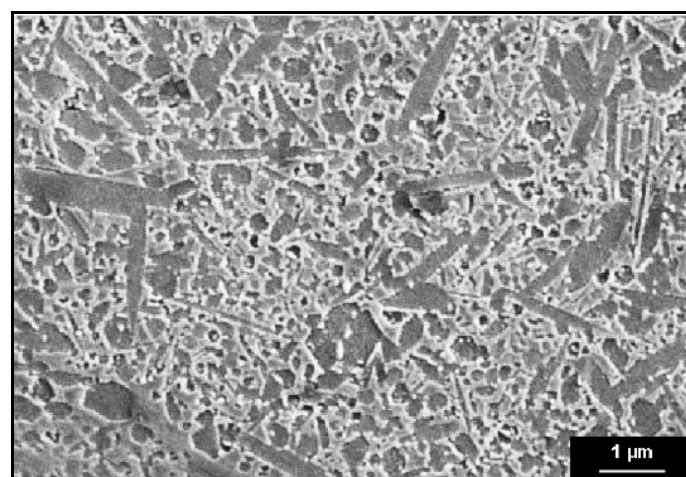


**Figure 2.7: Photomicrograph of Silicon nitride, Si<sub>3</sub>N<sub>4</sub> (Barsoum, 1997).**

## 2.6 Types and Applications of Ceramics

Ceramic materials can be categorized into different groups such as glasses, clay products, refractories, abrasive ceramic, cements and advanced ceramics, depending on their respective applications. Each type of ceramic and their applications are summarized in the table below (Callister, 2007).

**Table 2.5: Types and Applications of Ceramics (Callister, 2007).**

<b>Types of Ceramics</b>	<b>Descriptions</b>	<b>Applications</b>
<b>Glasses</b>	<ul style="list-style-type: none"> <li>□ <b>Glasses</b> <ul style="list-style-type: none"> <li>▪ Noncrystalline silicates.</li> </ul> </li> </ul>	<ul style="list-style-type: none"> <li>□ Containers, lenses and fiberglass.</li> </ul>
	<ul style="list-style-type: none"> <li>□ <b>Glass-Ceramics</b> <ul style="list-style-type: none"> <li>▪ Fine grained polycrystalline material.</li> <li>▪ High mechanical strength.</li> <li>▪ Low coefficients of thermal expansion.</li> </ul> </li> </ul>	<ul style="list-style-type: none"> <li>□ Ovenware, oven window and tableware.</li> </ul>
<b>Clay Products</b>	<ul style="list-style-type: none"> <li>□ <b>Structural clay products</b> <ul style="list-style-type: none"> <li>▪ High structural integrity.</li> </ul> </li> </ul>	<ul style="list-style-type: none"> <li>□ Bricks, tiles and sewer pipes.</li> </ul>
	<ul style="list-style-type: none"> <li>□ <b>Whitewares</b> <ul style="list-style-type: none"> <li>▪ Becoming white after high temperature firing.</li> </ul> </li> </ul>	<ul style="list-style-type: none"> <li>□ Porcelain, pottery and china.</li> </ul>
<b>Refractories</b>	<ul style="list-style-type: none"> <li>□ Capable of withstanding high temperatures.</li> <li>□ Inert to severe environments.</li> <li>□ Can be further divided into fireclay, silica, basic and special refractories.</li> </ul>	<ul style="list-style-type: none"> <li>□ Furnace and bricks.</li> </ul>
<b>Abrasive Ceramics</b>	<ul style="list-style-type: none"> <li>□ Used to wear, grind or cut away other materials.</li> <li>□ High degree of wear resistance, hardness and toughness.</li> </ul>	<ul style="list-style-type: none"> <li>□ Sandpaper</li> </ul>
<b>Cements</b>	<ul style="list-style-type: none"> <li>□ Used to chemically bind other materials together.</li> </ul>	<ul style="list-style-type: none"> <li>□ Plaster of Paris and lime.</li> </ul>
<b>Advanced Ceramics</b>	<ul style="list-style-type: none"> <li>□ Development of ceramic materials that exhibit special properties.</li> </ul>	<ul style="list-style-type: none"> <li>□ Optical fibers and ceramic ball bearings.</li> </ul>

## CHAPTER 3

### ALUMINA

#### 3.1 Introduction

Alumina, which is also known as aluminium oxide,  $\text{Al}_2\text{O}_3$ , is a compound consists of aluminium and oxygen. In actual fact, alumina has the same chemical formula with gems like sapphire or ruby. Unlike these gems, alumina is a transparent, white or nearly colourless ceramic substance. This is owing to alumina does not own any metal impurity that could act as colouring agent (Lide, 2004).

Alumina is usually extracted from bauxite, which is a rock that consists of gibbsite,  $\text{Al}(\text{OH})_3$ , boehmite,  $\gamma\text{-AlO}(\text{OH})$  and diaspore,  $\alpha\text{-AlO}(\text{OH})$ . In details, extraction of alumina is performed through Bayer process that encompasses a series of activities, starting from digestion of bauxite with hot caustic liquor,  $\text{NaOH}$  into solution form, crystallization and precipitation of the aluminium hydrate particles and lastly calcination to form alumina (Schmitz, 2006). Additional milling process is needed for producing fine alumina powder since the Bayer process tends to produce highly-aggregated powder (Lee and Rainforth, 1994).

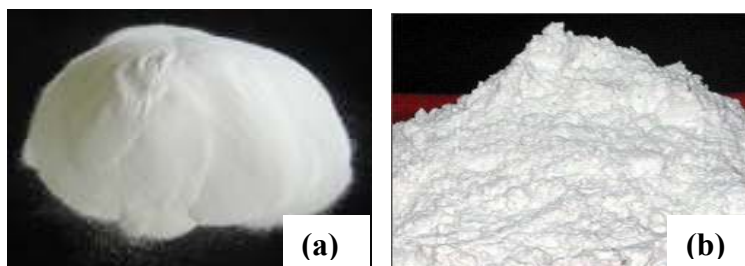


**Figure 3.1: (a) Fine and (b) Coarse Alumina Powder**

### 3.2 Grades of alumina powder

Reactive alumina powder could achieve nearly complete densification at relative low sintering temperature, usually ranging from 1550°C to 1600 °C. Reactive alumina powder is usually produced to be with higher purity, finer grain, spherical shape and alpha phase. Due to the high temperature mechanical behaviour of reactive alumina powder, it is widely used in application such as zirconia toughened alumina and SiC-reinforced alumina ceramic matrix composites (Southern, 1991).

Tabular refractory alumina powder is characterized with extremely high purity and low grain porosity. It is produced by heating the calcined Bayer alumina powder at temperatures, which are greater than 1925 °C but lower than its melting temperature. Through this heating process, fine and  $\alpha$ -phase crystallites of calcined Bayer alumina are transformed into large, hexagonal, elongated tablet shape crystallites. Tabular refractory alumina has good thermal conductivity and high crushing strength, making it become widely used in alumina-graphite refractories, low and high cement castable mixes (Lee and Rainforth, 1994).

Fused alumina can be produced in two forms, which are white and brown. White fused alumina, which has sharp grain and higher abrasiveness than brown fused alumina, is produced by using calcined Bayer alumina. Despite of using as an abrasive, white fused alumina is also used extensively in high temperature refractory bricks and monolithics. Meanwhile, brown fused alumina that has angular-shaped grain and higher toughness than white fused alumina, is made from bauxite. Brown fused alumina has melting temperature which is lower than white fused alumina due to the existence of impurities. It is usually used in refractories for blast furnace trough and continuous casting of steel (Lee and Rainforth, 1994).

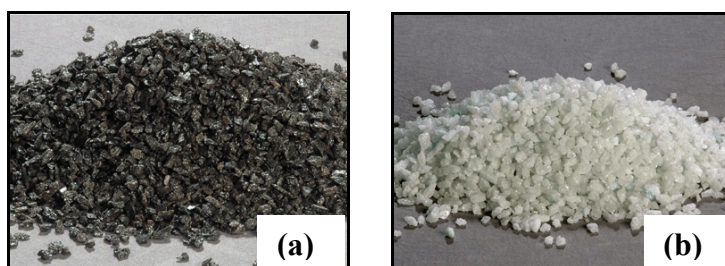


**Figure 3.2: (a) Brown and (b) White Fused Alumina.**



### 3.3 Phases of alumina

The formation of transitional metastable alumina phases such as gamma ( $\gamma$ ), eta ( $\eta$ ), chi ( $\chi$ ), iota ( $\iota$ ), epsilon ( $\epsilon$ ), delta ( $\delta$ ), theta ( $\theta$ ) and kappa ( $\kappa$ ) occurs during the processes such as oxidation of aluminium metal and formation of  $\alpha$ -alumina by heating boehmite, gibbsite and diaspore. As the heating temperature increases, each transition alumina transforms into another transition alumina with a different crystalline structure. However, each transition alumina would recrystallize into  $\alpha$ -alumina which has a very stable crystalline structure and remains unchanged up to its fusion point, at temperature above 1100 °C. The sequence of transitional alumina phases is dependent on the type of starting material and how the starting material was formed (Lee and Rainforth, 1994).

During the heating process of a pure boehmite,  $\gamma$ -AlO(OH), dehydration begins at between 300 °C and 400 °C. When the heating temperature increased to 500 °C, complete dehydration of boehmite occurs and gives rise to formation of  $\gamma$ -alumina,  $\gamma$ Al<sub>2</sub>O<sub>3</sub>. Through this dehydration process, about a quarter of oxygen, O<sub>2</sub> are removed in the form of water, H<sub>2</sub>O. With the continuous heating process, a number of transitional alumina phases occur, starting from  $\gamma$  to  $\delta$ ,  $\theta$  and finally to  $\alpha$ -alumina at about 1100 °C (Gitzen, 1970).

Throughout the heating process of gibbsite, Al(OH)<sub>3</sub>, the transition alumina phases develops from  $\chi$  to  $\iota$ ,  $\kappa$ ,  $\theta$  and finally transforms into  $\alpha$ -alumina. However, if the starting material is switched to diaspore,  $\alpha$ -AlO(OH), it transforms directly into  $\alpha$ -alumina without experiencing any transition phase change. The development of a highly porous powder microstructure takes place as the transformation process of hydrated compounds to transition alumina proceeds (Wilson, 1979).



**Figure 3.3: (a) Boehmite, (b) Gibbsite and (c) Diaspore.**



### 3.4 Crystal structures of transition aluminas

Alpha alumina has a hexagonal crystal structure in which the oxygen anions are packed in a hexagonal arrangement and the aluminium cations reside in some of the available octahedral positions (Askeland and Phulé, 2004). Each aluminium ions is surrounded by six oxygen ligands (Bär, 2004).

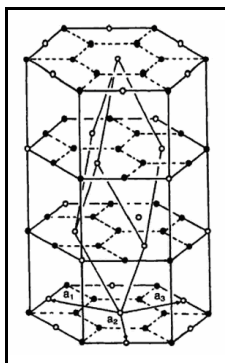


**Figure 3.4: Hexagonal Crystal Structure of  $\alpha$ -Alumina (Bär, 2004).**

The crystal structures of transition aluminas are partially disordered and depending on a closed oxygen sublattice with varying interstitial aluminium configurations. As the heating temperatures increase, the structures become more ordered, start forming a hexagonal oxygen sublattice until stable  $\alpha$ -alumina is formed. The crystallographic information for the transition aluminas is summarized in the Table 2.1 below (Lee and Rainforth, 1994).

**Table 3.1: Crystallographic Information of Transition Alumina (Lee and Rainforth, 1994).**

Transition Alumina	Crystal Structure
Gamma ( $\gamma$ )	Cubic
Eta ( $\eta$ )	Cubic
Chi ( $\chi$ )	Hexagonal
Iota ( $\iota$ )	Tetragonal
Epsilon ( $\epsilon$ )	Hexagonal
Delta ( $\delta$ )	Tetragonal
Theta ( $\theta$ )	Monoclinic
Kappa ( $\kappa$ )	Orthrhombic

### 3.5 Properties of alumina

#### 3.5.1 Mechanical properties

Alpha-alumina is a very hard material since it has a hardness of 9 on the Mohs scale or 2200 Knoop, which is much higher if compared with other ceramic materials. Besides, alumina ceramics have good wear resistance, making them become resistant to erosion. However, alumina ceramic is a brittle material, which would fracture under light impact or tensile loads. This is owing to low fracture toughness of alumina ceramics, usually in the range of  $4 \text{ MPa m}^{1/2}$ , which is lesser than zirconia ceramics that have  $9 \text{ MPa m}^{1/2}$  of fracture toughness (Lide, 2004). Alumina ceramic has an elastic modulus of 366 GPa, which is higher than cobalt chromium that has only 220 GPa of elastic modulus (Black and Hastings, 1998).

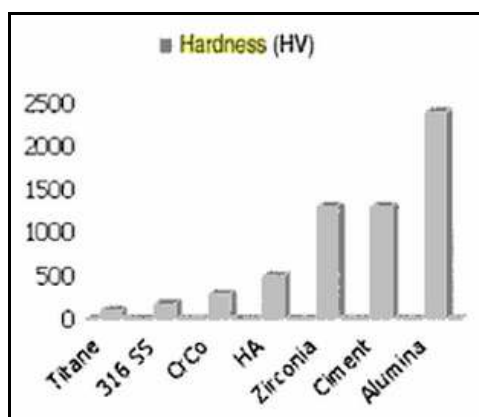


Figure 3.5: Vickers Hardness of Materials (Lide, 2004).

Table 3.2: Mechanical Properties of Alpha-Alumina at Room Temperature (Black and Hastings, 1998).

Mechanical Properties	Value
Hardness	22 GPa
Modulus of elasticity	366 GPa
Flexural strength	551 MPa
Compressive strength	3790 MPa
Tensile strength	310 MPa
Fracture toughness	$4.0 \text{ MPa m}^{1/2}$
Poisson's ratio	0.26

### 3.5.2 Physical properties

Similar with other ceramic oxides, alpha-alumina has comparatively low density if compared to those metals. This eventually makes the alumina-based materials or products become much lighter. Undeniably, alpha-alumina is heavier than polymers due to its higher density if compared to polymers (Lynch, 1975).

Alpha-alumina has excellent thermal properties due to its high melting point, which is about 2313 K and thermal conductivity of 36 W/m K at room temperature. These make alumina become widely used, especially as refractory that could withstand extreme heat or elevated temperature environment without deterioration. Besides, its relatively high specific heat capacity, which is about 774.997 J/kg K, gives rise to its ability to withstand temperature changes (Lide, 2004).

**Table 3.3: Physical Properties of  $\alpha$ -Alumina at Room Temperature (Lide, 2004).**

Physical Properties	Value
Density	3.98 g/cm <sup>3</sup>
Melting point	2313 K
Boiling point	3253 K
Thermal conductivity	36 W/m K
Specific heat capacity	774.977 J/kg K
Thermal expansion coefficient	6.5 K <sup>-1</sup>

### 3.5.3 Chemical properties

Alumina is a non hazardous substance and this makes it become a more favourable and desirable material to use than the beryllia or beryllium oxide which has enhanced thermal properties but higher toxicity (Lide, 2004). Moreover, alumina is chemically stable and corrosion resistant since it is unaffected under atmospheric or marine environment. Besides, it is also insoluble in inorganic acids at room temperature. However, alumina tends to dissolve slowly in molten salts and oxides at elevated temperature, usually greater than 1000 °C (Martin, 2007).

### 3.6 Applications of alumina

Due to its advantageous characteristics, alumina is used extensively in various engineering applications. As a review, alumina is an oxide ceramic which has relatively high hardness, good corrosion resistance, strength, thermal and electrical insulation characteristics and stability (Gitzen, 1970). In addition, its expansion coefficient is closer to those of metals than that of structural nitrogen ceramics, such as silicon nitride. Its ease of processing and availability in abundance make alumina become favourable used oxide ceramics (Sathiyakumar and DGnanam, 2002).

Alumina-based materials are used in various applications, ranging from the calcined bauxite anti-skid road dressings to high-purity, dense alumina hip prostheses. Other examples of alumina-based products are refractory bricks, whitewares, computer substrates, grinding media, spark plug insulators, abrasives, cutting tools and radomes (Lee and Rainforth, 1994). The ability of alumina to achieve densification with little or no glass phase formation makes its theoretical properties become attainable. This results in new applications of alumina such as envelopes for high-pressure sodium vapour lamps and microwave windows (Lynch, 1975).

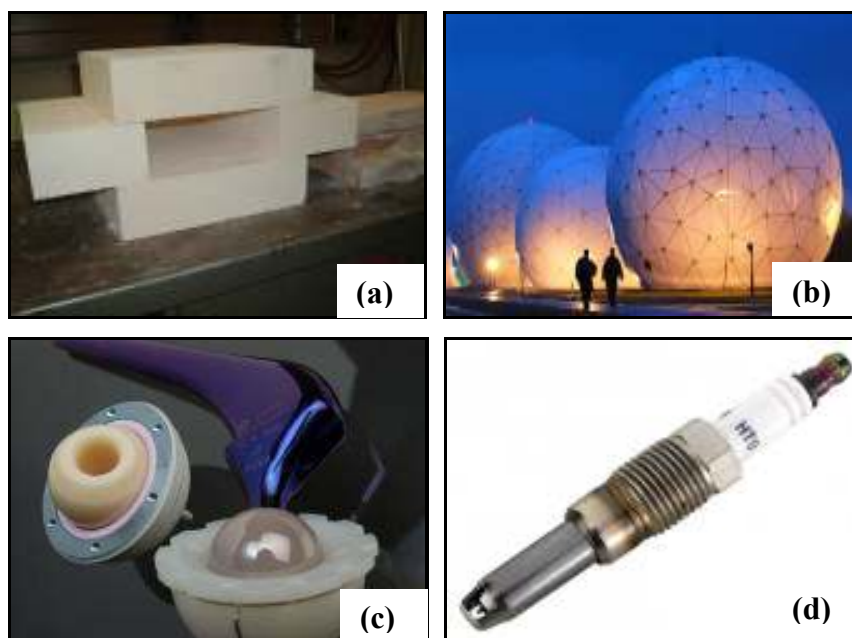


**Figure 3.6: Various Applications of Alumina: (a) Bricks, (b) Radomes, (c) Hip Prostheses, (d) Spark Plug.**

### 3.7 Consolidation Approach

#### 3.7.1 Uniaxial pressing

Uniaxial pressing involves consolidation of the powder by application of pressure in a single direction. In uniaxial pressing process, a hard steel die is initially filled with dry powder. Then, a hard metal punch is driven into the die to compress the powder and form a compact (Segal, 1989). The compact follows the configuration and shape of the die. Unlike hot pressing, sintering operation is required after the pressing operation (Callister, 2007).

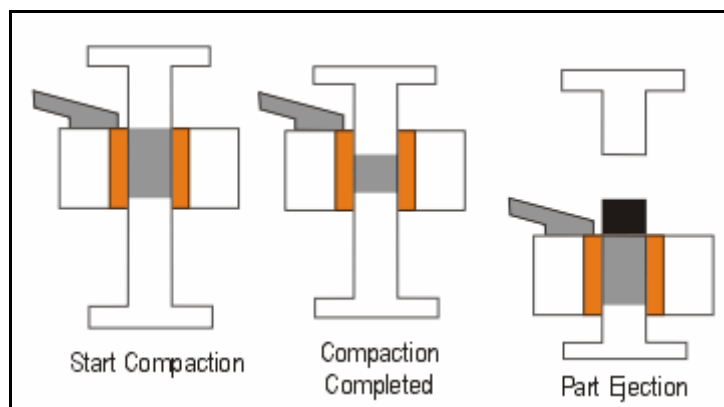


**Figure 3.7: Uniaxial Pressing Process (Materials, 2010).**

The main advantages of uniaxial pressing are high production rates and inexpensive processing cost (Callister, 2007). By using uniaxial pressing, the compacts or parts can be produced to close dimensional tolerances (Segal, 1989). However, it can only be used to form parts with simple shape and geometry, such as flat discs and bars. This is mainly due to the difficulty of powders to flow evenly in all directions perpendicular to the applied pressure. Another drawback of uniaxial pressing is the density variations tend to occur in the compacts after the pressing process (Groover, 2010).

### 3.7.2 Hot pressing

Hot pressing involves simultaneous application of heat and pressure during the entire consolidation process. In simpler words, the powder is compacted at an elevated temperature. Hot pressing is also known as hot uniaxial pressing since it also exerts pressure to the powder in a single direction. Unlike uniaxial pressing, hot pressing uses graphite die, which could withstand high temperature environment without deterioration. Moreover, no sintering operation is needed after the pressing process (Callister, 2007).

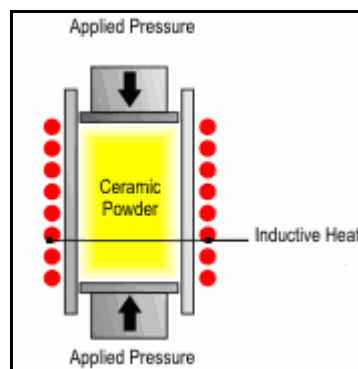


**Figure 3.8: Hot Pressing (Materials, 2010).**

If compared with uniaxial pressing, hot pressing could produce better green bodies at lower temperatures as these green compacts tend to have higher densities and smaller grain sizes. Similar with uniaxial pressing, it is only suitable for fabrication of simple parts such as flat plates, blocks and cylinders. Hot pressing is also limited by the low strength of graphite die (Segal, 1989). Hot pressing requires the mold and die to be heated and cooled during each cycle and thus, it is very time consuming. Moreover, the fabrication cost of mold is usually high and most of the molds are non-durable due to their short life time (Callister, 2007).

### 3.7.3 Isostatic pressing

Isostatic pressing involves the compaction of powder by application of uniform pressures in all directions. During the isostatic pressing process, a mold is initially filled with powder. Then, the mold is subjected to high and uniform pressures transmitted through pressure medium in a pressure vessel. The mold would deform as the pressure is applied and it would return to its original form when the pressure is released (Segal, 1989). Similar to uniaxial pressing, sintering operation is required after the pressing operation (Callister, 2007).

Isostatic pressing can be classified into two categories, which are hot isostatic pressing and cold isostatic pressing. By comparison, hot isostatic pressing is usually performed at high temperature and argon is used as its pressure medium (Chattopadhyay, 2004). Meanwhile, cold isostatic pressing is normally conducted at room temperature and liquid such as water or oil is often used as its pressure medium (DIANE, 1993). The costs of equipments and processing of hot isostatic pressing is significantly higher than those for cold isostatic pressing (Franklin and Wang, 1976).

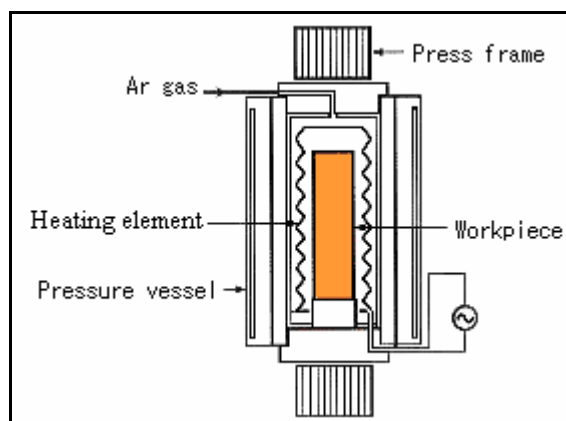


**Figure 3.9: Hot Isostatic Pressing (Franklin and Wang, 1976).**

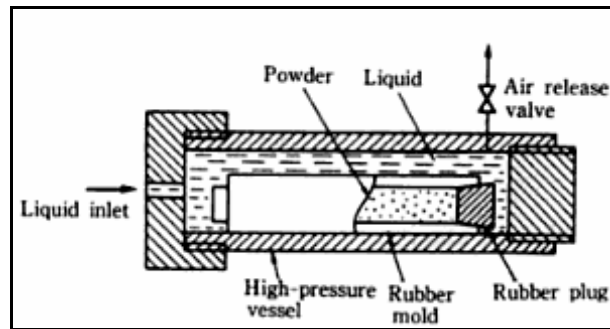


**Figure 3.10: Cold Isostatic Pressing (Mitsue Koizumi et al., 1991).**

If compared with uniaxial pressing, isostatic pressing could produce parts with more complicated shapes since there is no geometry constraints imposed by the hard tooling (Callister, 2007). Besides, isostatic pressing could yield green compacts with higher and more uniform density (Segal, 1989). By using isostatic pressing, fine and homogeneous microstructure of initial powders could be preserved and fabrication of large powdered compacts is possible (Zavaliangos et al., 2001). However, the isostatic pressing is more time consuming and expensive (Callister, 2007). Moreover, it is difficult to achieve good dimensional accuracy of samples in isostatic pressing due to the flexible mold (Groover, 2010).



### 3.8 Sintering Approach

#### 3.8.1 Pressureless sintering

Pressureless sintering involves no application of pressure throughout the entire heating process. Therefore, pressureless sintering requires less cost and energy if compared with other sintering approaches. It can be divided into two categories which are conventional and two-step sintering.

Conventional or single-step sintering involves constant heating rate cycle with a dwell time at the sintering temperature (Maca et al., 2010). Typically, the sample's surface is first heated and the heat would flow inwards to the core of the sample through conduction process. As a result, this leads to a temperature gradient from the surface to the inner region of the sample. In other words, the surface of the sample would have higher temperature than the core of the sample. The variation in temperature can lead to poor microstructural characteristics of the sample (Oghbaei et al., 2010).

Slower heating rate cycle is usually applied to prevent thermal gradient within the sample at high sintering temperatures. However, slower heating rate cycle tends to increase the overall sintering time and thus, leads to grain coarsening. Meanwhile, high heating rates cycle would contribute to the thermal gradient within the sample and hence, lead to sample distortion and inhomogeneous microstructure (Oghbaei et al., 2010).

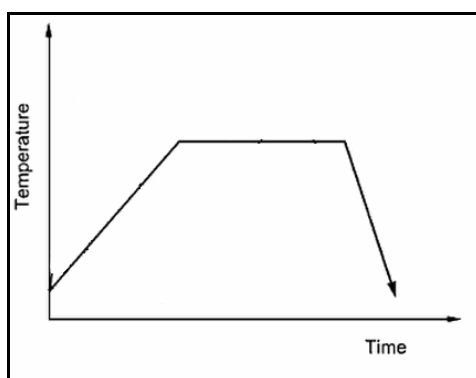


**Figure 3.11: Temperature Profile of Conventional Sintering (Oghbaei et al., 2010).**

As shown in the figure below, there are two different patterns of temperature profile for two-step sintering. For the first pattern, samples are first heated and maintained at a relatively low temperature in which surface diffusion predominates. Then, the samples are heated to a higher temperature for densification purpose (Hosokawa, 2007). For the second pattern, samples are initially heated to a high temperature through constant-heating-rate sintering so that initial high relative density could be achieved. After that, the samples are cooled rapidly to a lower temperature and then isothermal sintering is carried out for a long period of time in order to increase the density without significant grain growth and avoid the surface diffusion (Wang et al., 2009).

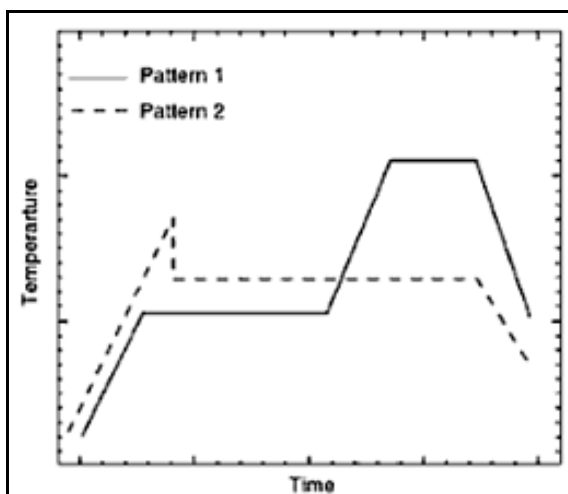


**Figure 3.12: Temperature Profile of Two-Step Sintering (Wang et al., 2009).**

The second type of two-step sintering is normally used to constrain the grain growth of sub-micron alumina powder. For instance, growth ratio or the ratio of final grain size to initial particle size could be reduced successfully by applying two-step sintering with suitable temperatures (Wang et al., 2009). By comparison, two-step sintering could cause a significant decrease of grain size down to 500 nm while conventional sintering only could produce a full dense structure with grain size ranges between 1 and 2  $\mu\text{m}$  (Hesabi et al, 2009). Two-step sintering could yield a sample with higher density but smaller grains if compared to the single-step sintering (Chen et al., 2000).

### 3.8.2 Spark plasma sintering

Spark plasma sintering is one of the non-conventional sintering approaches, which is also named as pulse electric current sintering, plasma-activated sintering, electric pulse assisted consolidation or field-assisted sintering (Zhou et al., 2003). The advantage of this sintering approach is its ability of achieving exclusively high heating rate, which is essential for improving densification and constraining grain growth (Harmer et al., 1981). Besides, this approach could attain full densification of ceramics at relatively low sintering temperature within a short period of time (Guo and Tuan, 2004).

During conventional sintering, smaller particle size of starting powder results in larger densification and grain growth rates (Kingery, 1975). This is similar when the alumina specimens are heated to high temperature under spark plasma sintering condition. Specimens with higher heating rates would achieve higher densities at the early stage of the spark plasma sintering process. Moreover, the effect of fast heating on reducing the grain growth rate would be greater when the starting powder was finer (Zhou et al., 2003).

The main drawback of spark plasma sintering is the microstructure of the sintered body is usually non-uniform. Furthermore, vapour deposits are often observed after this sintering process (Guo and Tuan, 2004).

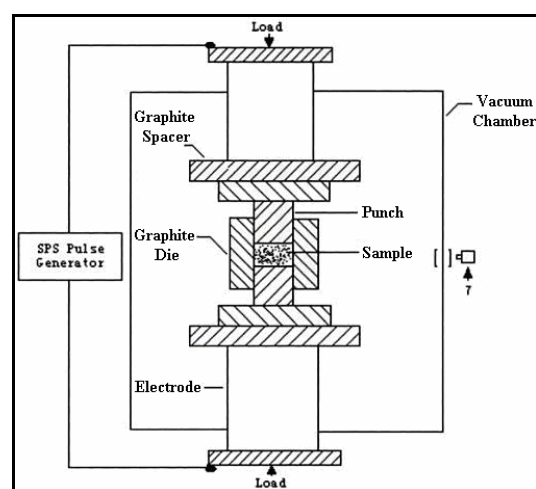


**Figure 3.13: Schematic Diagram of Spark Plasma Sintering (Guo and Tuan, 2004).**

### 3.8.3 Microwave sintering

Unlike conventional sintering, microwave sintering possesses the characteristics of uniform heating on a macroscopic scale and rapid heating rates. Microwave sintering involves the internal heating of a ceramic material volume. Moreover, the microwave sintering furnace is easily modified to operate under different atmospheric environment and pressures. The cooling time required by the microwave sintering furnace is usually negligible (Bengisu, 2001). The microwave sintering is an effective and energy saving processing method (Ohji et al, 2009).

The microwave-sintered samples usually have better microstructures due to the penetrating action of microwaves and shorter sintering time required (Bengisu, 2001). Microwave sintering could achieve higher increment of alumina relative density if compared to conventional sintering. Moreover, the relative density of alumina under microwave sintering is always higher than that for conventional sintering (Fang et al., 2003). Also, microwave sintering could achieve higher densification rates if compared to conventional sintering. From the research, microwave sintering could lead to significant reduction in sintering temperatures and improvement in the diffusion coefficients for alumina sintering (Cheng et al., 1992).

The main shortcoming is the occurrence of local thermal runaway, melting or cracking during rapid heating as the microwave absorption coefficient of many ceramics increases exponentially with temperature (Bengisu, 2001).

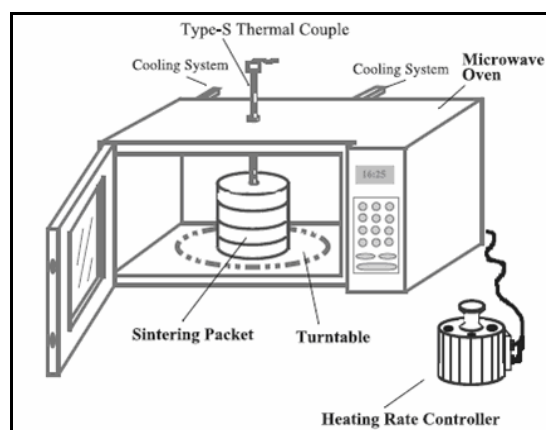


**Figure 3.14: Schematic Diagram of Microwave Sintering (Bengisu, 2001).**

### 3.9 Various types of additives

#### 3.9.1 Niobium oxide

The effects of niobium oxide on the densification and microstructural development of alumina were investigated by the research done by Hsu et al. (2007). In the experiment,  $\alpha$ -alumina powder with an average particle size of 100 nm was used as the starting powder while various amounts of niobium oxide,  $\text{Nb}_2\text{O}_5$ , ranging from 0 to 0.5 mol% were used as the additives. The samples were compressed by uniaxial pressing under 74 MPa and then sintered at temperatures, ranging from 1200 to 1450 °C for various period of time.

According to the experimental results, niobium oxide was good in enhancing the densification of alumina with lower sintering temperature and shorter sintering time. These effects could be reinforced as the amount of niobium oxide increased. For instance, the alumina sample doped with 0.5 mol% of niobium oxide had relative density of about 97%, which was higher than the 82% relative density of the pure alumina sample, at the sintering temperature of 1350°C. However, the addition of niobium oxide would promote the grain growth and the grain growth rate of alumina would increase slightly as the amount of niobium oxide increased. The relative densities and average grain sizes of all samples would increase as the sintering temperature and period increased (Hsu et al., 2007).

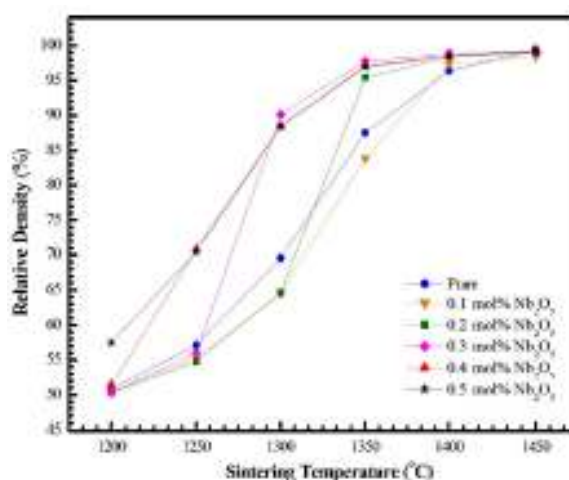


**Figure 3.15: Relative Density as a Function of Sintering Temperature for Various Compositions of Alumina Ceramic (Hsu et al., 2007).**

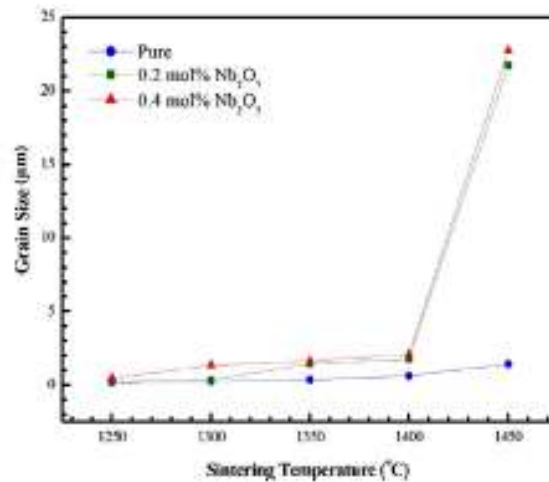


**Figure 3.16: Grain Size as a Function of Sintering Temperature for Various Compositions of Alumina Ceramics (Hsu et al., 2007).**

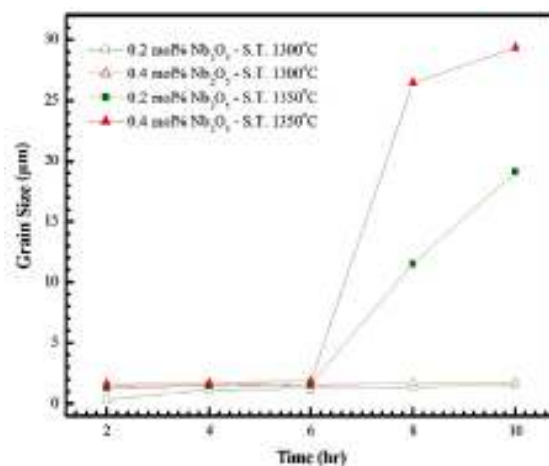


**Figure 3.17: Grain Size as a Function of Sintering Time for Various Compositions of Alumina Ceramic (Hsu et al., 2007)**

### 3.9.2 Titanium oxide

The influence of titanium oxide, TiO<sub>2</sub> on the density, microstructure and mechanical properties of alumina was studied by Sathiyakumar et al. (2002). In the experiment, the sol-gel derived alumina was used as the starting material while various amounts of titanium oxide, ranging from 0 to 4.0 wt% were used as the dopants. The mixed

powders were compressed uniaxially and sintered at various temperatures, ranging from 1400 to 1600 °C for 3 hours of sintering period.

Through the experiment, titanium oxide was found to be effective in improving the densification of alumina and the relative densities increased as the amount of titanium oxide increased. For instance, 98% of theoretical density could be achieved by alumina specimen doped with 0.2 wt% of titanium oxide sintered at lower temperature, which was 1400°C. Meanwhile, pure alumina specimen could only attain 96% of theoretical density even though the sintering temperature was increased to 1500°C (Sathiyakumar et al., 2002).

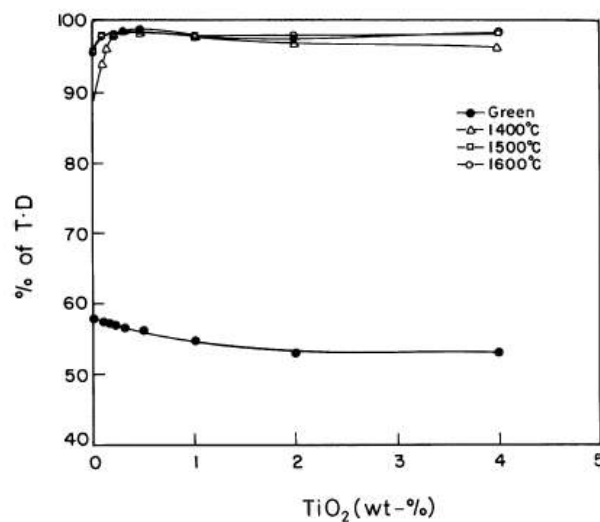


**Figure 3.18: Effect of Sintering Temperature on Sintered Density of TiO<sub>2</sub> doped Alumina Ceramics (Sathiyakumar et al., 2002).**

Grain growth was accelerated as the amount of titanium oxide increased from 0 to 0.2 wt% and reduced when the amount of titanium oxide raised from 0.2 to 4.0 wt% due to the formation of secondary phase or aluminium titanate, Al<sub>2</sub>TiO<sub>5</sub> which inhibited the grain growth of alumina. Addition of titanium oxide could improve the flexural strength of pure alumina, which was below 300 MPa. Nonetheless, maximum flexural strength, 409 MPa could be achieved with addition of 0.2 wt% of titanium oxide at sintering temperature of 1400 °C (Sathiyakumar et al., 2002).

### 3.9.3 Zirconium oxide

Wang et al. (2009) had discussed about the effects of zirconium oxide,  $ZrO_2$  or zirconia in affecting the sintering temperatures and microstructure of alumina through their works. In the experiment, the as-received  $\alpha$ -alumina powder with an average particle size of 150 nm and 5 wt% of zirconia content was used as the starting powder. The powder was uniaxially pressed at 150 MPa and heated by using two-step sintering with the temperatures of first step and second step sintering were varied at the range of 1400 to 1450 °C and 1300 to 1400°C respectively.

According to the research of Bodišová et al. (2007), a smaller grain growth from 0.47 to 0.62  $\mu\text{m}$  could be obtained for alumina sample doped with 5 wt% of zirconia. This is owing to zirconia provides a pinning effect to the grain growth of alumina (Wang et al., 2009).

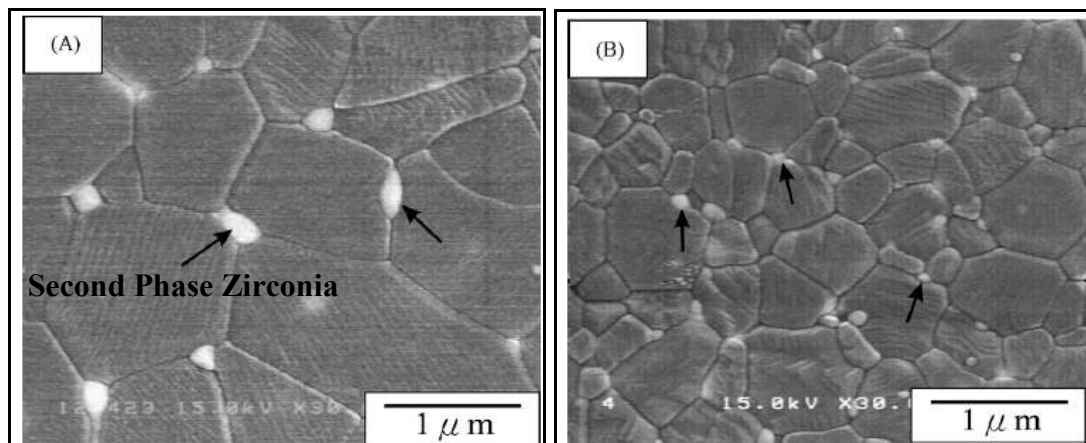


**Figure 3.19: Microstructures of Full Dense Alumina prepared by (A) Constant Heating Rate Sintering (1600 °C/0 h) and (B) Two-Step Sintering (T1 = 1450 °C, T2 = 1350 °C/12 h) (Wang et al., 2009).**



### 3.9.4 Magnesium oxide

The effects of magnesia or magnesium oxide, MgO on the densification and grain growth of pure alumina and alumina with various amounts of calcium oxide, CaO additives were analyzed in the research of Bae et al. (1994). During the experiment, ultrapure  $\alpha$ -alumina powder was used as the starting powder while various amounts of magnesium oxide and calcium oxide were used as the additives. The well mixed powders were compressed at 196.2 MPa by cold isostatic pressing and the compacts were sintered at 1900 °C for 1 hour under pressureless sintering.

According to their findings, minimum amount of magnesium oxide required to prevent the abnormal grain growth was linearly dependent to the concentration of calcium oxide. Besides, the addition of magnesium oxide to ultrapure alumina would enhance the grain growth and the increment in the amount of magnesium oxide would lead to linear increase in the average grain sizes of alumina. However, Bennison et al. (1983) concluded that magnesium oxide was effective in reducing the grain growth rate of commercial alumina with a purity level more than 99.99%. Based on the explanation of Bae et al. (1994), there might be still existence or presence of minor impurities within the commercial alumina of such purity level if compared to the ultrapure alumina used in this experiment.

Besides, the addition of magnesium oxide alone would improve the densification of ultrapure alumina during the pressureless sintering. For instance, 96.0% of relative density could be achieved by the ultrapure alumina with 200 ppm of magnesium oxide additives. While the ultrapure alumina with 200 ppm of calcium oxide additives could only achieve less than 90.0% of relative density at the same sintering temperature and period (Bae et al., 1994).

### 3.9.5 Manganese (II) oxide, MnO

The influences of manganese oxide, MnO on the density, microstructure and mechanical properties of alumina were studied by Sathiyakumar et al. (2002). In the research, various concentrations of manganese oxide, ranging from 0.1 to 3.0 wt. % were used as the additives. The mixed powders were compressed by uniaxial pressing and then sintered at temperatures between 1400 to 1600 °C for 3 hours.

Meanwhile, Keski et al. (1965) focused on examining the effects of manganese oxide on the sintering of alumina. In the experiment, starting powders with particle sizes ranging from 18 to 22  $\mu\text{m}$  and compositions of 99.8 wt.%  $\text{Al}_2\text{O}_3$ , 0.01 to 0.05 wt.%  $\text{Fe}_2\text{O}_3$ , 0.01 to 0.05 wt.%  $\text{SiO}_2$  and 0.01 to 0.08 wt.%  $\text{Na}_2\text{O}$  were used. Moreover, various amounts of manganese oxide, ranging from 0.1 to 1.0 wt% were used as the additives. The mixed powders were compressed uniaxially at 103 MPa and then, the compacts were sintered at temperatures between 1400 to 1550 °C.

The experimental results of Sathiyakumar et al. (2001) showed that 98.5% of theoretical density could be achieved by pure alumina while the doped samples which were sintered at 1550 °C for 3 hours, reached about 98 to 99% of the theoretical density. While the research of Keski et al. (1965) showed that a small amount of manganese oxide could improve the densification rate of alumina. Based on the shrinkage data, the sintering rate accelerated to a maximum value as the concentration of manganese oxide increased from 0 to 0.3 wt.% and then decreased as the concentration of manganese oxide increased more than 0.3 wt.%. The decrement was believed to be caused by the formation of a secondary phase. The addition of manganese oxide within a certain limits would increase the sintering rate of alumina but the activation energy would not change markedly. For instance, the activation energy of 140 kcal/mole was measured for both pure and doped samples.

By comparing the micrographs of samples sintered at 1550 °C, homogeneous grain growth with a few isolated pores was observed in the pure alumina while the addition of 0.1 wt. % manganese oxide would lead to inhomogeneous grain growth in which finer grains were surrounded by larger or coarser grains. As the concentration of manganese oxide increased up to 0.5 wt. %, significant grain

growths with grains as large as 20 to 100  $\mu\text{m}$  and considerable amount of intergranular and intragranular pores were observed. The presence of pores was unavoidable when manganese oxide was used as the additive and the amount of pores increased as the concentration of manganese oxide in the alumina increased (Sathiyakumar, 2002).

Besides, there was no secondary phase formation between the grains for alumina samples with 0.1 to 0.5 wt. % manganese oxide addition, which were sintered at 1550 to 1600  $^{\circ}\text{C}$ . The absence of secondary phase formation between the grains indicated that the volume or grain boundary diffusion mechanism acts as the controlling process during the later stages of densification. Meanwhile, at sintering temperature of 1550  $^{\circ}\text{C}$ , the addition of 1.5 wt. % manganese oxide to alumina would lead to the formation of secondary intergranular phase in the form of continuous layer and irregular shapes (Sathiyakumar, 2002).

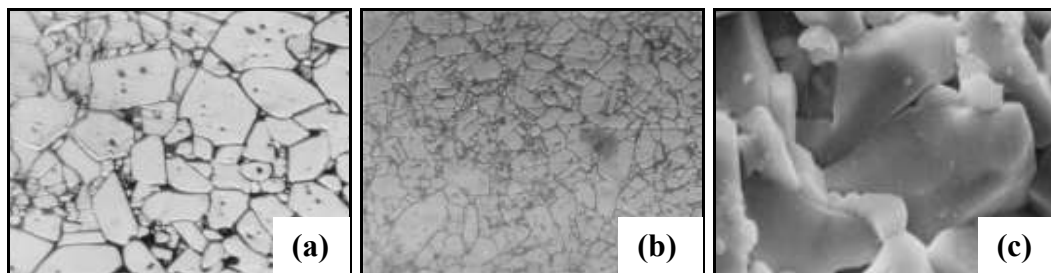


**Figure 3.20: Micrographs of Alumina Sintered at 1550  $^{\circ}\text{C}$ , (a) Pure or 0 wt. %, (b) 0.1 wt. %, (c) 1.5 wt. % Manganese Oxide (Sathiyakumar, 2002).**

For samples sintered at 1550  $^{\circ}\text{C}$ , there was a slight decrease in the hardness value as the concentration of manganese oxide increased up to 0.5 wt.%. After that, the hardness value increased with the increasing concentration of manganese oxide and reached a maximum value of 23 GPa when the concentration of manganese oxide was 3.0 wt. %. This might be attributed to the formation of a secondary intergranular phase in the form of continuous layers as the concentration of manganese oxide increased from 1.5 to 3.0 wt. %. A similar behaviour was also observed for the flexural strength of the alumina samples with various concentrations of manganese oxide (Sathiyakumar, 2002).

### 3.9.6 Manganese (IV) oxide, MnO<sub>2</sub>

The effects of minor amounts of manganese (IV) oxide, MnO<sub>2</sub> addition on the sintering behavior, microstructural development and mechanical properties of alumina were researched by C. Toy et al. (1995). In this study, various amounts of MnO<sub>2</sub>, varying from 0.1 to 0.5 % was mixed with AlCOA A-16SG grade alumina powder via colloidal method. Both doped and undoped powders were consolidated uniaxially under 100 MPa. After that, all samples were sintered at 1550, 1600 and 1650 °C for 1 hour with heating rate of 5 °C/min (Toy et al., 1995).

In the interim, similar topic was also investigated by Erkalfa et al. (1995). In this research, colloidal method was also used to mix the AlCOA A-16SG grade alumina powder with varying amounts of MnO<sub>2</sub>, ranging between 0, 0.1, 0.3, 0.5, 1.0, 1.5 and 3.0 wt%. Similar to previous research, uniaxial pressing was applied to all samples at 100 MPa. Subsequently, compositions with 0.1, 0.3 and 0.5 wt% MnO<sub>2</sub> were sintered at 1550, 1600 and 1650 °C for 1 hour. Meanwhile the compositions with 0.5, 1.0 and 1.5 wt% MnO<sub>2</sub> were sintered at 1550 °C for 2 hours after these samples were further isostatically cold pressed at 300 MPa. The undoped and composition with 3 wt% MnO<sub>2</sub> were sintered at temperatures ranging from 1250 to 1650 °C for 1 hour with a heating rate of 5-10 °C/min (Erkalfa et al, 1995).

Based on the result of Toy et al. (1995), full density can be achieved for undoped sample sintered at 1650 °C. However, addition of MnO<sub>2</sub> from 0 to 0.5 % would cause the relative density of the samples to drop from 100 to 98.5 %. This is owing to the increasing amount of MnO<sub>2</sub> addition would lead to higher amount of porosity under the same sintering temperature. Meanwhile, the experimental results of Erkalfa et al. (1995) showed that the addition of MnO<sub>2</sub> to alumina would improve the densification process if the sintering temperature was set to 1550 °C or lower. For instance, the relative densities of the samples increased from 89.9 % to 96.2 % when the concentration of MnO<sub>2</sub> was increased from 0 to 3 wt% and the sintering temperature was set to 1450° C. In fact, higher sintering temperature could eventually improve the relative density of alumina. But, it could also promote the grain-growth at the same instant, which was undesirable. As shown in the Table 3.4 below, sintering of samples with 3.0 wt% MnO<sub>2</sub> additions, up to 1450 °C indicates a

regular densification and grain growth behaviour. However, sample with same composition sintered at 1550°C exhibited abnormal grain-growth even though higher relative density could be attained (Erkalfa et al, 1995).

**Table 3.4: Relative Density and Grain Size of Alumina with 3.0 wt% MnO<sub>2</sub>.  
(Erkalfa et al., 1995)**

MnO <sub>2</sub> (wt. %)	Sintering Conditions	Relative Density (%)	Grain Size (μm)
3.0	1250 °C, 1h	73.0	0.51
	1350 °C, 1h	86.3	0.84
	1450 °C, 1 h	96.2	1.34
	1550 °C, 1 h	98.7	13.84

From the micrographs, fairly homogeneous grain-growth with a small amount of intergranular pores could be observed in those undoped samples sintered at higher temperatures wherein the average grain size increased from 1.38 to 3.05 μm as the sintering temperature was raised from 1550 to 1650 °C. Conversely, more intensive and inhomogeneous grain-growth with a large number of intragranular pores could be observed in those doped samples sintered at higher temperatures. For instance, the average grain sizes of the samples with 0.5 % of manganese addition were found to increase from 9.5 to 30 μm as the sintering temperature was increased from 1550 to 1650 °C (Toy et al., 1995). MnO<sub>2</sub> was found to promote the grain growth of the alumina. As a proof, the average grain size of the alumina would increase from 1.48 to 13.48 μm as the concentration of MnO<sub>2</sub> addition was increased from 0 to 3 wt% for samples sintered at 1550 °C (Erkalfa et al., 1995).

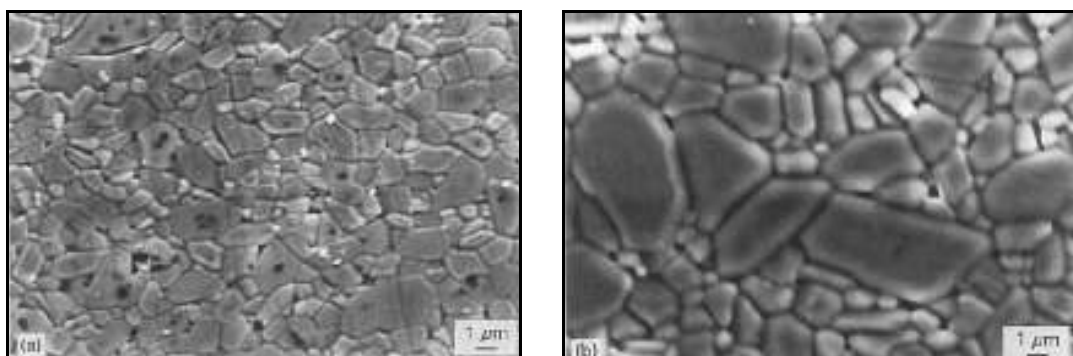


**Figure 3.21: Micrographs of Undoped Alumina Samples after Sintering at  
(a) 1550 °C, (b) 1650 °C (Toy et al., 1995).**

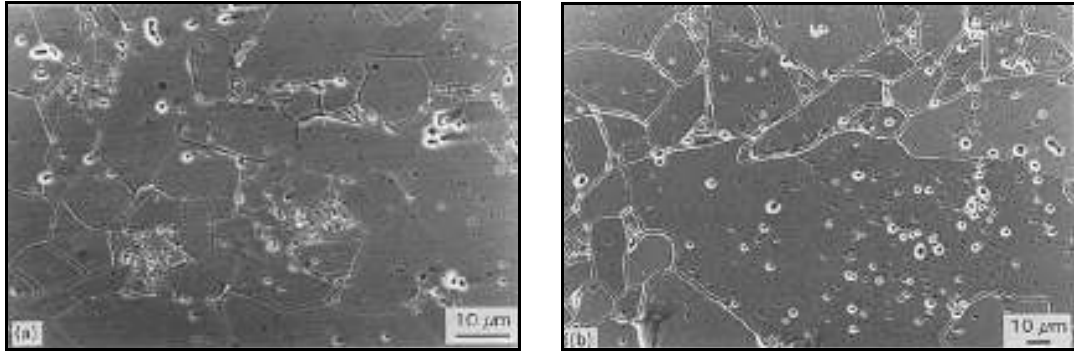


**Figure 3.22: Micrographs of Alumina with 0.5% Manganese addition after Sintering at (a) 1550 °C, (b) 1650 °C (Toy et al., 1995)**

Besides, there was no secondary phase formation between the grains within the limits of this study up to 0.5 % of manganese additions (Toy et al, 1995). However, secondary phase was detected in those samples doped with 0.5 to 1.5 wt%  $\text{MnO}_2$ , sintered at 1550 °C for 2 hours. Based on these observations, the composition and sintering conditions during the later stages of densification act as the primary factors that contribute to the presence of secondary phase. Moreover, according to the phase diagram, the minimum temperature for the secondary phase to exist in the alumina is 1520 °C. From the micrographs, the  $\text{MnO}_2$ -rich secondary phase seems to be squeezed out of the grain boundaries in needle-like shapes. This phenomenon had justified the conclusion that a eutectic liquid phase formed between the grains (Erkalfa et al., 1995).

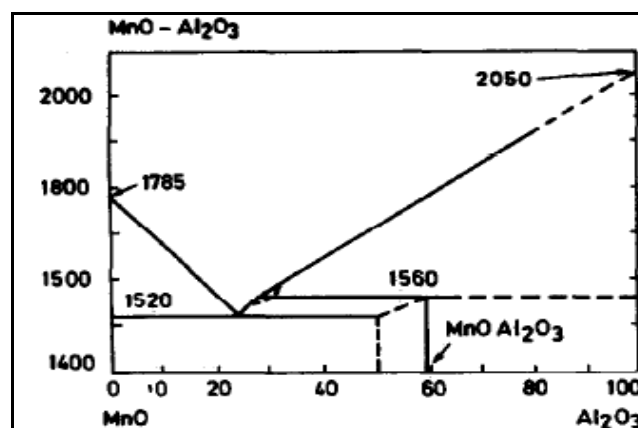


**Figure 3.23: The Phase Diagram of  $\text{MnO-Al}_2\text{O}_3$  System (Erkalfa et al., 1995).**

Regardless of the dopant portion, the hardness of the samples would increase as the sintering temperature was raised. Moreover, the addition of  $\text{MnO}_2$  would cause the hardness of the alumina to decrease. For example, the microhardness values of alumina would decrease slightly from 20.29 to 19.53 GPa as the concentration of  $\text{MnO}_2$  increased from 0 up to 0.5 % at 1650 °C (Toy et al., 1995). However, the hardness of the alumina would recover and keep increasing when the addition of  $\text{MnO}_2$  was more than 0.5 wt%. For instance, at sintering temperature of 1550 °C, the hardness of the alumina decreased from 18.98 to 18.30 GPa as the addition of  $\text{MnO}_2$  was raised from 0 to 0.5 wt% and it bounced to 24.8 GPa when the composition of  $\text{MnO}_2$  was increased to 3 wt% (Erkalfa et al., 1995).

There was no certain relationship between the strength of alumina and the concentration of  $\text{MnO}_2$ . This was because there was a trend of strength reduction for samples sintered at 1550 and 1600 °C, but there was an increment in the strength when the concentration of  $\text{MnO}_2$  was in the range of 0.3 to 0.5 % at 1650 °C (Toy et al., 1995). By comparison, the sample that did not go through cold isostatic pressing process would have lower strength, which was about 200 MPa. While the sample that was further cold isostatically pressed, owned a strength value of 439 MPa even though both samples were doped with equal amount of  $\text{MnO}_2$ , which was 0.5 wt% (Erkalfa et al., 1995).

## CHAPTER 4

### METHODOLOGY

#### 4.1 Introduction

In this chapter, some standard experimental equipments and techniques which would be used throughout the entire alumina research work, are discussed in details. At the same time, experimental procedures of specific techniques would also be explained with the aid of some diagrams or tables.

#### 4.2 Powder Preparation

During the experiment, the as received commercially available materials which are 99.5% pure alumina (NanoAmor, USA) and 99.0% pure manganese (IV) oxide,  $\text{MnO}_2$  powders are used as the starting powders. The chemical compositions and properties of these powders are summarized in Table 4.1 and Table 4.2. Five different amounts of  $\text{MnO}_2$  powder, ranging from 0, 0.5, 1.5, 3.0 and 5.0 wt% are used as the additives for the pure alumina powder through a process involving ultrasonification and ball milling.

The  $\text{MnO}_2$  and  $\text{Al}_2\text{O}_3$  powders were measured according to the composition required and poured into a beaker containing 200 ml of ethanol. The solution was then subject to ultrasonic pulses at 28 – 34 kHz for half an hour to enhance the dispersion and homogeneity of  $\text{MnO}_2$  in the  $\text{Al}_2\text{O}_3$  powder. The mixture was then



poured into a bottle with high density polyethelene (HDPE) followed by zirconia's ball milling process for at least 1 hour. Sieve was used to separate the milling balls from the slurry. The slurry was put into the oven for drying over night at 60°C so that ethanol could be removed via evaporation process. The dried cake subsequently was crushed and sieved through a 212  $\mu\text{m}$  mesh stainless steel sieve to obtain ready-to-press powders.

**Table 4.1: Characteristics of the Starting Pure Alumina,  $\text{Al}_2\text{O}_3$  Powder.**

Chemical composition	$\text{Al}_2\text{O}_3$	Unit
Aluminium dioxide ( $\text{Al}_2\text{O}_3$ )	99.50	wt%
Magnesium oxide (MgO)	0.001	wt%
Silicon dioxide ( $\text{SiO}_2$ )	0.05	wt%
Iron oxide ( $\text{Fe}_2\text{O}_3$ )	0.3	wt%
Titanium dioxide ( $\text{TiO}_2$ )	-	wt%
Manganese oxide ( $\text{MnO}_2$ )	-	wt%
Mean particle size	27	nm
Theoretical density	3.98	$\text{g/cm}^3$

**Table 4.2: Characteristics of the Doping manganese oxide,  $\text{MnO}_2$  Powder.**

Chemical composition	$\text{MnO}_2$	Unit
Manganese oxide ( $\text{MnO}_2$ )	99.0	%
Barium (Ba)	0.0002	%
Calcium (Ca)	0.01	%
Cadmium (Cd)	0.0003	%
Niobium (Nb)	0.07	%
Phosphorous (P)	0.27	%
Plumbum (Pb)	0.006	%
Strontium (Sr)	0.0002	%
Zirconium (Zr)	0.019	%
Mean particle size	5.0	nm
Theoretical density	3.9	$\text{g/cm}^3$

### 4.3 Green Body Preparation

The pure alumina and well-mixed powders were compressed uniaxially at about 2.5 MPa into disc (20 mm diameter x 5 mm thickness) and rectangular bars (32 x 13 x 6) mm. For each powder composition, one disc (each weighing 2.5 g) and one bar (weighing 2.5 g) were made. Then, the green compacts were marked by using the sample identification codes shown in Table 4.3. The samples subsequently were compressed again by using cold isostatic pressing at 200 MPa. This step is performed in order to ensure homogeneous compaction, induce uniform shrinkage and ultimately improve densification.

**Table 4.3: Sample Identification Codes Employed in Present Study.**

MnO <sub>2</sub> (wt. %)	Sintering Temperature		
	1250°C	1350°C	1450°C
0	A1	A2	A3
0.5	F1	F2	F3
1.5	G1	G2	G3
3.0	H1	H2	H3
5.0	I1	I2	I3

### 4.4 Sintering

The pressureless sintering was applied to the green bodies under ambient condition, using a standard rapid heating furnace, at various temperatures ranging from 1250°C to 1450°C. Sintering profile of 10°C/min. ramp rate and 1 hour of soaking time were employed for all samples.

#### 4.5 Grinding and Polishing

The sintered disc samples were firstly ground by various grade of SiC papers range from 120, 240, 600, 800 and 1200 successively. Polishing was done with 6  $\mu\text{m}$  and 1  $\mu\text{m}$  diamond paste on the samples to achieve a fine surface finish prior to Vickers hardness testing, XRD and SEM evaluation.

#### 4.6 Bulk Density Measurement

The bulk densities of dense compacts (low porosity) were measured by employing the water immersion technique based on the Archimedes principle. Distilled water was used as the immersion medium in this measurement.

Nonetheless, special attention was needed when measuring the low density samples (high porosity) in the water. The measurement could only be taken when the reading from the balance is constant so that water could penetrate the pores completely. The excess weight of the water in the pore was taken out from the calculation in order to avoid from overestimating the density of the samples. The relative density was calculated by taking the theoretical density of alumina as 3.98  $\text{Mgm}^{-3}$ . The bulk density ( $\rho$ ) of the samples was calculated by using equation (4.1).

$$\rho = \frac{W_a}{W_a - W_w} \rho_w \quad (4.1)$$

Where

$\rho$  = Bulk density of the sample

$W_a$  = Weight of the sample in air

$W_w$  = Weight of the sample in water and

$\rho_w$  = Density of the distilled water which vary with temperature

#### 4.7 Young's Modulus Determination

The sonic resonance technique was used to measure the Young's modulus of the rectangular samples by a commercial testing instrument. The vibrations were physically induced in the samples by tapping and the resonant frequency of the samples was measured by monitoring and evaluating the vibration harmonics of the samples by a transducer. The Young's modulus is calculated based on the standard test method (ASTM E1876-97). The Young's modulus (E) is computed by using equation (4.2):

$$E = 0.9465 \left( \frac{m F_f^2}{b} \right) \left( \frac{L}{t} \right)^3 T_1 \quad (4.2)$$

where

- E = Young's Modulus (Pa)
- m = mass of the rectangular bar (g)
- b = width of the bar (mm)
- L = length of the bar (mm)
- t = thickness of the bar (mm)
- $F_f$  = fundamental resonant frequency of bar in flexure, (Hz)
- $T_1$  = correction factor for fundamental flexural mode to account for finite thickness of bar, Poisson's ratio etc., calculated using equation (4.3)

$$T_1 = 1 + 6.585 \left( 1 + 0.0752\mu + 0.8109\mu^2 \right) \left( \frac{t}{L} \right)^2 - 0.868 \left( \frac{t}{L} \right)^4 - \frac{8.340 \left( 1 + 0.2023\mu + 2.173\mu^2 \right) \left( \frac{t}{L} \right)^4}{1 + 6.338 \left( 1 + 0.1408\mu + 1.536\mu^2 \right) \left( \frac{t}{L} \right)^2} \quad (4.3)$$

where

- $\mu$  = poisson's ratio which was taken as  $\mu = 0.23$  (Munro, 1997).

#### 4.8 Vickers Hardness Determination

The Vickers Hardness testing method was used to measure the hardness of the sintered alumina samples. The indentations were made by using a pyramidal diamond indenter with an applied load of 0.5 kg and 1.0 kg.

During the test, the load was applied slowly, without impact, and held for 10 seconds to create an impression. The physical quality of the indenter and the accuracy of the applied load as defined clearly in ASTM E384-99 and ISO 14705 must be always controlled in order to obtain accurate results. After the load was removed, the two impression diagonals,  $D_1$  and  $D_2$ , as shown in Fig. 4.1 were measured with a filar micrometer built in the attached microscope on the Vickers machine to the nearest  $0.1 \mu\text{m}$ , and then averaged. The Vickers hardness ( $H_v$ ) is calculated based on the surface area of the indent using equation (4.4):

$$H_v = \frac{1.854P}{(D)^2} \quad (4.4)$$

where

$P$  = applied load

$D$  = average diagonals =  $H_v = \frac{D_1 + D_2}{2}$

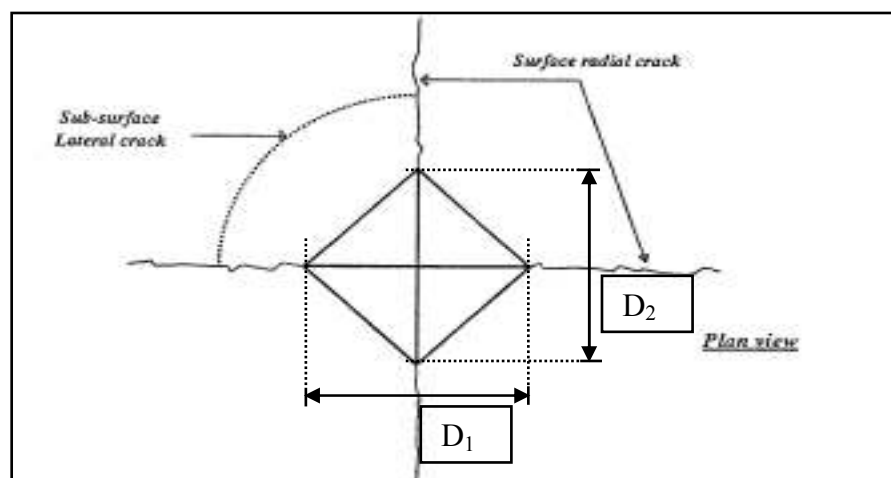


**Figure 4.1: Schematic Indentation Fracture Pattern of an Idealized Vickers Palmqvist Crack System.**

#### **4.9 Microstructure Examination**

The morphology of the starting powders and the microstructural evolution of the sintered samples were examined using a Hitachi scanning electron microscope (SEM). With SEM, the resolution of the sub-micron dimensional features on the surface of a material and the element composition of the samples were determined.

SEM focuses a small spot of electrons on the thick specimen with electrostatic or electromagnetic force and the samples were scanned in a series of line. Electrons emerging from the upper specimen surface are collected by an electron detector and used to produce an image on a T.V. monitor as a series of lines.

Before SEM analysis was performed, selected sintered samples were thermally etched at 50°C below the sintering temperature of the sample at a heating and cooling rate of 10°C/min, with a holding time of 30 minutes prior to cooling. Upon cooling down, the samples were coated with a gold palladium, which is a conductive layer to prevent charging in the microscope. This is to obtain a clearer microstructure especially the grain boundary.

The grain size of the alumina ceramics would be measured by using linear interpolation method.

#### **4.10 X-Ray Diffraction (XRD)**

X-Ray diffraction (XRD) provides information that relates to the crystal lattice of the material and the presence of crystalline phases. The information on the degree of crystallization and the orientation texture in the material could be determined by using XRD.

In the present work, the phases present in the powders as well as the sintered samples were determined at room temperature using X-Ray diffraction (Shimadzu X-

Ray Diffractometer, Japan) with Cu-K $\alpha$  as the radiation source using a scan speed and step scan of 0.5° /min and 0.02° respectively, at 35 kV and 15 mA.

The peaks obtained were compared to standard reference JCPDS-ICDD (Joint Committee of Powder Diffraction Standard – International Center for Diffraction Data) files for alumina (No. 10-0173), pyrolusite MnO<sub>2</sub> (No. 24-0735) and MnAl<sub>2</sub>O<sub>4</sub> (No. 29-0880).

## CHAPTER 5

### RESULTS AND DISCUSSIONS

#### 5.1 Bulk Density and Average Shrinkage

From the previous literature review, the research of Erkalfa et al. (1995) showed that the bulk or relative density of the alumina ceramics would increase as the sintering temperature was raised. By referring to Figure 5.1, similar trend could also be observed in the experimental results. For instance, the bulk density of the alumina ceramic doped with 5 wt. %  $\text{MnO}_2$  would increase from 3.655 to 3.788  $\text{g/cm}^3$  as the sintering temperature was raised from 1250 to 1450  $^\circ\text{C}$ .

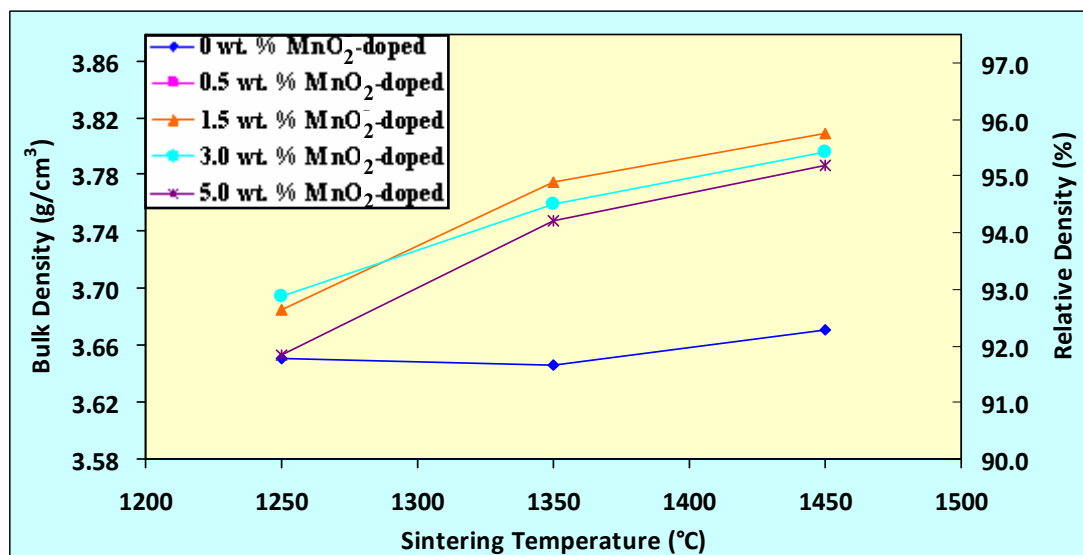
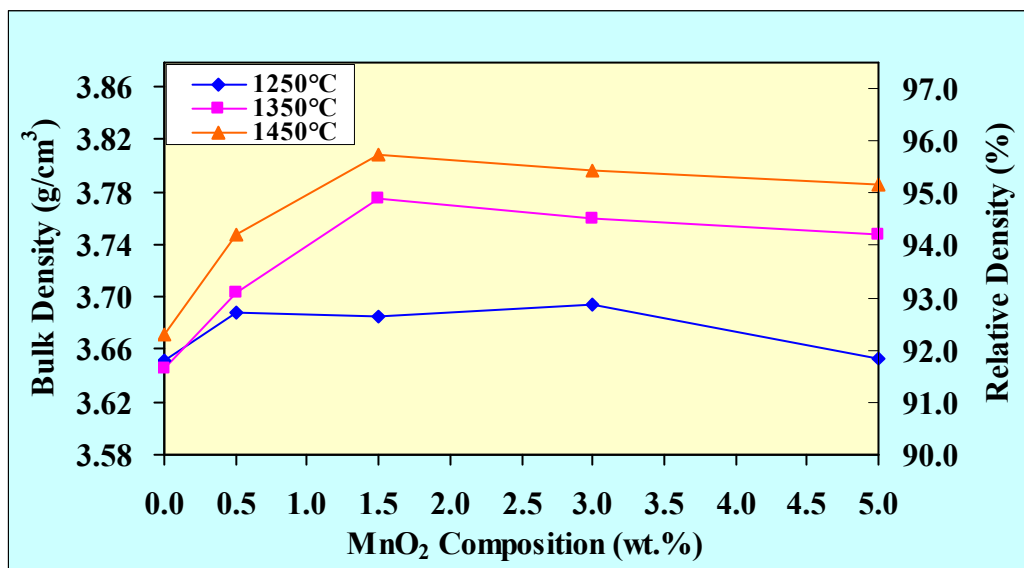


Figure 5.1: Graph of Bulk and Relative Density against Sintering Temperature for Various Concentration of  $\text{MnO}_2$  Addition



Based on Figure 5.2, the addition of  $\text{MnO}_2$  could indeed improve the bulk or relative density of the alumina ceramics as the sintering temperature was  $1450^\circ\text{C}$  or lower. This could be supported by the research done by Erkalfa et al. (1995) in which the relative density of the alumina samples would increase when the concentration of  $\text{MnO}_2$  addition was increased. Moreover, it could be observed that the addition of  $\text{MnO}_2$  from 0 wt. % up to certain concentration level would increase the relative density of the alumina ceramics. However, further addition of  $\text{MnO}_2$  could actually cause the relative density of the alumina ceramics to drop to a level, which would be still higher if compared to the relative density that could be achieved by the undoped sample at the same sintering temperature. For example, at the sintering temperature of  $1450^\circ\text{C}$ , the relative density of the alumina sample would increase from 92.29 to 95.75 % as the concentration of  $\text{MnO}_2$  addition was raised from 0 to 1.5 wt. %. Nonetheless, further addition of  $\text{MnO}_2$  up to 5 wt. % would cause a minor decline in the relative density of the alumina ceramics, which was from 95.75 to 95.18 %. But, it was still higher than the relative density of the undoped sample, which was 92.29 %. This might be due to the increasing amount of porosity in the alumina ceramics as the concentration of  $\text{MnO}_2$  addition was increased more than certain limit that could diminish its effect in enhancing the densification of alumina ceramics (Toy et al., 1995).



**Figure 5.2: Graph of Bulk and Relative Density against Concentration of  $\text{MnO}_2$  Addition for Various Sintering Temperature**

From the Figure 5.3, it could be observed that the experimental relative density of either undoped samples or samples doped with 3.0 wt. %  $\text{MnO}_2$  addition would be higher if compared with the results obtained by Erkalfa et al. (1995) regardless of the sintering temperature portion. This might be due to smaller particle size of the experimental major powder was used, which was  $0.027 \mu\text{m}$  if compared to the major powder used in the research of Erkalfa et al. (1995), which was  $0.37 \mu\text{m}$ . According to the research of Maca et al. (1995), it was held that the temperature for the alumina ceramics to reach certain level of relative density would increase as the particle size of the major powder increases. This could be clearly illustrated by the undoped sample of Erkalfa et al. (1995) in which the sintering temperature needed to be increased to  $1450^\circ \text{C}$  in order to attain 90 % of the relative density. On the other hand, the experimental undoped sample could achieve more than 90 % of the relative density when the sintering temperature was only  $1250^\circ \text{C}$ . Besides, the pores in the sample would become larger as the particle size of the major powder increases, which in turn would affect the relative density of the alumina ceramics negatively (Maca et al., 1995).

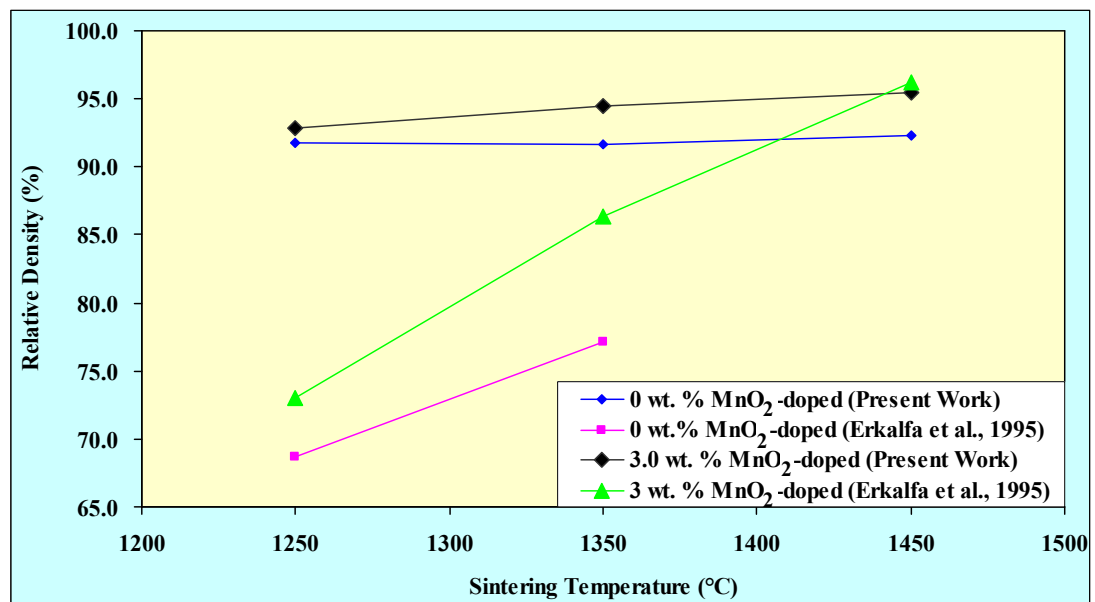


**Figure 5.3: Comparison of Relative Density between Experimental Result and Researcher's Result (Erkalfa et al., 1995).**

By referring to the graph shown in Figure 5.4, it could be observed that in general, the addition of  $\text{MnO}_2$  was found to be more effective in improving the density of the alumina ceramics if compared to  $\text{MgO}$ , which was usually doped into the alumina ceramics with minor amount in order to reduce the grain growth rate. For example, at the sintering temperature of  $1450^\circ\text{C}$ , the bulk density of the alumina samples which doped with  $\text{MgO}$  would increase from  $3.673$  to  $3.737$   $\text{g/cm}^3$  when the concentration of  $\text{MgO}$  addition was increased from  $0$  to  $1.5$  wt. %. However, further increment in the concentration of the  $\text{MgO}$  addition up to  $5$  wt. % would lead to drastic reduction in the bulk density of the alumina ceramics to a value of  $3.663$   $\text{g/cm}^3$ , which was lower than the bulk density of the undoped alumina sample. Similar trend could be observed on the alumina samples doped with  $\text{MnO}_2$  addition in which the bulk density of the alumina ceramic would increase initially from  $3.673$  to  $3.811$   $\text{g/cm}^3$  as the concentration of the  $\text{MnO}_2$  addition was raised from  $0$  to  $1.5$  wt. %. Further addition of  $\text{MnO}_2$  up to  $5$  wt. % would also lead to a reduction in the bulk density of the alumina ceramic to a value of  $3.788$   $\text{g/cm}^3$ , but it was still higher if compared to the bulk density of the undoped alumina ceramic.

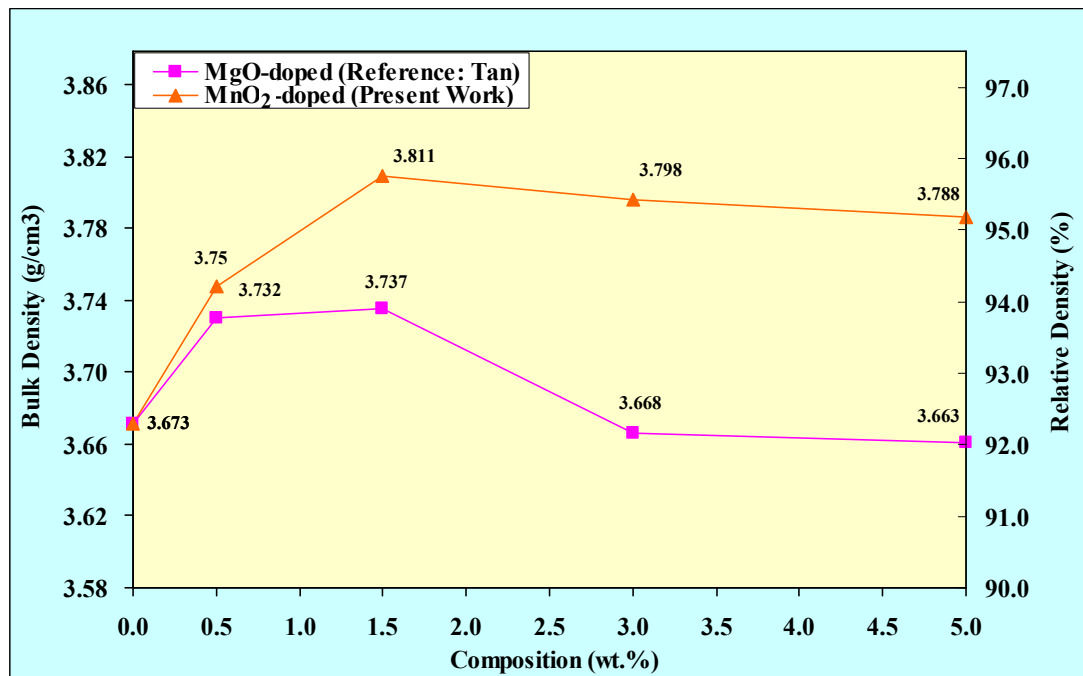


**Figure 5.4: Comparison of Bulk and Relative Density of Alumina Samples which were doped with  $\text{MnO}_2$  and  $\text{MgO}$  independently and sintered at  $1450^\circ\text{C}$**

From Figure 5.5, it is apparent that the average shrinkage of the samples would increase with the sintering temperature despite the concentration of  $\text{MnO}_2$  addition. Besides that, the average shrinkage would also raise with the concentration of  $\text{MnO}_2$  addition, which can be clearly illustrated in the Figure 5.6. In addition, the maximum average shrinkage that could be achieved by the samples was 25.35 % when the concentration of  $\text{MnO}_2$  addition was 5.0 wt. % and sintered at 1450 °C. Meanwhile, the minimum average shrinkage, which was about 5.10 %, was attained by undoped sample that was sintered at 1250 °C.

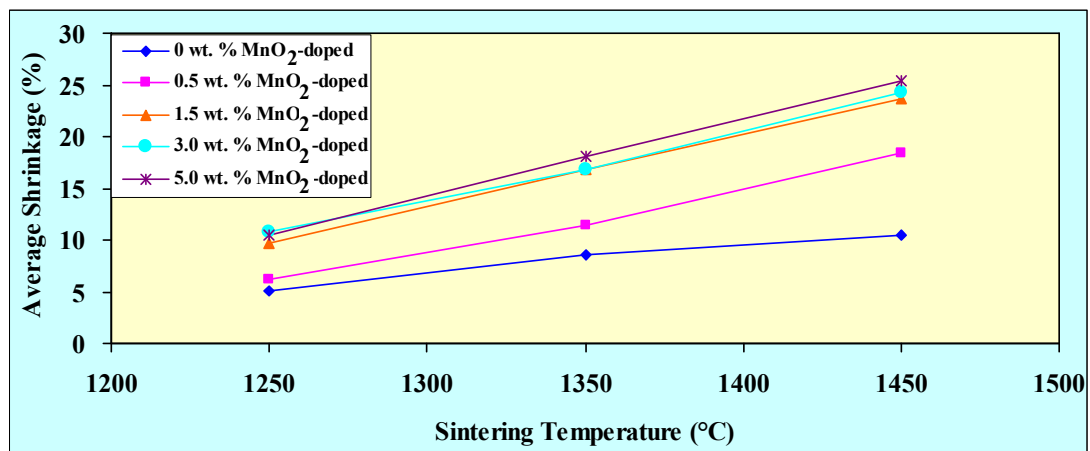


**Figure 5.5: Graph of Average Shrinkage against Sintering Temperature for Various Concentrations of  $\text{MnO}_2$  Addition**

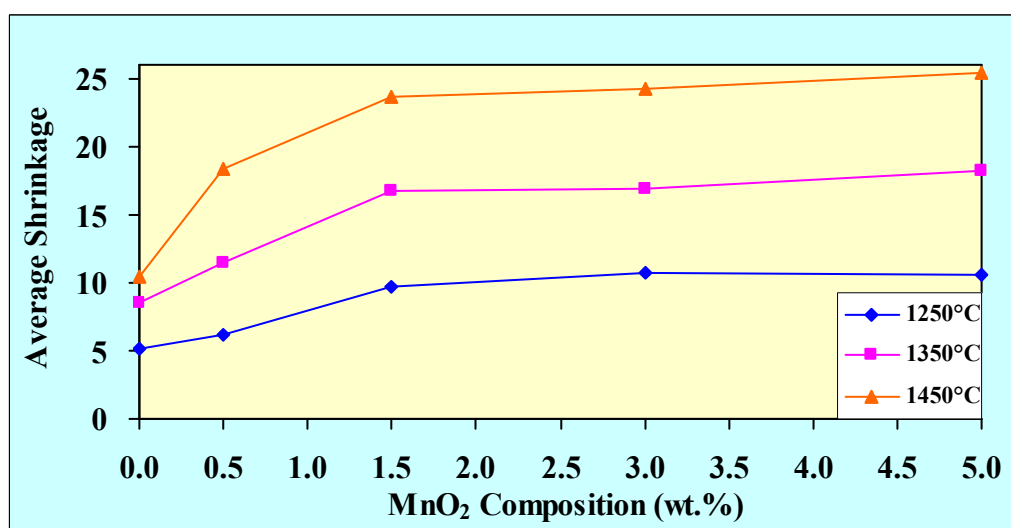


**Figure 5.6: Graph of Average Shrinkage against Concentrations of  $\text{MnO}_2$  Addition for Various Sintering Temperatures**

## 5.2 Young Modulus

From the Figure 5.7, the modulus of elasticity for various compositions of alumina samples would increase with the sintering temperature. As an evidence, the modulus of elasticity of alumina samples doped with 5.0 wt. % of  $\text{MnO}_2$ , would raise from 44.82 to 221.63 GPa as the sintering temperature increased from 1250 to 1450 °C. Similar circumstances also took place on the pure alumina samples, in which the modulus of elasticity of the pure alumina samples would increase from 21.55 to 49.43 GPa as the sintering temperature raised from 1250 to 1450 °C. Furthermore, if compared to the pure alumina samples, alumina samples which were doped with  $\text{MnO}_2$  would have higher increment in the modulus of elasticity as the sintering temperature was raised from 1250 to 1450 °C. For instance, the alumina samples with 3.0 wt. % of  $\text{MnO}_2$  addition would have the highest increment in the modulus of elasticity, which was about 202.42 GPa as the sintering temperature increased from 1250 to 1450 °C. Conversely, the pure alumina samples would have the lowest increment in the modulus of elasticity, which was only 27.88 GPa, at sintering temperature of 1250 °C.

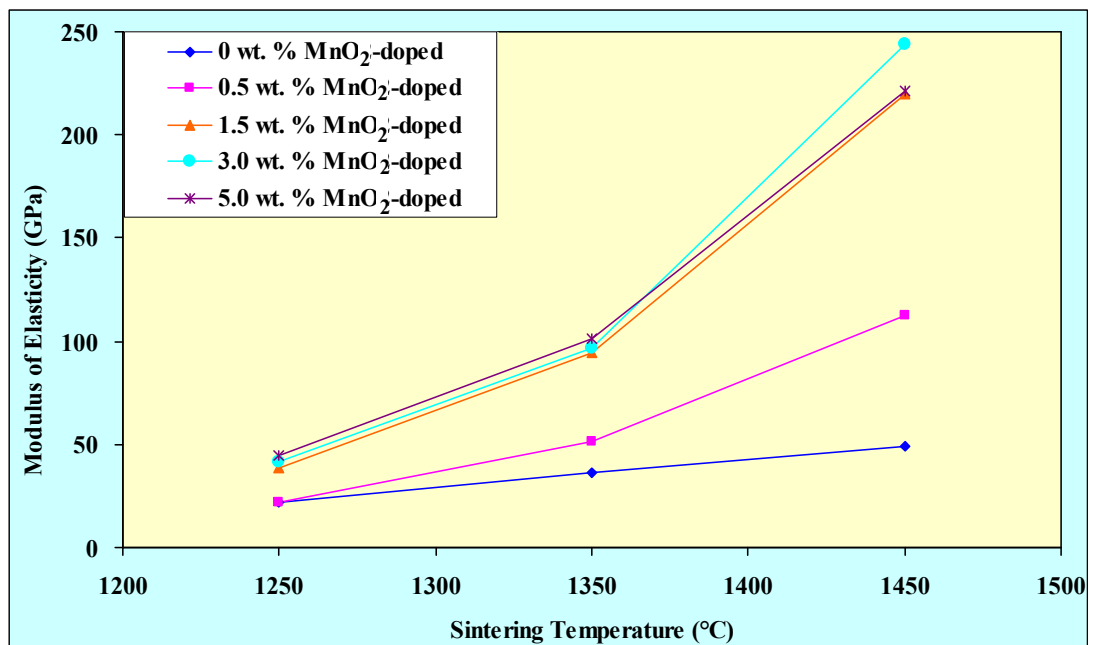


**Figure 5.7: Graph of Modulus of Elasticity against Sintering Temperature for Various Concentration of  $\text{MnO}_2$  Addition**

In general, the addition of  $\text{MnO}_2$  would have positive effect on improving the modulus of elasticity of alumina. This could be observed in the graph shown in Figure 5.8, in which those samples with  $\text{MnO}_2$  addition would have higher modulus of elasticity, if compared to those pure alumina samples regardless of sintering temperature portion. For example, the maximum modulus of elasticity, which can be achieved by the pure alumina sample at the sintering temperature of  $1450^\circ\text{C}$ , was only 49.43 GPa. On the other hand, the maximum modulus of elasticity, which could be attained by alumina sample doped with 3.0 wt. % of  $\text{MnO}_2$  at the same sintering temperature, was about 244.13 GPa or nearly five fold of the maximum modulus of elasticity that could be reached by the pure alumina sample. In addition, it could be observed that the modulus of the elasticity would increase sharply when the addition of  $\text{MnO}_2$  was raised from 0 up to 1.5 wt. %. However, the modulus of elasticity seemed to stay constant when the addition of  $\text{MnO}_2$  was increased more than 1.5 wt. %.

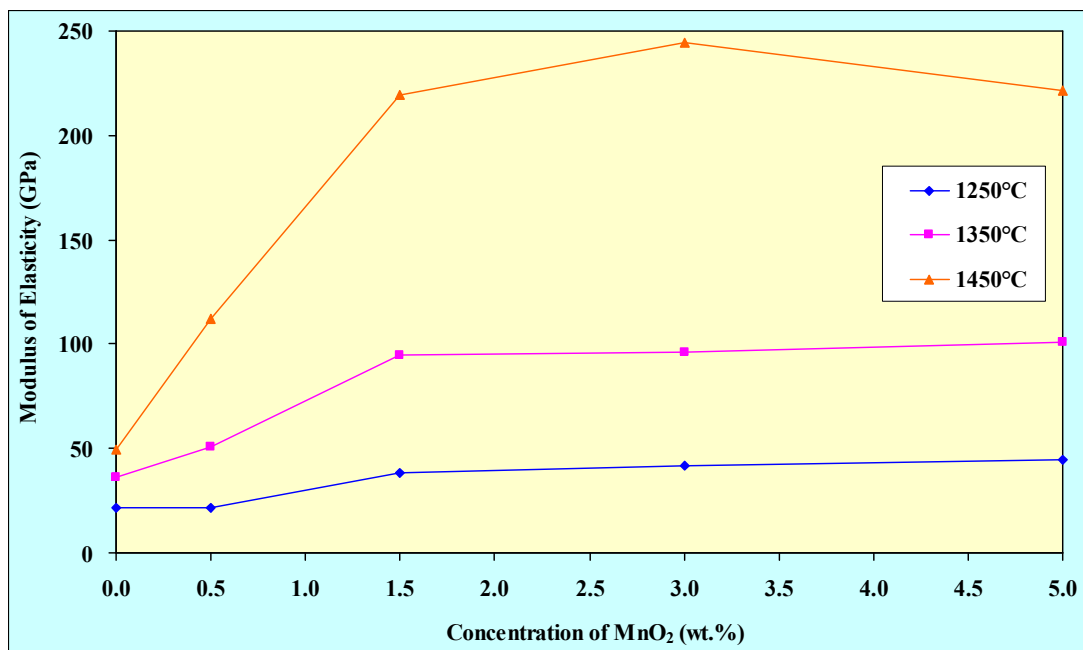


**Figure 5.8: Graph of Modulus of Elasticity against Concentration of  $\text{MnO}_2$  Addition for Various Sintering Temperature**

By reviewing Figure 5.9, it would be apparent that the addition of  $\text{MnO}_2$  was more effectual in enhancing the modulus of elasticity of the alumina ceramics if

compared to the addition of MgO. By comparison, the maximum modulus of elasticity that could be achieved by samples doped with MnO<sub>2</sub> was 244.13 GPa, which was much higher if compared to that could be attained by the sample doped with MgO, which was only 63.63 GPa at the sintering temperature of 1450 °C and concentration of dopant addition of 3 wt. %. Besides, it could be noticed that alumina samples doped with MnO<sub>2</sub> and MgO separately would exhibit similar trend in the relation of modulus of elasticity with respect to the concentration of dopant addition. For instance, the modulus of elasticity of the alumina samples doped with MgO would increase from 49.43 to 63.63 GPa as the concentration of MgO addition was increased from 0 to 3.0 wt. %. Nevertheless, further addition in the concentration of the MgO up to 5 wt. % would cause the modulus of elasticity to decline slightly from 63.63 to 61.08 GPa. Similarly, the modulus of elasticity of the alumina samples doped with MnO<sub>2</sub> would increase significantly from 49.43 to 244.13 GPa as the concentration of the MnO<sub>2</sub> addition was raised from 0 to 3.0 wt. %. Likewise, further addition of MnO<sub>2</sub> up to 5 wt. % would also cause the modulus of elasticity to reduce from 244.13 to 211.63 GPa.

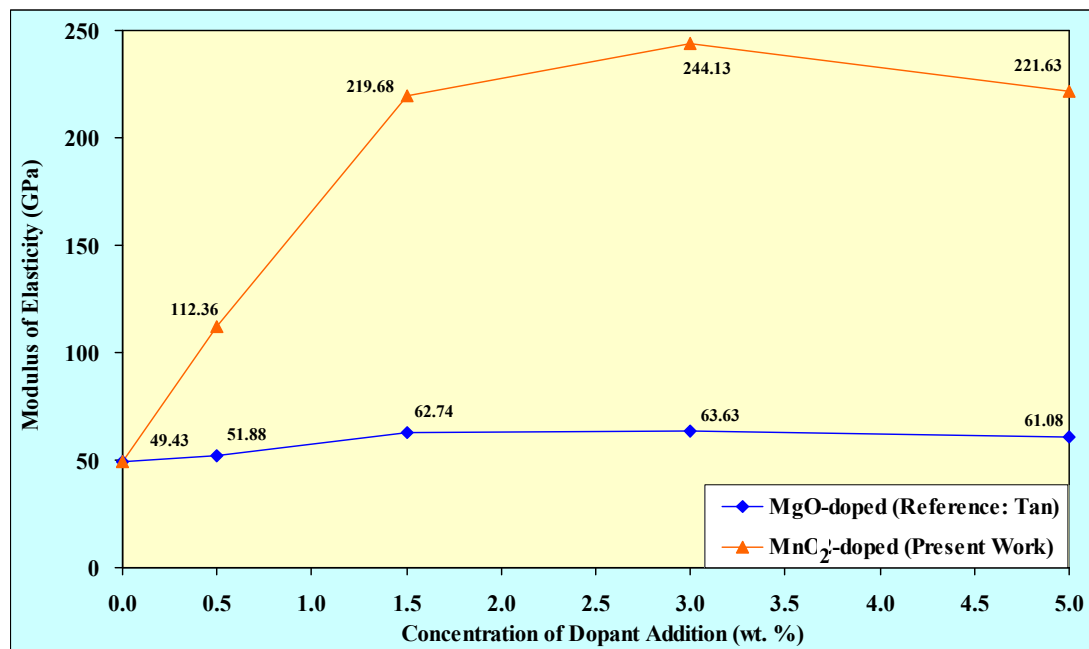


**Figure 5.9: Comparison of Modulus of Elasticity of Alumina Samples doped with MnO<sub>2</sub> and MgO independently and sintered at 1450 °C**

### 5.3 Vickers Hardness

From the Figure 5.10, it was very obvious that the Vickers hardness of the alumina samples, which were doped with various concentration of  $\text{MnO}_2$ , would increase with the sintering temperature. This trend also occurred on the pure alumina samples even though the increment of the Vickers hardness was comparatively less significant if compared with those doped alumina samples. For instance, the Vickers hardness of the pure alumina samples would increase from 0.74 to 1.79 GPa as the sintering temperature was increased from 1250 to 1450 °C. However, for the alumina samples which were doped with 5 wt. % of  $\text{MnO}_2$ , would experience a dramatic increase in the Vickers hardness due to the raise in the sintering temperature. For example, the Vickers hardness of the alumina samples doped with 5 wt. % of  $\text{MnO}_2$  would boost up significantly from 2.780 to 13.050 GPa as the sintering temperature was raised from 1250 to 1450 °C. Toy et al. (1995) and Erkalfa et al. (1995) experimental results showed similar trend in which the hardness of the samples increase with the sintering temperature.

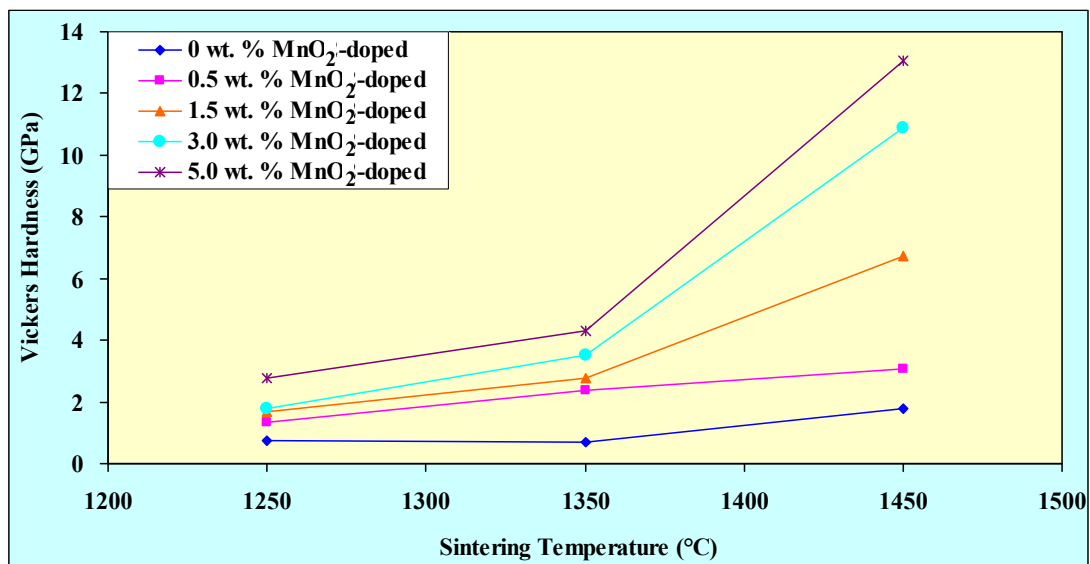


**Figure 5.10: Graph of Vickers Hardness against Sintering Temperature for Various Concentration of  $\text{MnO}_2$  Addition**



By observing Figure 5.11, it could be deduced that the addition of  $\text{MnO}_2$  in alumina samples, could lead to the improvement of the Vickers hardness. This is owing to the Vickers hardness of the alumina would increase as the amount of  $\text{MnO}_2$  addition was increased. For instance, at the sintering temperature of  $1450^\circ\text{C}$ , the Vickers hardness of the alumina sample would increase vividly from 1.79 to 13.05 GPa as the concentration of  $\text{MnO}_2$  addition was raised from 0 to 5 wt.%. Similar trend was also observed by Erkalfa et al. (1995). It could be observed that the increment in the Vickers hardness of the alumina samples would be much more significant as the sintering temperature was higher. For instance, the increments in the Vickers hardness of the samples sintered at 1450, 1350 and  $1250^\circ\text{C}$  were 11.26, 3.62 and 2.040 GPa respectively as the concentration of the  $\text{MnO}_2$  addition was raised from 0 to 5 wt. %.

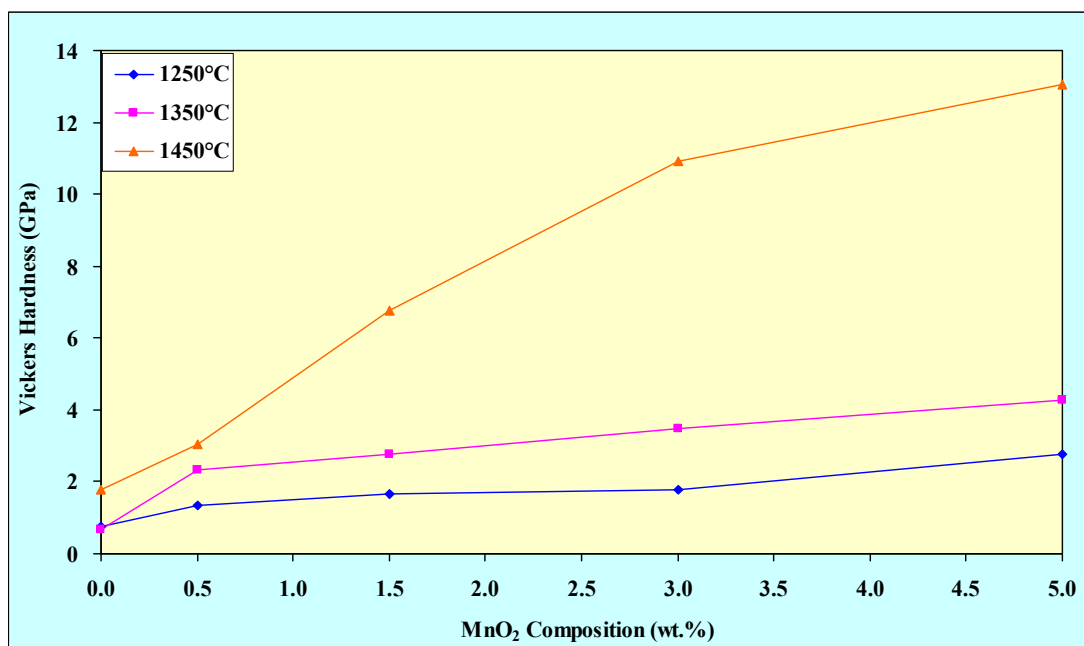


**Figure 5.11: Graph of Vickers Hardness against Concentration of  $\text{MnO}_2$  Addition for Various Sintering Temperatures**

In general, the addition of  $\text{MnO}_2$  would have a better effect on improving the hardness of the alumina ceramics if compared with other types of dopant such as  $\text{MgO}$  and  $\text{TiO}_2$ . From the comparison as shown in Figure 5.12, it could be observed that the samples doped with  $\text{MnO}_2$  would have an increasing trend in which the Vickers Hardness would increase as the concentration of  $\text{MnO}_2$  addition increases.

Meanwhile, the samples doped with  $\text{TiO}_2$  would exhibit a fluctuating trend in the relation of Vickers Hardness with respect to the concentration of  $\text{TiO}_2$  addition. In addition, the Vickers Hardness of samples doped with  $\text{MgO}$  would deem to remain constant within certain region due to the insignificant changes in the Vickers Hardness of the samples as the concentration of the  $\text{MgO}$  addition increases. By comparison, at the sintering temperature of  $1450\text{ }^\circ\text{C}$ , the maximum Vickers Hardness that could be attained by the samples doped with  $\text{MnO}_2$  was  $13.05\text{ GPa}$  when the concentration of  $\text{MnO}_2$  addition was  $5.0\text{ wt. }%$ . This would be about  $70\%$  and  $430\%$  higher than the Vickers Hardness which could be achieved by the samples doped with  $\text{TiO}_2$  and  $\text{MgO}$  respectively. This is owing to the maximum Vickers Hardness that could be reached by samples doped with  $\text{TiO}_2$  was only  $7.60\text{ GPa}$  when the concentration of  $\text{TiO}_2$  addition was  $0.5\text{ wt. }%$ . On the other hand, the samples doped with  $\text{MgO}$  could only attain maximum Vickers Hardness of only  $2.44\text{ GPa}$  when the concentration of  $\text{MgO}$  addition was  $3.0\text{ wt. }%$ . Moreover, this increment was only slightly higher than the Vickers Hardness that could be attained by undoped alumina sample, which was about  $1.79\text{ GPa}$ .

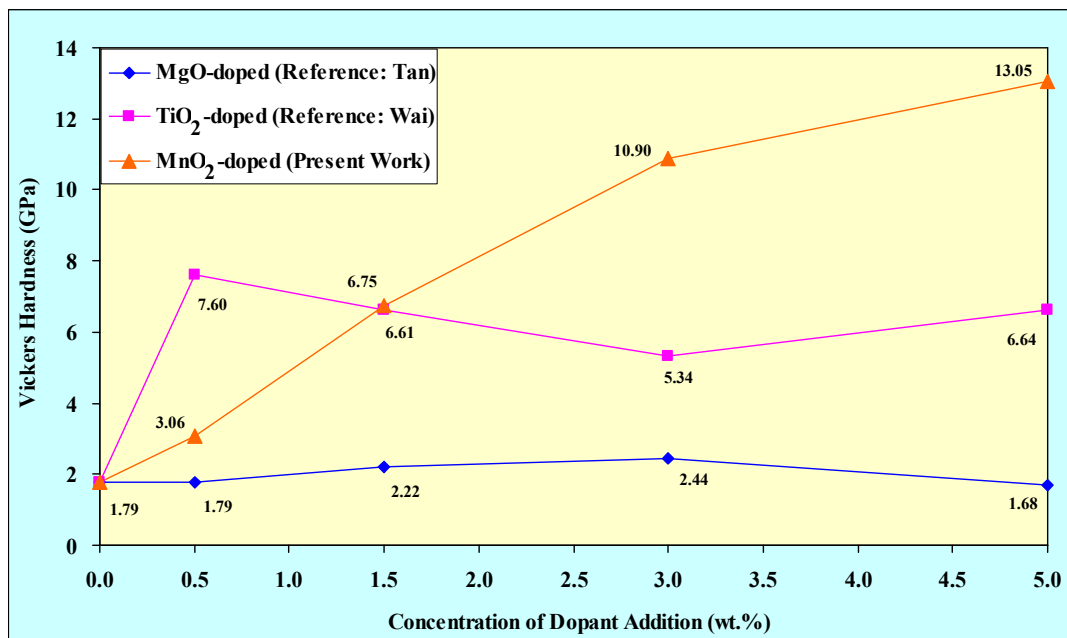


**Figure 5.12: Comparison of Vickers Hardness of Alumina Samples doped with  $\text{MnO}_2$ ,  $\text{MgO}$  and  $\text{TiO}_2$  independently and sintered at  $1450\text{ }^\circ\text{C}$**

#### 5.4 X-Ray Diffraction (XRD) Analysis

From X-Ray Diffraction (XRD) analysis, small traces of  $\text{MnO}_2$  could be detected in the doped alumina powder (before sintering), when the concentration of  $\text{MnO}_2$  was increased more than 1.5 wt. %. By referring to the Figure 5.13, the intensity of the peak at approximately  $29^\circ$  was found to be increasing as the concentration of  $\text{MnO}_2$  addition was raised from 1.5 to 5.0 wt. %. However,  $\text{MnO}_2$  was not detected in the alumina sample with 0.5 wt. %  $\text{MnO}_2$  addition (before sintering).

After the samples were sintered at 1250, 1350 and 1450  $^\circ\text{C}$ , it was found that  $\text{MnO}_2$  could no longer be detected in the alumina samples (Figures 5.14 & 5.16). This is because major amount of  $\text{MnO}_2$  might dissolve in the alumina to form a solid solution after the sintering process and thus it would be difficult to detect the existence of  $\text{MnO}_2$  in the sintered samples. Furthermore, this also indicated that the concentration of  $\text{MnO}_2$  addition up to 5.0 wt. % was below the solubility limit of the  $\text{MnO}_2\text{-Al}_2\text{O}_3$  system for sintering temperature varied from 1250 to 1450 $^\circ\text{C}$  since there was no excess  $\text{MnO}_2$  compound could be detected through the XRD analysis.

By referring to the phase diagram of  $\text{MnO}_2\text{-Al}_2\text{O}_3$  system as depicted in Figure 3.23, a eutectic composition is present in the  $\text{MnO}_2$ -rich side of the binary  $\text{MnO}_2\text{-Al}_2\text{O}_3$  system at 1520 $^\circ\text{C}$  (Erkalfa et al., 1995). In other words, the secondary phase would only exist in the alumina ceramic when the sintering temperature was 1520  $^\circ\text{C}$  or above. This is also supported by the research done by Erkalfa et al. (1995) in which the intergranular grain boundary phase or secondary phase could only be detected in the alumina samples which were doped with 0.5 to 1.5 wt. %  $\text{MnO}_2$  and sintered at 1550 $^\circ\text{C}$  for 2 hours.

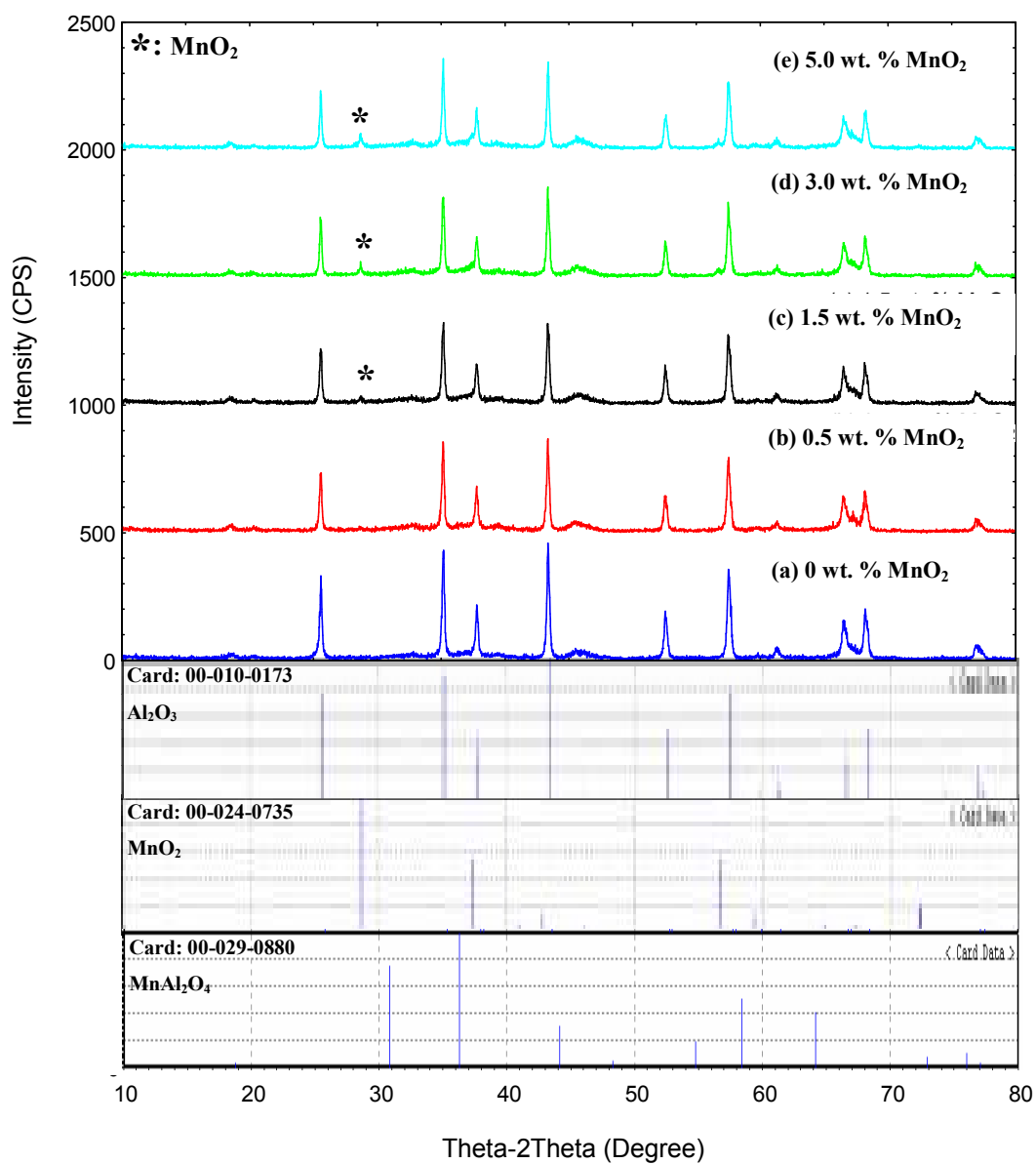


**Figure 5.13: XRD Analysis of Samples Doped with (a) 0 wt. %, (b) 0.5 wt. %, (c) 1.5 wt. %, (d) 3.0 wt. %, (e) 5.0 wt. % of MnO<sub>2</sub> before Sintering**

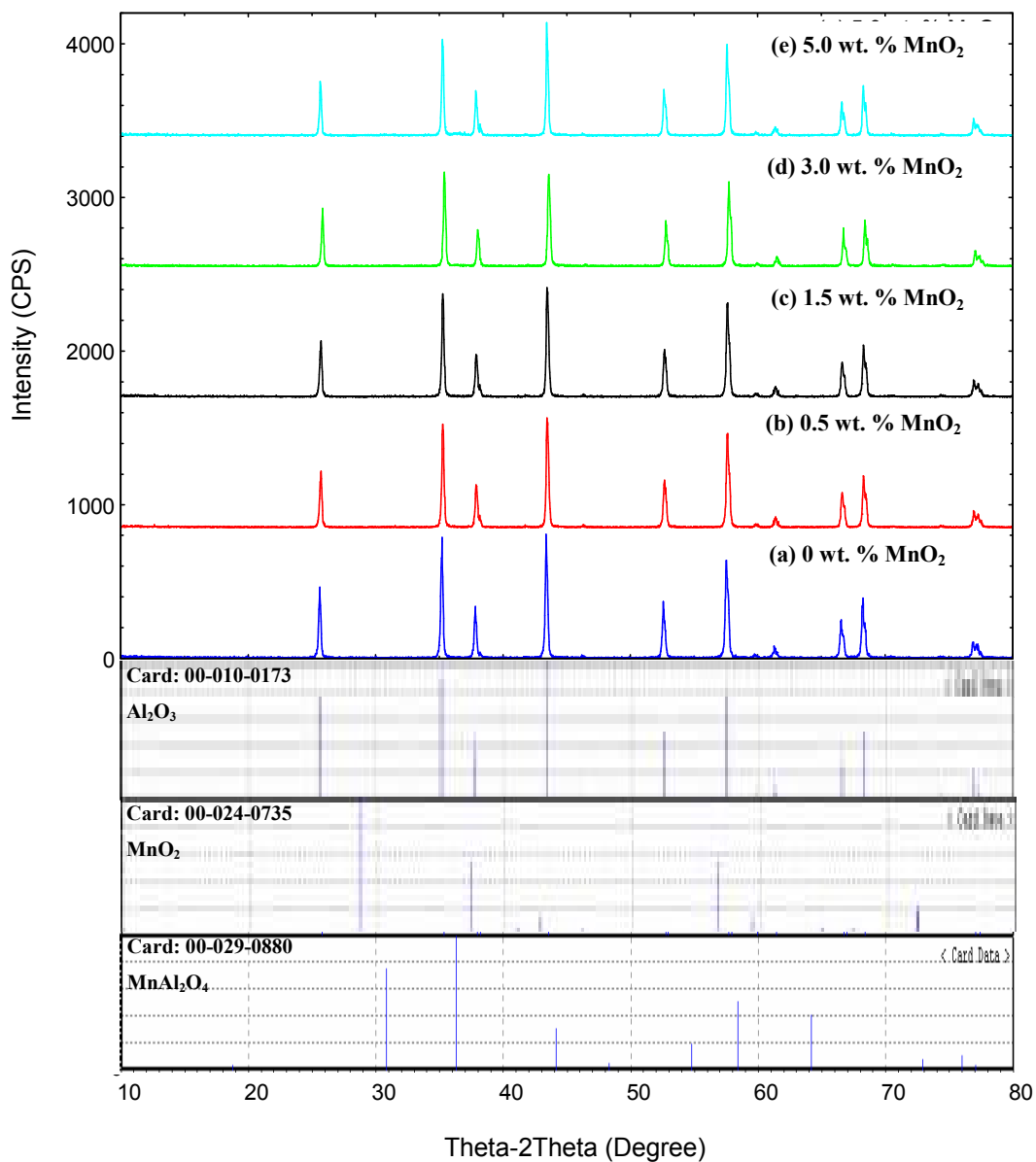


**Figure 5.14: XRD Analysis of Samples Doped with (a) 0 wt. %, (b) 0.5 wt. %, (c) 1.5 wt. %, (d) 3.0 wt. %, (e) 5.0 wt. % of MnO<sub>2</sub> after Sintering at 1250 °C**

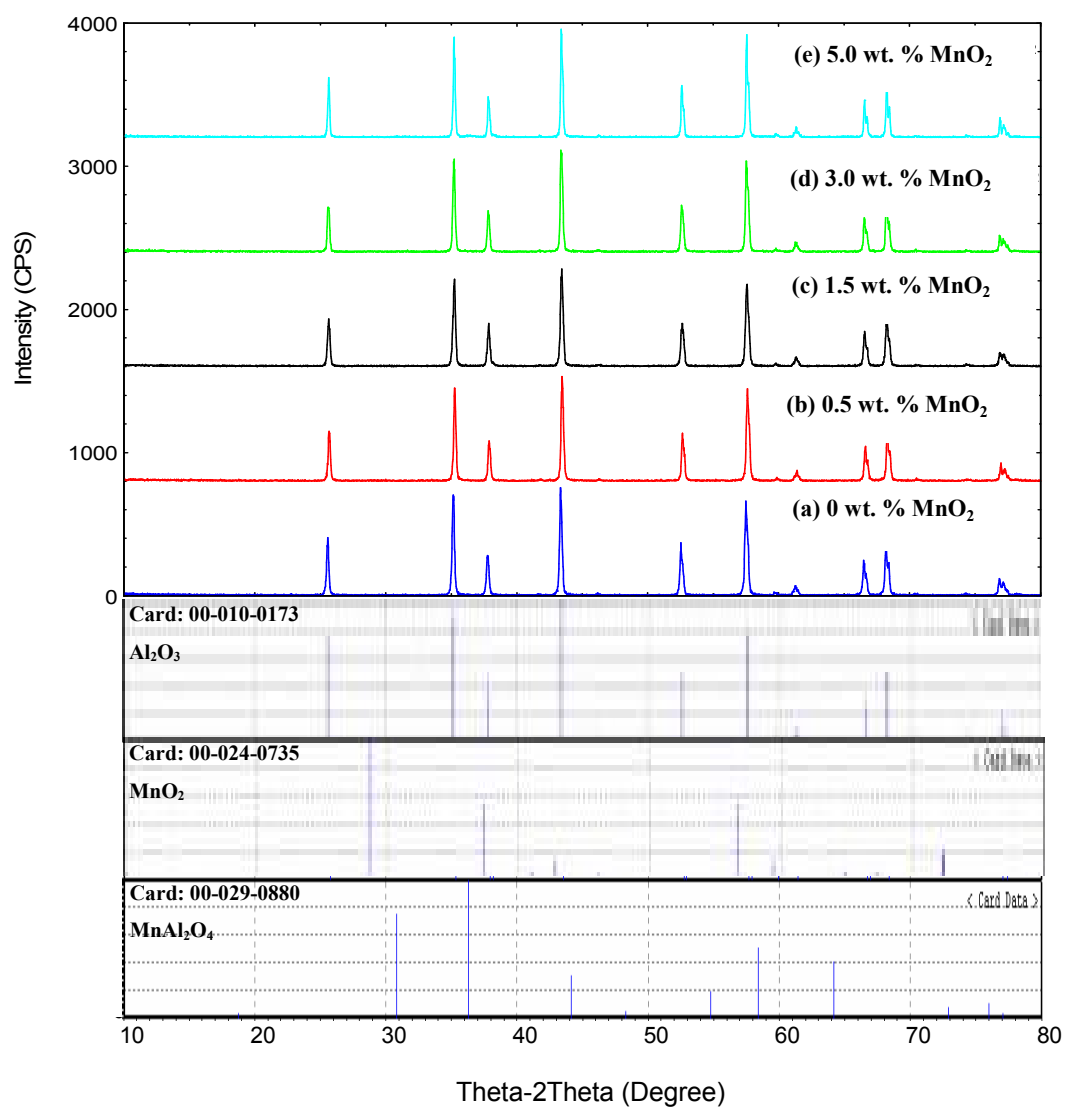


**Figure 5.15: XRD Analysis of Samples Doped with (a) 0 wt. %, (b) 0.5 wt. %, (c) 1.5 wt. %, (d) 3.0 wt. %, (e) 5.0 wt. % of MnO<sub>2</sub> after Sintering at 1350 °C**

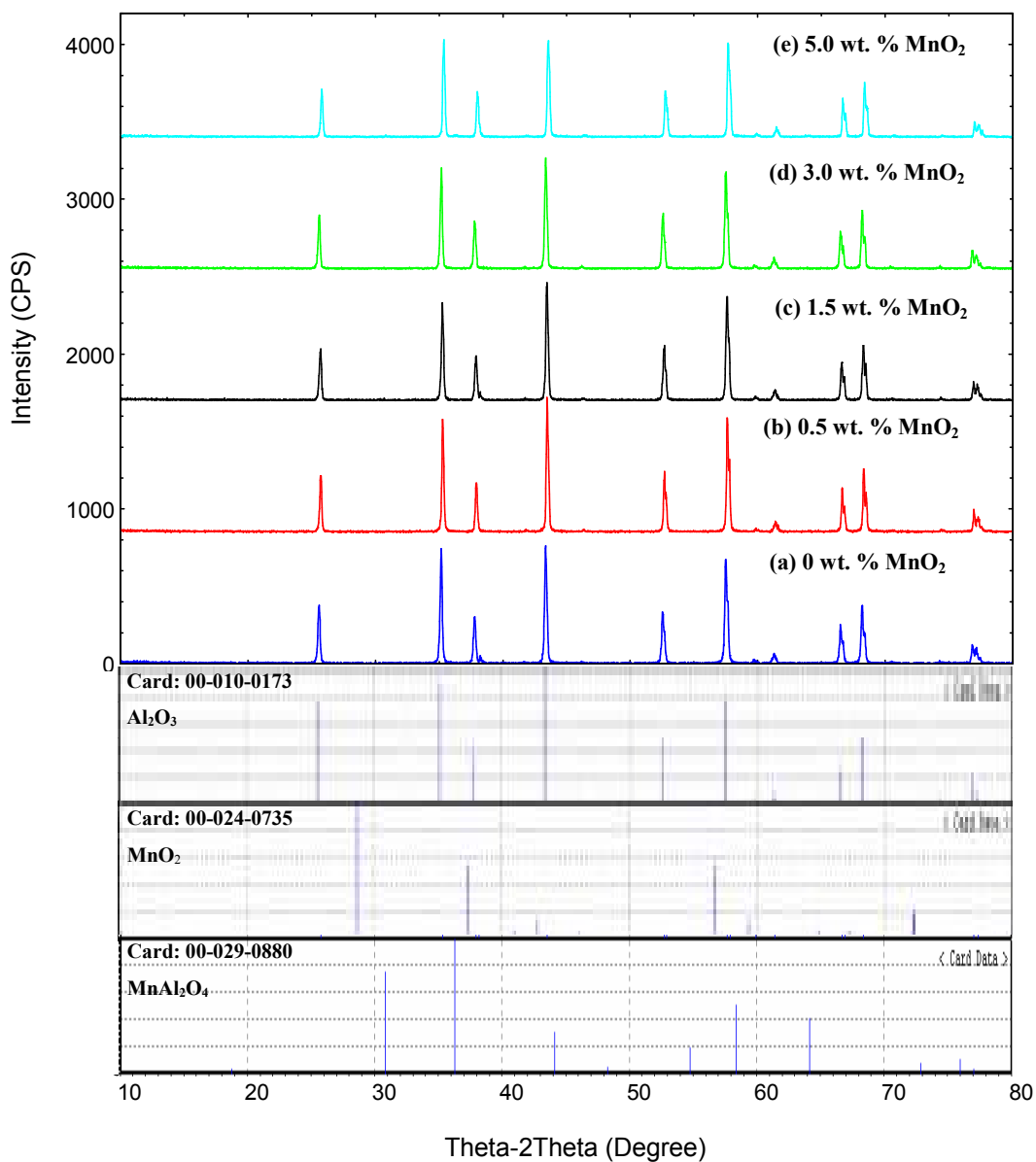


**Figure 5.16: XRD Analysis of Samples Doped with (a) 0 wt. %, (b) 0.5 wt. %, (c) 1.5 wt. %, (d) 3.0 wt. %, (e) 5.0 wt. % of MnO<sub>2</sub> after Sintering at 1450 °C**

**Table 5.1: Summary of Compounds found in Samples before and after Sintering (A and M represents Al<sub>2</sub>O<sub>3</sub> and MnO<sub>2</sub> respectively).**

Sintering Temperature (°C)	MnO <sub>2</sub> Concentration (wt. %)				
	0	0.5	1.5	3.0	5.0
Before Sintering	A	A	A + M	A + M	A + M
1250	A	A	A	A	A
1350	A	A	A	A	A
1450	A	A	A	A	A

## 5.5 Grain Size

By referring to the micrographs as shown in Figure 5.17, it could be observed that the amount of intergranular pores of the pure alumina samples would decrease as the sintering temperature increases. This might be due to the occurrence of relatively homogeneous and uniform grain growth as the pure alumina samples were sintered from 1250 to 1450 °C (Erkalfa et al., 1995).

The addition of MnO<sub>2</sub> into the alumina ceramics would lead to inhomogeneous grain growth and this effect would be further magnified as the sintering temperature increases. This occurrence could be observed clearly in the micrographs shown in Figure 5.15 in which the alumina sample that was doped with highest concentration of MnO<sub>2</sub>, which was 5 wt. % and sintered at 1450° C, exhibiting significant abnormal grain growth with grains as large as  $4.6 \pm 0.58 \mu\text{m}$ . A significant amount of intergranular and intragranular pores could be observed in the microstructures of the alumina samples doped with MnO<sub>2</sub>. This could be clearly illustrated in the Figures 5.18 to 5.21 in which the pores could be observed between the grains and within the grains. Moreover, these micrographs indicate that samples with 0.5 to 5.0 wt. % MnO<sub>2</sub> addition and sintered at 1250 to 1450° C, do not show the presence of any grain boundary phase formation between the grains. This observation could also be supported by the research of Erkalfa et al. (1995) in which intergranular grain boundary phase could only be observed or detected between the grains in those samples with 0.5 to 1.5 wt. % MnO<sub>2</sub> additions sintered at 1550 °C for 2 hour.



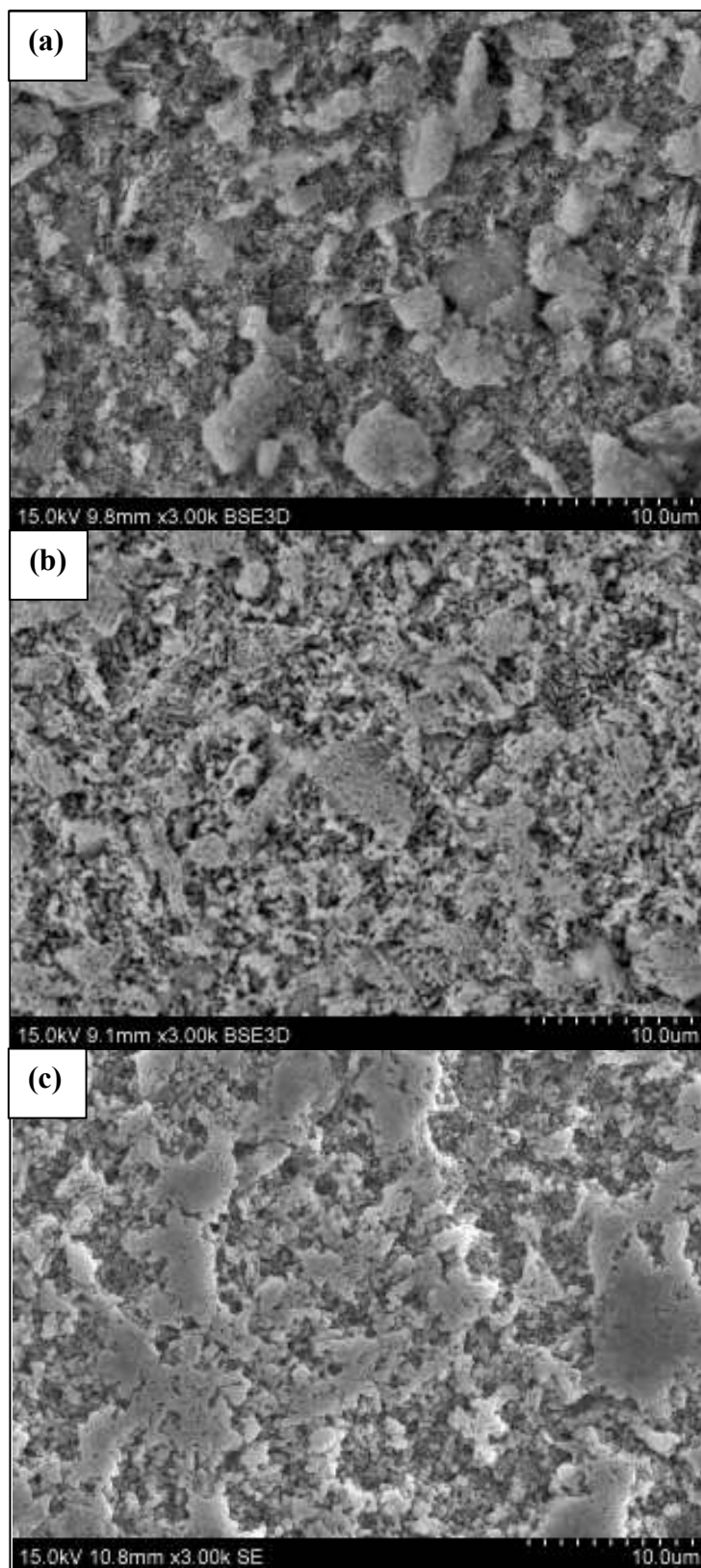


**Figure 5.17: SEM Analysis of Pure Alumina Samples Sintered at (a) 1250 °C, (b) 1350 °C and (c) 1450 °C**

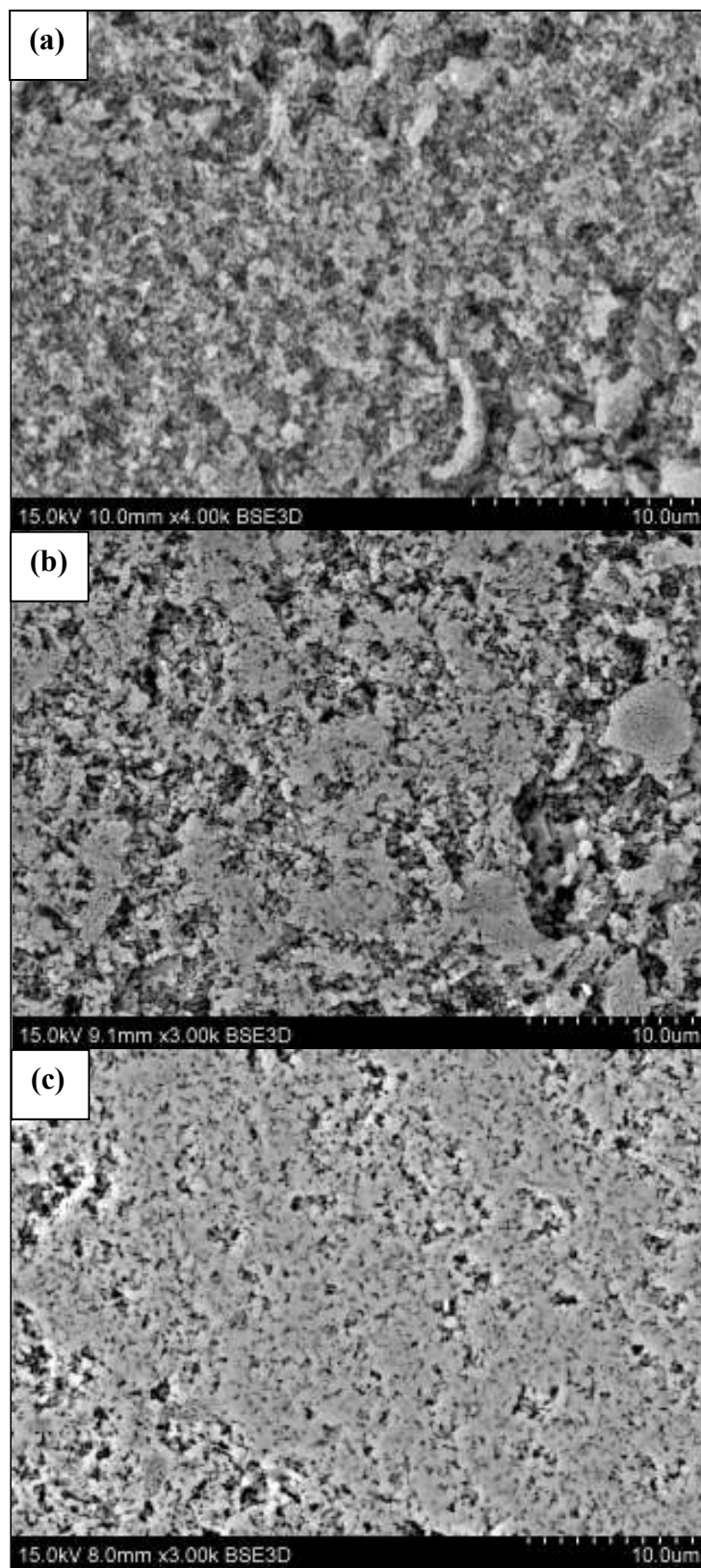


**Figure 5.18: SEM Analysis of Samples Doped with 0.5 wt. % MnO<sub>2</sub> Sintered at (a) 1250 °C, (b) 1350 °C and (c) 1450 °C**

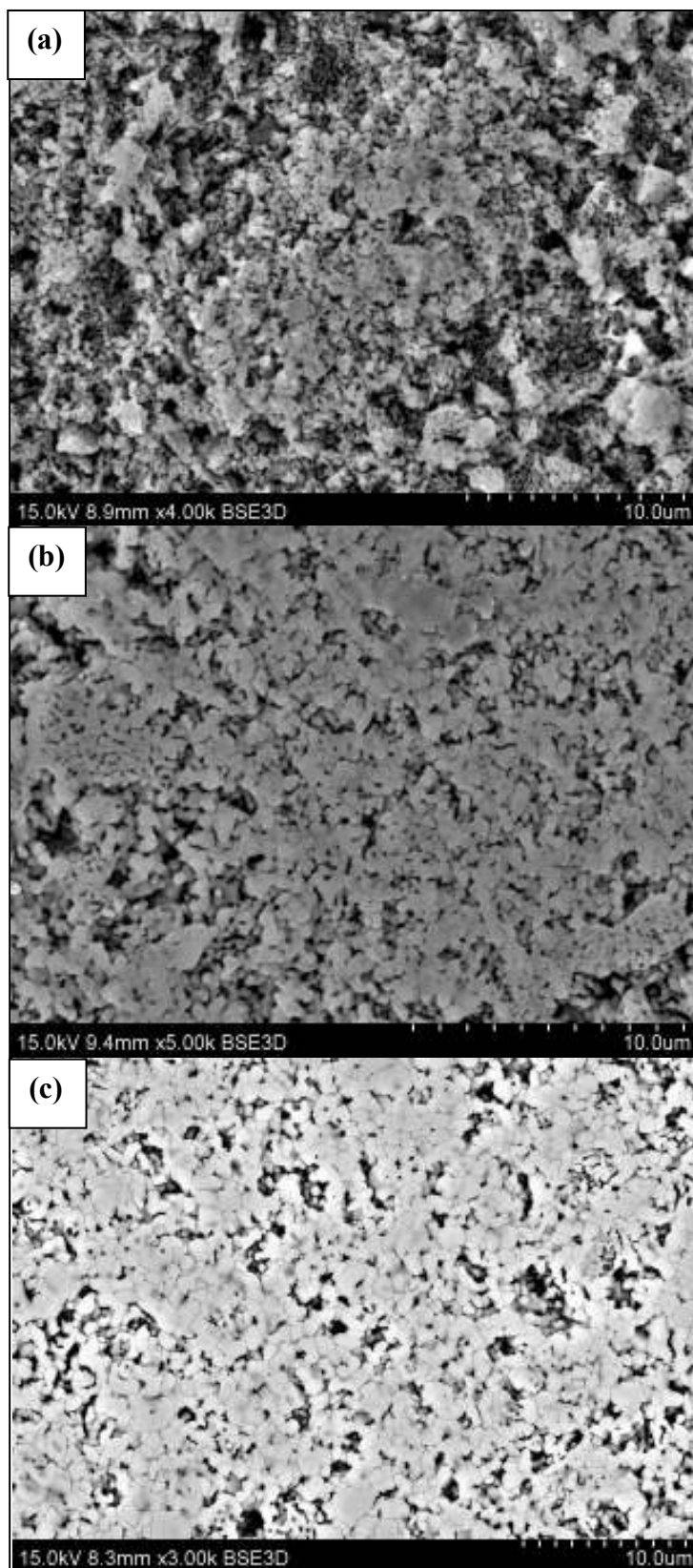


**Figure 5.19: SEM Analysis of Samples Doped with 1.5 wt. % MnO<sub>2</sub> Sintered at (a) 1250 °C, (b) 1350 °C and (c) 1450 °C**

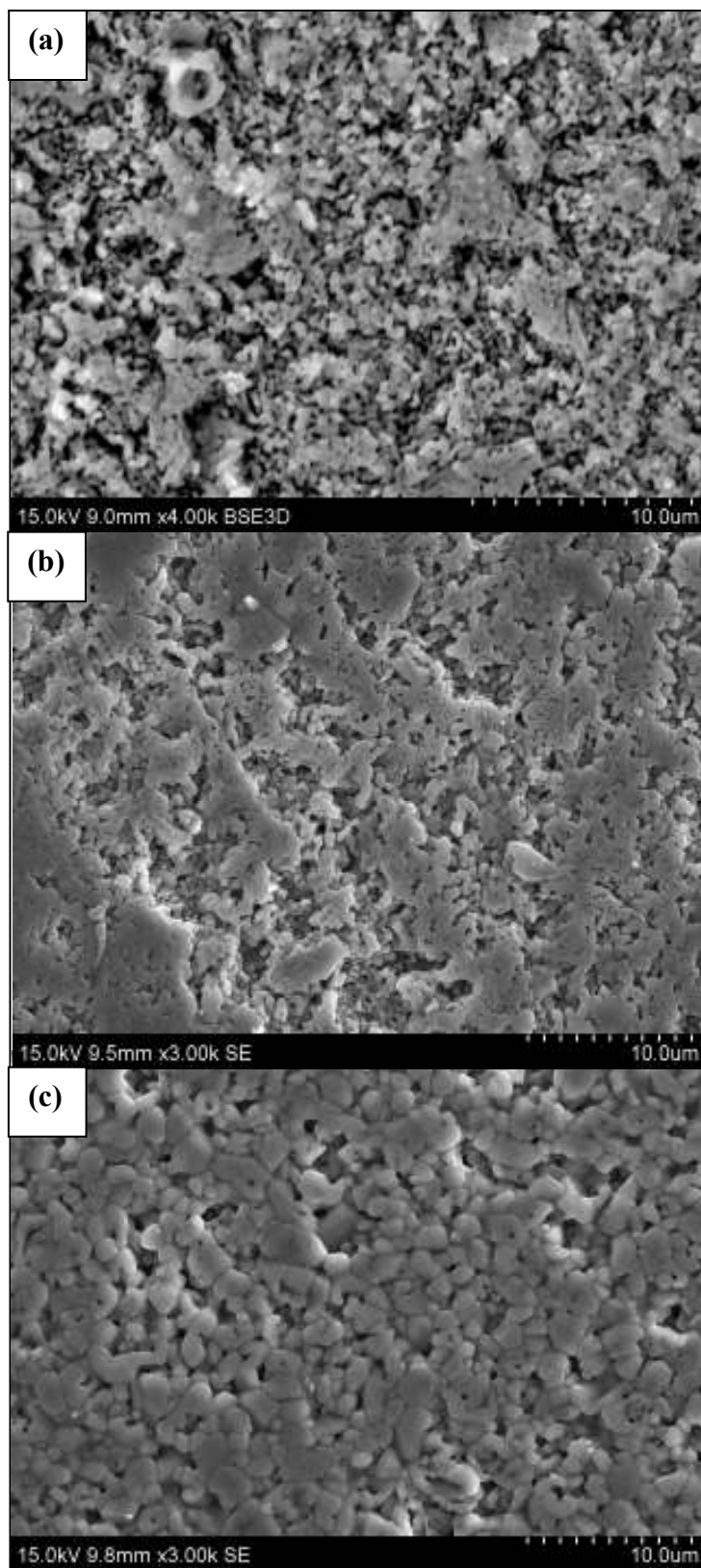


**Figure 5.20: SEM Analysis of Samples Doped with 3.0 wt. % MnO<sub>2</sub> Sintered at (a) 1250 °C, (b) 1350 °C and (c) 1450 °C**

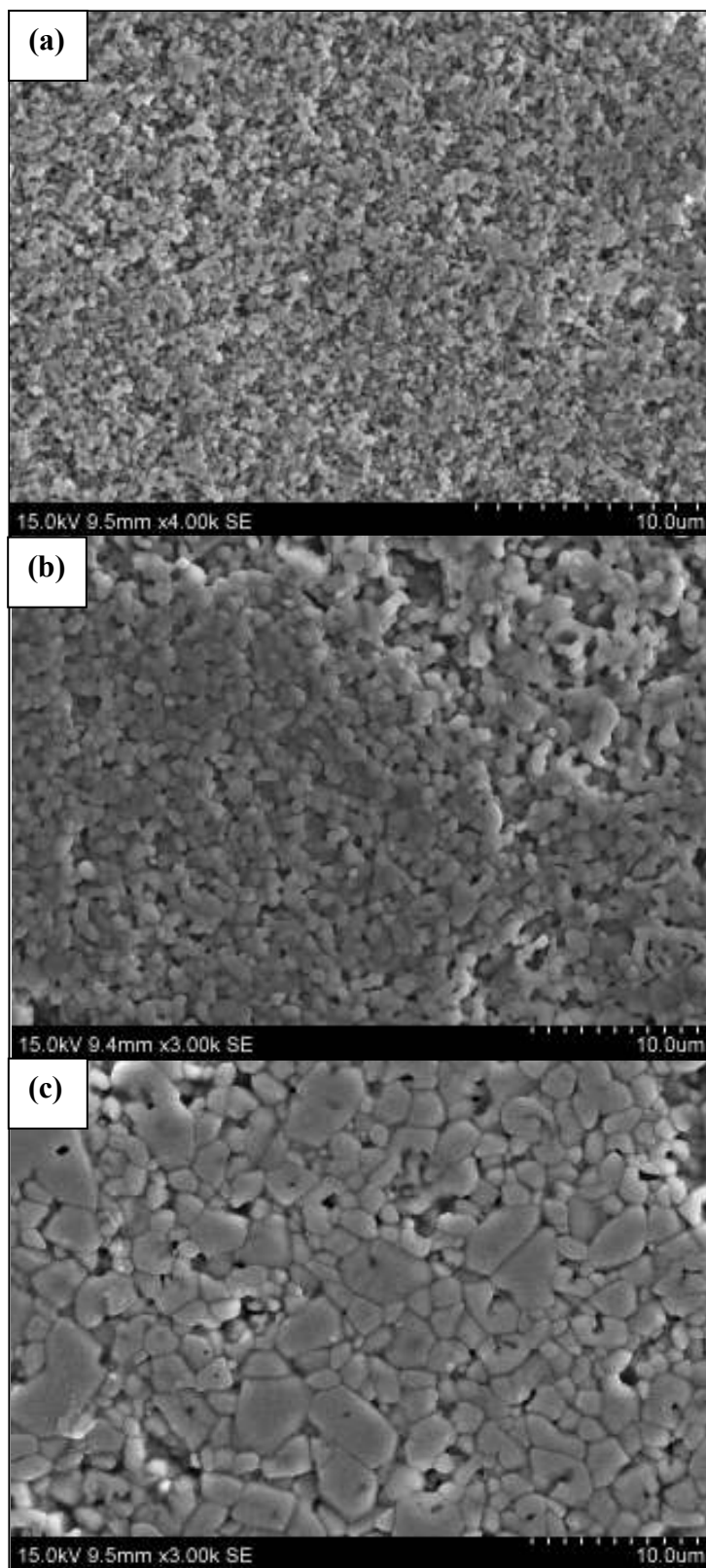


**Figure 5.21: SEM Analysis of Samples Doped with 5.0 wt. % MnO<sub>2</sub> Sintered at (a) 1250 °C, (b) 1350 °C and (c) 1450 °C**

According to the literature review, high sintering temperatures would promote the grain growth of the alumina samples (Toy et al, 1995). This could be observed from Figure 5.22 in which the average grain size of the alumina samples would increase with the sintering temperature regardless of the concentration of  $\text{MnO}_2$  addition. Moreover, it was also found that higher concentration of  $\text{MnO}_2$  addition would lead to higher increment in the average grain size of the alumina ceramic as the sintering temperature was increased from 1250 to 1450 °C. Meanwhile, relatively less increment in the average grain size could be observed on the undoped or pure alumina samples as the sintering temperature was raised. For instance, the average grain size of the pure alumina samples was found to be increasing from 0.17 to 0.37  $\mu\text{m}$  while the average grain size of the alumina samples doped with 5 wt. %  $\text{MnO}_2$  was observed to rise from 0.31 to 1.68  $\mu\text{m}$  as the sintering temperature was increased from 1250 to 1450 °C.

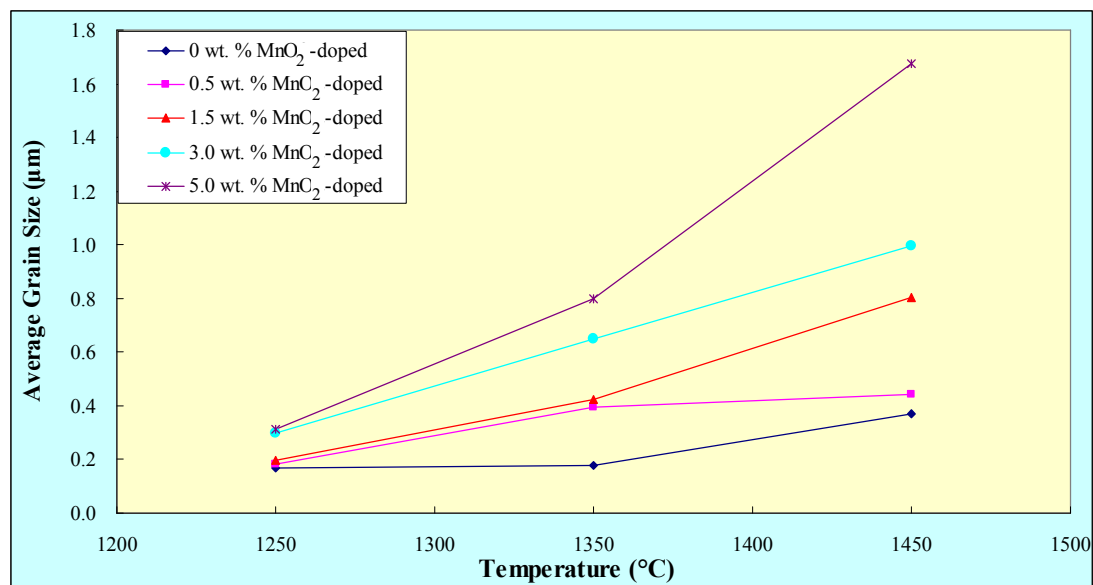


**Figure 5.22: Graph of Average Grain Size against Temperature for Various Concentration of  $\text{MnO}_2$  Addition**

Generally, the addition of the  $\text{MnO}_2$  could indeed promote the grain growth of the alumina ceramic. This could be shown clearly in the graph as depicted in Figure 5.23 in which the average grain size of the alumina ceramics would increase as the concentration of the  $\text{MnO}_2$  increased. For instance, at the sintering temperature of 1350 °C, the average grain size of the alumina ceramics was observed to be raised

from 0.18 to 0.80  $\mu\text{m}$  as the concentration of  $\text{MnO}_2$  addition was increased from 0 to 5.0 wt. %. Besides that, the largest average grain size, which was about 1.68  $\mu\text{m}$ , could be observed on the alumina sample which was doped with 5 wt. %  $\text{MnO}_2$  and sintered at 1450  $^\circ\text{C}$ . Meanwhile, the smallest average grain size, which was about 0.17 $\mu\text{m}$ , could be noticed on the pure alumina sample which was sintered at 1250  $^\circ\text{C}$ .

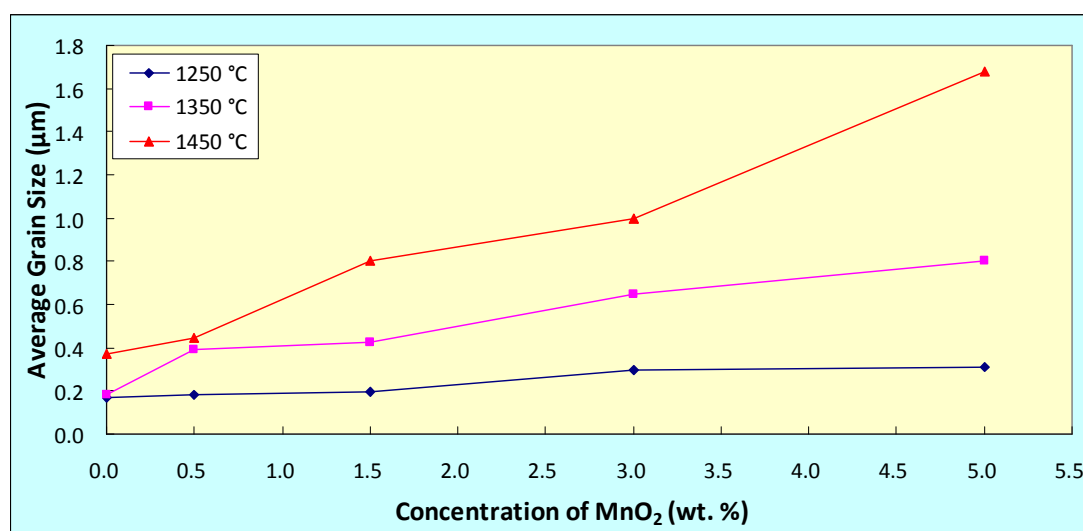


**Figure 5.23: Graph of Average Grain Size against Concentration of  $\text{MnO}_2$  Addition for Various Sintering Temperatures.**

The Figure 5.24 shows the comparison between the experimental result and the result achieved by Erkalfa et al. (1995). It could be noticed that for either pure alumina samples or samples doped with 3 wt. %  $\text{MnO}_2$ , the average grain size of the experimental result was found to be lower if compared to the result of Erkalfa et al. (1995). This might be probably due to smaller particle size of experimental major powder was used, which was 0.027  $\mu\text{m}$  if compared to the major powder used in the research of Erkalfa et al. (1995), which was 0.37 $\mu\text{m}$ .



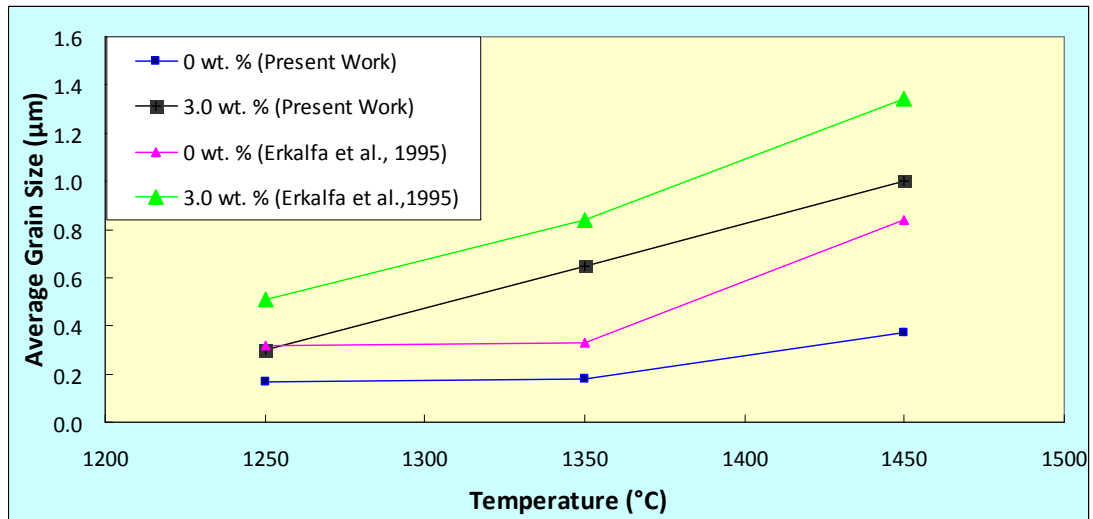


**Figure 5.24: Comparison of Average Grain Size between Experimental Result and Researcher's Result (Erkalfa et al., 1995).**

Based on Figure 5.25, it is significant that the alumina ceramics doped with 3.0 wt. %  $\text{MnO}_2$  would have better controlled grain growth if compared with the alumina ceramics doped with 3.0 wt. %  $\text{MnO}_2$  and various concentration of  $\text{TiO}_2$  together. For instance, the alumina ceramics doped with 3 wt. %  $\text{MnO}_2$  would have smaller average grain size for various sintering temperatures if compared to the alumina ceramics which were doped with these two additives together. This is because similar to the  $\text{MnO}_2$ , the addition of  $\text{TiO}_2$  would also promote the grain growth of the alumina ceramics. Therefore, it would be expected that the average grain size of the alumina ceramics doped with these two additives together was found to be higher than the average grain size of the alumina ceramics which were only doped with either one of them. Besides, it was also found that the grain growth of the alumina ceramics would be greater when the concentration of  $\text{TiO}_2$  was increased provided the concentration of  $\text{MnO}_2$  remained constant. For example, at the sintering temperature of 1450 °C, the maximum average grain size of the alumina ceramic doped with 3.0 wt. %  $\text{MnO}_2$  and 2.0 wt. %  $\text{TiO}_2$  together was 4.22 µm, which was much higher if compared to other alumina ceramics which were doped with lesser amount of  $\text{TiO}_2$  or only doped with  $\text{MnO}_2$ .



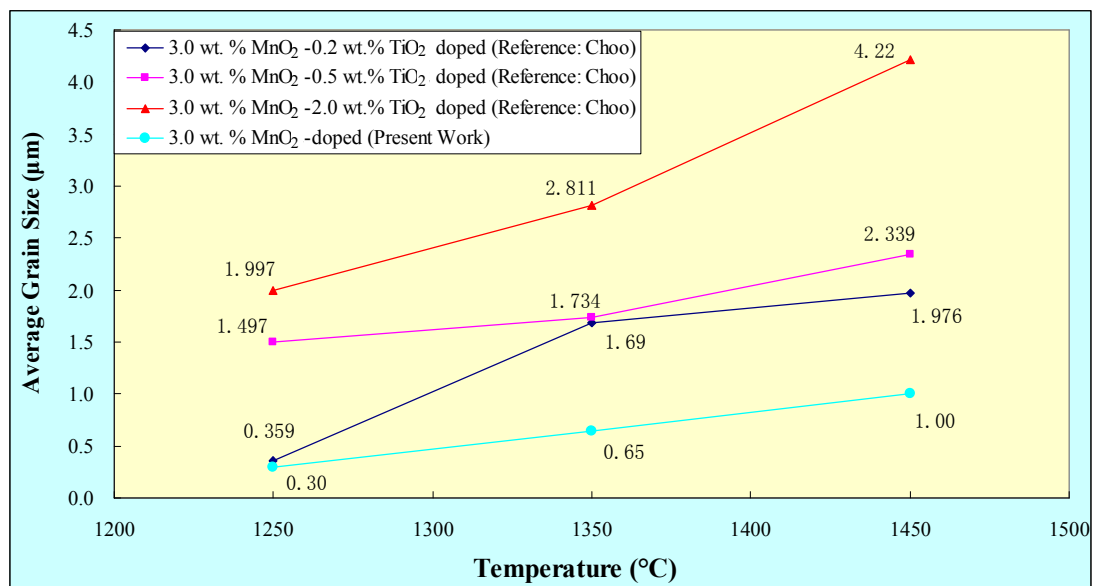


**Figure 5.25: Comparison of Average Grain Size of Alumina Ceramics with Various Concentrations of Additives.**

## CHAPTER 6

### CONCLUSION AND RECOMMENDATIONS

#### 6.1 Conclusion

The densification of the alumina ceramics could be improved by increasing the sintering temperature. Moreover, a minor amount of  $\text{MnO}_2$  addition was found to be effective in enhancing the densification of the alumina ceramics as the sintering temperatures were ranging from 1250 to 1450 °C. For instance, at the sintering temperature of 1450 °C, 95.754 % of theoretical density could be attained by sample doped with 5 wt. %  $\text{MnO}_2$  if compared to 92.286 % of theoretical density of the undoped sample. Similarly, the average shrinkage of the alumina ceramics would increase with the sintering temperature and concentration of  $\text{MnO}_2$  addition.

Besides, the modulus of elasticity for various compositions of alumina ceramics would also increase with the sintering temperature. The addition of  $\text{MnO}_2$  would improve the modulus of elasticity of the alumina ceramics and the maximum modulus of elasticity, which was 244.13 GPa could be achieved when the concentration of  $\text{MnO}_2$  addition was 3.0 wt. % and sintered at 1450 °C.

The Vickers hardness of the alumina ceramics was also found to be dependent on the sintering temperature as the Vickers hardness of the alumina ceramics with various concentrations of  $\text{MnO}_2$  addition, would increase with the sintering temperature. For example, the Vickers hardness of the alumina ceramic with 5 wt. % of  $\text{MnO}_2$  addition would increase extensively from 2.78 to 13.05 GPa as the sintering temperature was raised from 1250 to 1450 °C. Furthermore, the

Vickers hardness of the alumina ceramics could also be improved by increasing the amount of the  $\text{MnO}_2$  addition. For instance, the Vickers hardness of the alumina ceramics would increase significantly from 1.79 to 13.05 GPa when the concentration of  $\text{MnO}_2$  addition was raised from 0 to 5.0 wt. % at the sintering temperature of 1450 °C. The objective of this final year project was achieved with the successful enhancement in the hardness of the alumina ceramics through the addition of  $\text{MnO}_2$ .

No evidence could be found for liquid phase nor secondary phase formation within the limits of the dopant and sintering temperature level studied. The addition of  $\text{MnO}_2$  into the alumina ceramics would promote the grain growth and this effect would be further magnified as the sintering temperature and concentration of  $\text{MnO}_2$  addition was increased.

## **6.2 Recommendations**

In fact, when a small amount of additives is mixed with major powder, there is frequently a problem of insufficient mixing. One of the recommendations which could be used to improve the accuracy and precision of the experimental result would be the application of colloidal technique during the powder mixing process. This is owing to the advantage of the colloidal technique in which it allows a uniform distribution of the minor amounts of additive, which is  $\text{MnO}_2$  within the alumina ceramic. Besides that, the wet ball milling technique which was used in this research might have its limitations when doping a minor amount of submicron particles (Toy et al, 1995).

Besides, the sample should be dipped into the water slowly when the water immersion technique is used to measure the bulk density of the alumina ceramics. This is because the formation of air bubbles would occur on the surfaces of the sample when it is dropped into water from air. In addition, the air bubbles which are surrounding the surfaces of the sample would cause the reading of the measurement keep fluctuating and lead to difficulty in taking the measurement since the

measurement could only be taken when the reading from the balance is constant. Moreover, the air bubbles formed on the surfaces of the sample tend to restrain water from penetrate the pores completely, which in turn affects the accuracy of the bulk density measurement.

## REFERENCES

- American Ceramic Society. (2010). History of Ceramics. Retrieved June 27, 2010, from <http://ceramics.org/learn-about-ceramics/history-of-ceramics/>.
- Ashby, M.F., Messler, R.W., & Asthana, R. (2009). Engineering materials and processes desk reference. United States: Butterworth-Heinemann.
- Askeland, D.R., & Phulé, P.P. (2006). The science and engineering of materials. (5<sup>th</sup> ed.). United States: Cengage Learning.
- Bae, S.I., & Baik, S. (1994). Critical concentration of MgO for the prevention of abnormal grain growth in alumina. *Journal of American Ceramic Society*, 77 (10), 2499-2504.
- Bär, S. (2004). Crystalline rare earth-doped-sesquioxide PLD-films on [alpha]-alumina. CUVILLIER VERLAG.
- Bengisu, M. (2001). Engineering ceramics. Germany: Springer-Verlag Berlin Heidelberg, 192-195.
- Bennison, S.J., & Harmer, M.P. Effect of MgO solute on the grain growth kinetics of grain growth in Al<sub>2</sub>O<sub>3</sub>. *Journal of American Ceramic Society*, 66 (5), C90-C92.
- Black, J., & Hastings, G.W. (1998). Handbook of biomaterial properties. London, United Kingdom: Chapman & Hall.
- Bodišová, K., Šajgalík, P., Galusek, D., & Švancárek, P. (2007). Two-stage sintering of alumina with submicrometer grain size. *Journal of American Ceramic Society*, 90 (1), 330-332.
- Callister, W.D. (2007). Materials Science and Engineering. (7<sup>th</sup> ed.). John Wiley & Sons. Inc.
- Chattopadhyay, R. (2004). Advanced thermally assisted surface engineering processes. Chapter 13 Hot Isostatic Press. Springer.

- Chen, I.W., & Wang, X.H. (2000). Sintering dense nanocrystalline ceramics without final-stage grain growth. *Nature*, 404, 168–171.
- Cheng, J.Q., Zhou, J., & Ye, N. (1992). Densification kinetics of alumina during microwave sintering. *Material Research Society*, 323-328.
- DIANE. (1993). *New Materials Society, Challenges and Opportunities: New Materials Science and Technology*. DIANE Publishing.
- Erkalfa, H., Misirli, Z., Demirci, M., Toy, C. & Baykara, T. (1995). The Densification and Microstructural Development of Al<sub>2</sub>O<sub>3</sub> with Manganese Oxide Addition. *Journal of the European Ceramic Society*, 15, 165-171.
- Fan, J. H., & Chen, H. (2008). *Advances in Heterogeneous Material Mechanics*. Lancaster: DEStech Publications, Inc.
- Fang, Y., Cheng, J.P., & Agrawal, D.K. (2003). Effect of powder reactivity on microwave sintering of alumina. *Material Letters*, 58, 498-501.
- Franklin F. Y. W. (1976). *Ceramic fabrication processes, Volume 9*. Academic Press.
- Gitzen W.H. (1970). *Alumina as a ceramic material*. The American Ceramic Society, Columbus, 14.
- Groover, M.P. (2010). *Fundamentals of Modern Manufacturing: Materials, Processes, and Systems*. John Wiley and Sons.
- Guo, J.K., & Tuan, W.H. (2004). *Multiphased ceramic materials: processing and potential*. Germany: Springer-Verlag Berlin Heidelberg.
- Harmer, M.P., & Brook, R.J. (1981). *Journal of British Ceramic Society*. 80:147.
- Hesabi, Z.R., Haghightzadeh, M., Mazaheri, M., Galusek, D., & Sadmezhaad, S.K. (2009). Suppression of grain growth in sub-micrometer alumina via two-step sintering method. *Journal of the European Ceramic Society*, 29, 1371–1377.
- Hosokawa, M. (2007). *Nanoparticle technology handbook. Structure control of nanoparticle collectives by sintering and bonding*, 222-225; *Suppression of Particle Growth in Sintering Nanoparticles*. Elsevier.
- Hsu, Y.F., Wang, S.F., Wang, Y.R., & Chen, S.C. (2007). Effect of niobium doping on the densification and grain growth in alumina. *Journal of Ceramics International*.
- Keski, J.R., & Cutler, I.B. (1965). Effect of manganese oxide on sintering of alumina. *American Ceramic Society*, 48, 653-654.

- Kingery, W.D., Bowen, H.K., & Uhlmann, D.R. (1975). Introduction to ceramics. New York: John Wiley & Sons.
- Koch, C.C. (2007). Nanostructured Materials, Second Edition: Processing, Properties and Applications. United States: William Andrew, Inc.
- Koizumi, M., & Nishihara, M. (1991). Isostatic pressing: technology and applications. England: Elsevier Science Publishers Ltd, 32.
- Lee, W.E., & Rainforth, W.M. (1994). Ceramic microstructures: property control by processing. London, UK: Chapman & Hall.
- Lide, D.R. (2004). CRC Handbook Chemistry and Physics (85th ed). United States: CRC Press LLC.
- Lynch, C.T. (1975). CRC Handbook of Materials Science: Metals, composites, and refractory materials. CRC Press.
- Maca, K., Pouchly, V., & Zalud, P. (2010). Two-Step Sintering of oxide ceramics with various crystal structures. *Journal of the European Ceramic Society*, 30, 583-589.
- Materials. (2010). Powder Metallurgy – Component Manufacture by Uniaxial Pressing. Retrieved at 17<sup>th</sup> October 2010, from <http://www.azom.com/Details.asp?ArticleID=155>
- Materials. (2010). Production and Processing of Engineering Ceramics including Forming, Firing and Finishing by Dynamic-Ceramic. Retrieved at 17<sup>th</sup> October 2010, from <http://www.azom.com/Details.asp?ArticleID=4123>
- Murayama, N., & Shin, W. (2000). *Journal of Japan Ceramic Society*. 108:799.
- Oghbaei, M., & Mirzaee, O. (2010). Microwave versus conventional sintering: A review of fundamentals, advantages and applications. *Journal of Alloys and Compounds*, 494, 175–189.
- Ohji, T., & Singh, M. (2009). Advanced processing and manufacturing technologies for structural and multifunctional materials II. Canada: John Wiley & Sons, Inc, 19.
- Richerson, D.W. (2005). Modern ceramic engineering: properties, processing, and use in design (3<sup>rd</sup> ed). CRC Taylor & Francis.
- Sathiyakumar, M., & Gnanam, F.D. (2001). Influence of MnO and TiO<sub>2</sub> additives on density, microstructure and mechanical properties of Al<sub>2</sub>O<sub>3</sub>. *Ceramics International* 28 (2002) 195–200

- Sathiyakumar, M., & Gnanam, F.D. (2002). Influence of additives on density, microstructure and mechanical properties of alumina. *Journal of Materials Processing Technology*, 133, 282-286.
- Schmitz, C. (2006). *Handbook of aluminium recycling*. Germany: Vulkan-Verlag GmbH.
- Segal, D. (1989). *Chemical Synthesis of Advanced Ceramic Materials*. University of Cambridge: Press Syndicate, 25-27.
- Toy, C., Demirci, M., Onurlu, S., Tasar, M.S., & Baykara, T. (1995). A colloidal method for manganese oxide addition to alumina powder and investigation of properties. *Journal of Material Science*, 30, 4183-4187.
- Wang, C.J., Huang, C.Y., & Wu, Y.C. (2009). Two-step sintering of fine alumina–zirconia ceramics. *Ceramics International*, 35, 1467-1472.
- Wefer, K., & Bell, G.M. (1972). *Oxides and hydroxides of aluminium*. Aluminium Company of America, 19.
- Zavaliangos, A., & Laptev, A. (2001). *Recent developments in computer modeling of powder metallurgy processes*. IOS Press.
- Zhou, Y., Hirao, K., Yamauchi, Y., & Kanzaki, S. (2003). Effects of heating rate and particle size on pulse electric current sintering of alumina. *Journal of Scripta Materialia*, 48, 1631-1636.



## APPENDICES

### APPENDIX A: Experimental Data

#### **Bulk density (g/cm<sup>3</sup>) by using water immersion method**

Temperature (°C)	Concentration of MnO <sub>2</sub> (wt. %)				
	0 wt.%	0.5 wt.%	1.5 wt.%	3.0 wt.%	5.0 wt.%
1250	3.653	3.69	3.687	3.696	3.655
1350	3.648	3.706	3.777	3.761	3.749
1450	3.673	3.75	3.811	3.798	3.788

#### **Relative density (%) by using water immersion method**

Temperature (°C)	Concentration of MnO <sub>2</sub> (wt. %)				
	0 wt.%	0.5 wt.%	1.5 wt.%	3.0 wt.%	5.0 wt.%
1250	91.784	92.714	92.638	92.864	91.834
1350	91.658	93.116	94.899	94.497	94.196
1450	92.286	94.221	95.754	95.427	95.176

#### **Average shrinkage (%) of alumina ceramics with various concentration of MnO<sub>2</sub>**

Temperature (°C)	Concentration of MnO <sub>2</sub> (wt. %)				
	0 wt.%	0.5 wt.%	1.5 wt.%	3.0 wt.%	5.0 wt.%
1250	5.10	6.20	9.65	10.75	10.55
1350	8.55	11.40	16.80	16.90	18.15
1450	10.50	18.35	23.70	24.25	25.35

**Modulus of Elasticity (GPa) by using original formula (mass in air)**

Temperature (°C)	Concentration of MnO <sub>2</sub> (wt. %)				
	0 wt.%	0.5 wt.%	1.5 wt.%	3.0 wt.%	5.0 wt.%
1250	21.55	21.67	38.44	41.71	44.82
1350	35.97	51.09	94.61	96.39	101.20
1450	49.43	112.36	219.68	244.13	221.63

**Vickers Hardness (GPa) by using microhardness tester**

Temperature (°C)	Concentration of MnO <sub>2</sub> (wt. %)				
	0 wt.%	0.5 wt.%	1.5 wt.%	3.0 wt.%	5.0 wt.%
1250	0.740	1.360	1.660	1.780	2.780
1350	0.670	2.350	2.750	3.500	4.290
1450	1.790	3.060	6.750	10.900	13.050

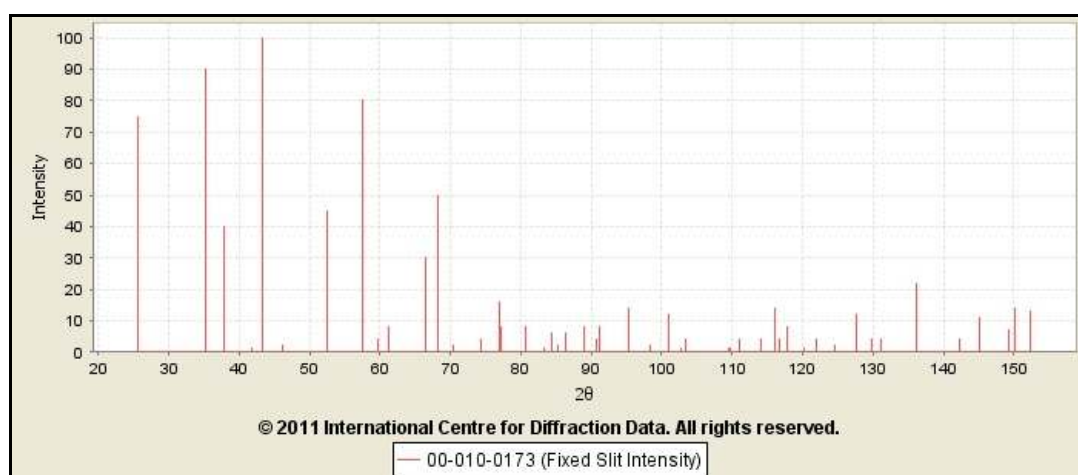
**Average Grain Size by using linear interpolation method**

Temperature (°C)	Concentration of MnO <sub>2</sub> (wt. %)				
	0 wt.%	0.5 wt.%	1.5 wt.%	3.0 wt.%	5.0 wt.%
1250	0.17	0.18	0.20	0.30	0.31
1350	0.18	0.39	0.42	0.65	0.80
1450	0.37	0.44	0.81	1.00	1.68

**Maximum Grain Size by using linear interpolation method**

Temperature (°C)	Concentration of MnO <sub>2</sub> (wt. %)				
	0 wt.%	0.5 wt.%	1.5 wt.%	3.0 wt.%	5.0 wt.%
1250	0.40 ± 0.08	0.34 ± 0.07	0.39 ± 0.12	0.72 ± 0.10	0.75 ± 0.27
1350	0.38 ± 0.02	0.75 ± 0.12	0.78 ± 0.11	1.27 ± 0.30	1.72 ± 0.47
1450	1.18 ± 0.13	0.86 ± 0.14	2.13 ± 0.57	2.38 ± 0.67	4.60 ± 0.58

## APPENDIX B: X-Ray Diffraction (XRD) Card Data

**1. Card Data: 00-010-0173**(a) d-Spacings ( $\lambda = 1.54056$ )

## (b) Fixed Slit Intensity

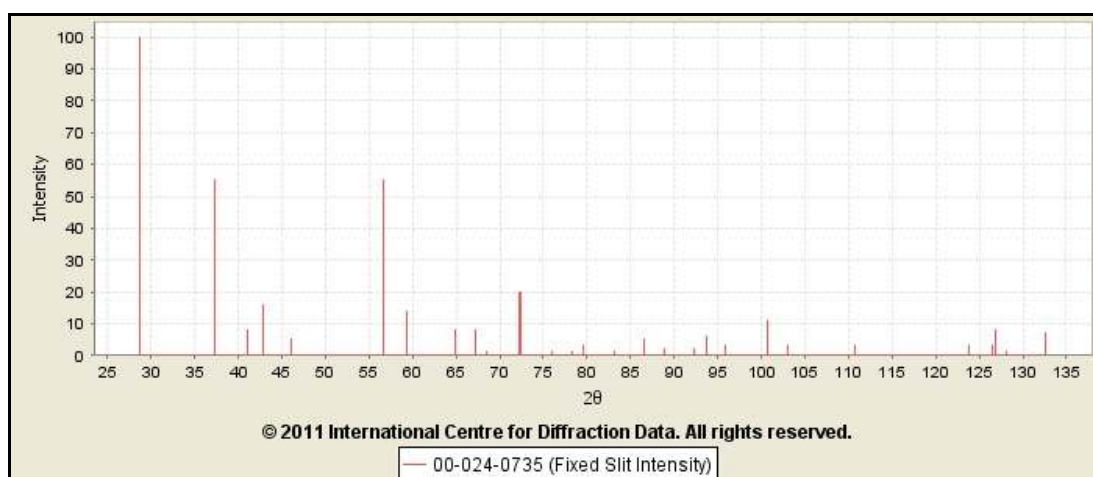
2θ	d (Å)	Intensity	h	k	l	*
25.5835	3.479000	75	0	1	2	
35.1355	2.552000	90	1	0	4	
37.7838	2.379000	40	1	1	0	
41.6834	2.165000	<1	0	0	6	
43.3620	2.085000	100	1	1	3	
46.1829	1.964000	2	2	0	2	
52.5512	1.740000	45	0	2	4	
57.5175	1.601000	80	1	1	6	
59.7675	1.546000	4	2	1	1	
61.1638	1.514000	6	1	2	2	

61.3437	1.510000	8	0	1	8	
66.5468	1.404000	30	2	1	4	
68.1963	1.374000	50	3	0	0	
70.3569	1.337000	2	1	2	5	
74.2662	1.276000	4	2	0	8	
76.8800	1.239000	16	1	0	10	
77.2267	1.234300	8	1	1	9	
80.6919	1.189800	8	2	2	0	
83.2164	1.160000	<1	3	0	6	
84.3755	1.147000	6	2	2	3	
85.1811	1.138200	2	1	3	1	
86.3751	1.125500	6	3	1	2	
86.4611	1.124600	4	1	2	8	
89.0176	1.098800	8	0	2	10	
90.6620	1.083100	4	0	0	12	
91.2011	1.078100	8	1	3	4	
95.2600	1.042600	14	2	2	6	
98.4066	1.017500	2	0	4	2	
101.0920	0.997600	12	2	1	10	
102.7880	0.985700	<1	1	1	12	
103.3450	0.981900	4	4	0	4	
109.5220	0.943100	<1	3	2	1	
109.8330	0.941300	<1	1	2	11	
111.0290	0.934500	4	3	1	8	
114.1260	0.917800	4	2	2	9	
116.1410	0.907600	14	3	2	4	
116.6300	0.905200	4	0	1	14	
117.9020	0.899100	8	4	1	0	
120.2330	0.888400	<1	2	3	5	
122.0710	0.880400	4	4	1	3	
124.6460	0.869800	2	0	4	8	
127.7310	0.858000	12	1	3	10	
129.9160	0.850200	4	3	0	12	
131.1480	0.846000	4	2	0	14	

136.1620	0.830300	22	1	4	6	
142.3960	0.813700	4	1	1	15	
145.2080	0.807200	11	4	0	10	
149.2870	0.798800	7	0	5	4	
150.2440	0.797000	14	1	0	16	
152.4450	0.793100	13	3	3	0	

## 2. Card Data: 00-024-0735

(a) d-Spacings ( $\lambda = 1.54056$ )



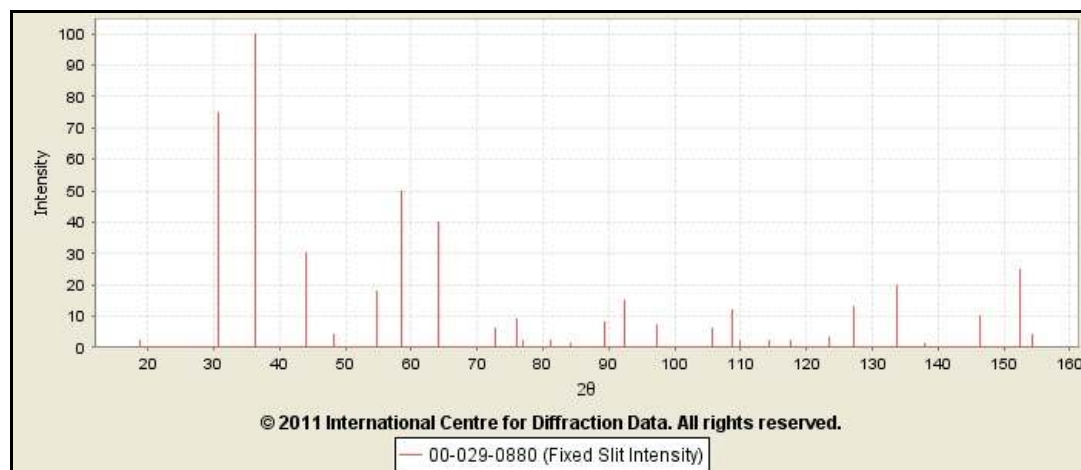
(b) Fixed Slit Intensity

2 $\theta$	d (Å)	Intensity	h	k	l	*
28.6804	3.110000	100	1	1	0	
37.3279	2.407000	55	1	0	1	
41.0097	2.199000	8	2	0	0	
42.8228	2.110000	16	1	1	1	
46.0811	1.968100	5	2	1	0	
56.6517	1.623400	55	2	1	1	
59.3699	1.555400	14	2	2	0	
64.8279	1.437000	8	0	0	2	
67.2395	1.391200	8	3	1	0	

68.5538	1.367700	<1	2	2	1	
72.2603	1.306400	20	3	0	1	
72.3818	1.304500	20	1	1	2	
75.9100	1.252400	1	3	1	1	
78.3646	1.219200	<1	3	2	0	
79.6360	1.202900	3	2	0	2	
83.1814	1.160400	1	2	1	2	
86.5957	1.123200	5	3	2	1	
88.8950	1.100000	2	4	0	0	
92.3241	1.067900	2	4	1	0	
93.7239	1.055600	6	2	2	2	
95.9406	1.037000	3	3	3	0	
100.7860	0.999800	11	3	1	2	
103.0650	0.983800	3	4	2	0	
110.7620	0.936000	3	1	0	3	
123.7530	0.873400	3	4	0	2	
126.4200	0.862900	3	5	1	0	
126.8170	0.861400	8	2	1	3	
128.0860	0.856700	<1	4	1	2	
132.6710	0.841000	7	3	3	2	

### 3. Card Data: 00-029-0880

(a) d-Spacings ( $\lambda = 1.54056$ )



## (b) Fixed Slit Intensity

$2\theta$	$d(\text{\AA})$	Intensity	h	k	l	*
18.7447	4.730000	2	1	1	1	
30.8069	2.900000	75	2	2	0	
36.2812	2.474000	100	3	1	1	
44.1183	2.051000	30	4	0	0	
48.3202	1.882000	4	3	3	1	
54.7573	1.675000	18	4	2	2	
58.3959	1.579000	50	5	1	1	
64.1770	1.450000	40	4	4	0	
72.8676	1.297000	6	6	2	0	
76.0103	1.251000	9	5	3	3	
77.0273	1.237000	2	6	2	2	
81.1698	1.184000	2	4	4	4	
84.1944	1.149000	1	7	1	1	
89.3058	1.096000	8	6	4	2	
92.3132	1.068000	15	7	3	1	
97.3759	1.025500	7	8	0	0	
105.6070	0.967000	6	8	2	2	
108.8060	0.947300	12	7	5	1	
109.8850	0.941000	2	6	6	2	
114.2800	0.917000	2	8	4	0	
117.6060	0.900500	2	9	1	1	
123.4840	0.874500	3	6	6	4	
127.1900	0.860000	13	9	3	1	
133.8400	0.837300	20	8	4	4	
138.0300	0.825000	1	9	3	3	
146.4570	0.804500	10	10	2	0	
152.4450	0.793100	25	9	5	1	
154.4060	0.789900	4	10	2	2	

## APPENDIX C: Gantt Chart and Flow Chart

**Gantt Chart of Final Year Project (Part I)**

Tasks \ Week	Week														
	1	2	3	4	5	6	7	8	9	10	11	12	13	14	15
Title Selection	■														
Literature Review		■	■	■	■	■	■	■	■	■	■	■	■	■	
Study on ceramics		■	■	■	■	■									
Study on alumina ceramics							■	■	■	■	■	■	■		
Study on methodology												■	■		
Weekly Report							■	■	■	■	■	■	■		
Report – Chapter 1				■											
Report – Chapter 2					■	■	■								
Report – Chapter 3								■	■	■	■	■	■		
Report – Chapter 4												■	■		
Oral Presentation 1														■	■

**Gantt Chart of Final Year Project (Part II)**

Tasks \ Week	Week									
	1	2	3	4	5	6	7	8	9	10
Preparation of MnO <sub>2</sub> – doped alumina ceramics	■	■	■	■						
Body preparation and sintering				■	■	■	■			
Body characterization and testing							■	■	■	■



### Gantt Chart of Final Year Project (Part III)

Week Task	1	2	3	4	5	6	7	8	9	10	11	12	13	14	15	16	17
Analysis of Data	■	■	■	■	■												
Thesis Writing	■	■	■	■	■	■	■	■	■	■	■	■	■	■	■	■	■
Report – Chapter 5		■	■	■	■												
Report – Chapter 6						■	■	■	■								
Thesis (First Draft)										■	■	■	■				
Final Thesis														■	■	■	■
Oral Presentation 2														■	■		

### Flow Chart of Processes of Final Year Project

